UCSF
UC San Francisco Electronic Theses and Dissertations

Title
The Recognition, Regulation and Roles of Misfolded Proteins in the Cell

Permalink
https://escholarship.org/uc/item/8rf373zp

Author
Smith, Melanie Hennebry

Publication Date
2014

Peer reviewed|Thesis/dissertation

eScholarship.org Powered by the California Digital Library
University of California

The Recognition, Regulation and Roles of Misfolded Proteins in the Cell

by

Melanie Hennebry Smith

DISSERTATION

Submitted in partial satisfaction of the requirements for the degree of

DOCTOR OF PHILOSOPHY

in

Biophysics

in the

GRADUATE DIVISION

of the

UNIVERSITY OF CALIFORNIA, SAN FRANCISCO

Copyright 2014
by
Melanie Hennebry Smith

ACKNOWLEDGMENTS

Non nobis solum nati sumus.
Not for us alone are we born.

- Marcus Tullius Cicero

I must first thank Professor Jonathan Weissman, a wonderful mentor without whom this thesis would never have been possible. I was extremely fortunate to find a scientific home at UCSF that prioritizes both learning as well as technological development and supported me in my interests and goals. I would also like to thank my thesis committee, Professors David Agard and Jack Taunton, for their input on and critical assessment of my work. The Peter Strauss Fellowship from the Hertz Foundation funded my graduate research; I am deeply appreciative of the Foundation's commitment not only to advancing research, but also to the creation of a well-connected scientific community.

My scientific training started with my high school biology teacher Alan Hargus who instilled in me a genuine curiosity in the biological world; as his teaching assistant, he let me dissect critters from his pond while I was meant to be grading papers. At Haverford College, Professor Robert Fairman gave me the confidence to pursue a career in science by entrusting me with the freedom to start a new project in his lab.

Research does not happen in a vacuum and many people contributed to both my learning while at UCSF in the Weissman lab as well as the research presented in this thesis.

I would like to thank the PSI subgroup, Brandon Toyama, Cat Foo, and Katie Verges, as well as Clement Chu for orienting me to the lab. In my early PhD years, Clement was always around to help when I was confused, needed technical assistance or had broken the Äkta for the nth time.

In making the switch from prions to ERAD I thank Edwin Rodriguez and Erin Quan Toyama for all of their reagents, notes, and advice. I would also like to thank the most recent iteration of the ERAD subgroup, Yi-Chang Liu and Professor Danica Fujimori, for all of their helpful discussions concerning my endeavors with Yos9.

Onn Brandman conceived of the mammalian screening system I worked on in my final year and this project was greatly accelerated when Britt Adamson joined the lab. Britt taught me a vast amount about working in mammalian cells and made me realize how satisfying it is to work closely with someone else on a problem. I thank them both for their excitement and drive – and for making this project fun.

In addition to these individuals, I would like to acknowledge all members of the Weissman lab for creating an amazing work environment. There was always interesting science, lively discussion, group lunches around our extended lunchroom table, and fantastic espresso (originally thanks to Clement and then to Yi-Chang and Calvin Jan).

I give many thanks to all of the people who provided administrative help, technical support or guidance: Manny De Vera our lab manger who is indispensible (as we realize every year when he goes on vacation); Christopher Reiger our ultra-efficient lab admin whose sense of humor surrounding bureaucratic nonsense is definitely appreciated; Rebecca Brown in the Biophysics graduate program; Jana Toutolmin and Catherine Norton in the MSTP office; and the MSTP Directors Professors Kevin Shannon and Mark Anderson.

Finally, I would like to thank my family and friends for contributing to my success and happiness. At different times, they have all had an impact through their willingness to listen, make me laugh, do new things, travel, be outside and generally have a good time. I am particularly thankful for the continual support of my parents, Josh and Laura, as I make my way

through the long training towards an MD/PhD. I am also grateful for the support of my very soon to be husband Vivek Tata. I'm not sure if he knew what he was getting himself into when we met just prior to my start in the lab, but his non-science perspective has provided an important source of balance over the years. His positive, yet rational, outlook has helped shape both my personal and professional lives. I also want to give a huge thanks to my brother, Garrett, who is in San Francisco and convinced me that it would be a fun place to live while going to school. The Hump Night Dinner Crew (Garrett, Rob Benson, Caroline Stanculescu and Vivek) deserves special mention for feeding me after many a long day in lab and providing me with nicer wine than any graduate student should probably be allowed to consume.

I hope to be able to repay the generosity and patience granted to me by these people by helping colleagues and friends, training the next generation, and doing research that will have an impact on the lives of others.

M.H.S.
San Francisco
May 19, 2014

ABSTRACT

The three dimensional structure of a protein, or its native state, determines its function. Yet, the process of folding into the native state is not straightforward; proteins can stay unfolded, misfold and even aggregate. This dissertation addresses the issue of how the cell responds to these non-native species.

In the first part, I explored the cellular regulation of a specific type of protein aggregate: prions. Prions, made from the ordered-aggregation of single proteins in non-native conformations, can exist as multiple heritable strains that have distinct structures and result in different phenotypes. Here, I investigated how the sequence of a prion protein influences its ability to propagate specific strains using the PNM2 variant of the yeast prion [*PSI*$^{+}$]. We found that the PNM2 mutation, which prevents propagation of a specific strain, interfered with the delivery of that strain to daughter cells, illustrating that delivery is a crucial step in prion inheritance.

The remainder of this thesis addresses how the cell responds to misfolded proteins in the endoplasmic reticulum (ER). As the first part of the sectretory pathway, the ER receives all proteins destined for the extracellular space or insertion into the membrane. Some of these nascent proteins never reach their native states and are degraded by a series of pathways collectively referred to as ER-associated degradation (ERAD). In order to determine how ERAD factors accurately identify substrates for removal, I studied the substrate-binding abilities of Yos9, which in addition to its role as a lectin can also bind the protein components of substrates. I showed that Yos9 exhibits sequence specific recognition of peptides *in vitro* and binding of Yos9 to its substrates results in their cooperative aggregation, which is a novel phenomenon that may play a role in the regulation of ERAD.

While the response to misfolded proteins in the ER is well-studied in yeast, we sought to better understand this process in metazoans through the development of a pathway-specific screening approach that employs a reporter of the unfolded protein response. While this work is ongoing, it has the potential to reveal key mammalian-specific aspects of protein homeostasis in the ER.

CONTRIBUTIONS

Chapter 3, "Strain conformation, primary structure and the propagation of the yeast prion [*PSI*$^{+}$]", first appeared as a manuscript published in *Nature Structure & Molecular Biology* in April 2011, Vol. 18, pp. 493-499. Katherine Verges initiated this work and performed the initial experiments concerning the characterization of PNM2, the Hap-ClpPtrap translocation assays and the mother-daughter propagon partitioning. I performed the Hsp104ΔNTD experiments, analysis of fiber sizes and the high copy PNM2 suppression screen. Brandon Toyama designed, performed and analyzed the H/X NMR experiments. Dr. Jonathan S. Weissman supervised the work.

Chapter 4, "Road to ruin: targeting proteins for degradation in the endoplasmic reticulum" appeared in print November 25, 2011 in *Science*, Vol. 334, pp. 1056-1090 and is reproduced with permission form AAAS. This review was written in collaboration with the authors listed.

Chapter 5, "Binding of unfolded proteins by the lectin Yos9 induces aggregation", will be submitted for publication. Edwin Rodriguez performed the limited proteolysis defining the Yos9 truncation variant. I performed all other experiments with the assistance of those acknowledged in that chapter and Dr. Jonathan S. Weissman supervised the work.

The methodology for Chapter 6, "Defining the core regulators of protein homeostasis in the mammalian endoplasmic reticulum", was originally conceived of by Dr. Onn Brandman. Dr. Britt Adamson and myself jointly performed the experiments, and both Drs. Onn Brandman and Jonathan S. Weissman supervised the work.

With the exception of those items listed above, Melanie H. Smith performed the work presented in this dissertation under the supervision of Dr. Jonathan S. Weissman.

PERMISSIONS

THE AMERICAN ASSOCIATION FOR THE ADVANCEMENT OF SCIENCE LICENSE TERMS AND CONDITIONS

Mar 26, 2014

This is a License Agreement between Melanie H Smith ("You") and The American Association for the Advancement of Science ("The American Association for the Advancement of Science") provided by Copyright Clearance Center ("CCC"). The license consists of your order details, the terms and conditions provided by The American Association for the Advancement of Science, and the payment terms and conditions.

All payments must be made in full to CCC. For payment instructions, please see information listed at the bottom of this form.

License Number	3356660213271
License date	Mar 26, 2014
Licensed content publisher	The American Association for the Advancement of Science
Licensed content publication	Science
Licensed content title	Road to Ruin: Targeting Proteins for Degradation in the Endoplasmic Reticulum
Licensed content author	Melanie H. Smith, Hidde L. Ploegh, Jonathan S. Weissman
Licensed content date	Nov 25, 2011
Volume number	334
Issue number	6059
Type of Use	Thesis / Dissertation
Requestor type	Author of the AAAS published paper
Format	Print and electronic
Portion	Full Text
Order reference number	
Title of your thesis / dissertation	The recognition, regulation and roles of misfolded proteins in the cell
Expected completion date	May 2014
Estimated size(pages)	100
Total	0.00 USD
Terms and Conditions	

American Association for the Advancement of Science TERMS AND CONDITIONS

Regarding your request, we are pleased to grant you non-exclusive, non-transferable permission, to republish the AAAS material identified above in your work identified above, subject to the terms and conditions herein. We must be contacted for permission for any uses other than those specifically identified in your request above.

The following credit line must be printed along with the AAAS material: "From [Full Reference Citation]. Reprinted with permission from AAAS."

All required credit lines and notices must be visible any time a user accesses any part of the AAAS material and must appear on any printed copies and authorized user might make.

This permission does not apply to figures / photos / artwork or any other content or materials included in your work that are credited to non-AAAS sources. If the requested material is sourced to or references non-AAAS sources, you must obtain authorization from that source as well before using that material. You agree to hold harmless and indemnify AAAS against any claims arising from your use of any content in your work that is credited to non-AAAS sources.

If the AAAS material covered by this permission was published in Science during the years 1974 - 1994, you must also obtain permission from the author, who may grant or withhold permission, and who may or may not charge a fee if permission is granted. See original article for author's address. This condition does not apply to news articles.

The AAAS material may not be modified or altered except that figures and tables may be modified with permission from the author. Author permission for any such changes must be secured prior to your use.

Whenever possible, we ask that electronic uses of the AAAS material permitted herein include a hyperlink to the original work on AAAS's website (hyperlink may be embedded in the reference citation).

AAAS material reproduced in your work identified herein must not account for more than 30% of the total contents of that work.

AAAS must publish the full paper prior to use of any text.

AAAS material must not imply any endorsement by the American Association for the Advancement of Science.

This permission is not valid for the use of the AAAS and/or Science logos.

AAAS makes no representations or warranties as to the accuracy of any information contained in the AAAS material covered by this permission, including any warranties of

merchantability or fitness for a particular purpose.

If permission fees for this use are waived, please note that AAAS reserves the right to charge for reproduction of this material in the future.

Permission is not valid unless payment is received within sixty (60) days of the issuance of this permission. If payment is not received within this time period then all rights granted herein shall be revoked and this permission will be considered null and void.

In the event of breach of any of the terms and conditions herein or any of CCC's Billing and Payment terms and conditions, all rights granted herein shall be revoked and this permission will be considered null and void.

AAAS reserves the right to terminate this permission and all rights granted herein at its discretion, for any purpose, at any time. In the event that AAAS elects to terminate this permission, you will have no further right to publish, publicly perform, publicly display, distribute or otherwise use any matter in which the AAAS content had been included, and all fees paid hereunder shall be fully refunded to you. Notification of termination will be sent to the contact information as supplied by you during the request process and termination shall be immediate upon sending the notice. Neither AAAS nor CCC shall be liable for any costs, expenses, or damages you may incur as a result of the termination of this permission, beyond the refund noted above.

This Permission may not be amended except by written document signed by both parties.

The terms above are applicable to all permissions granted for the use of AAAS material. Below you will find additional conditions that apply to your particular type of use.

FOR A THESIS OR DISSERTATION
If you are using figure(s)/table(s), permission is granted for use in print and electronic versions of your dissertation or thesis. A full text article may be used in print versions only of a dissertation or thesis.

Permission covers the distribution of your dissertation or thesis on demand by ProQuest / UMI, provided the AAAS material covered by this permission remains in situ.

If you are an Original Author on the AAAS article being reproduced, please refer to your License to Publish for rules on reproducing your paper in a dissertation or thesis.

FOR JOURNALS:
Permission covers both print and electronic versions of your journal article, however the AAAS material may not be used in any manner other than within the context of your article.

FOR BOOKS/TEXTBOOKS:
If this license is to reuse figures/tables, then permission is granted for non-exclusive world rights in all languages in both print and electronic formats (electronic formats are defined below).

If this license is to reuse a text excerpt or a full text article, then permission is granted for non-exclusive world rights in English only. You have the option of securing either print or electronic rights or both, but electronic rights are not automatically granted and do garner additional fees. Permission for translations of text excerpts or full text articles into other languages must be obtained separately.

Licenses granted for use of AAAS material in electronic format books/textbooks are valid only in cases where the electronic version is equivalent to or substitutes for the print version of the book/textbook. The AAAS material reproduced as permitted herein must remain in situ and must not be exploited separately (for example, if permission covers the use of a full text article, the article may not be offered for access or for purchase as a stand-alone unit), except in the case of permitted textbook companions as noted below.

You must include the following notice in any electronic versions, either adjacent to the reprinted AAAS material or in the terms and conditions for use of your electronic products: "Readers may view, browse, and/or download material for temporary copying purposes only, provided these uses are for noncommercial personal purposes. Except as provided by law, this

material may not be further reproduced, distributed, transmitted, modified, adapted, performed, displayed, published, or sold in whole or in part, without prior written permission from the publisher."

If your book is an academic textbook, permission covers the following companions to your textbook, provided such companions are distributed only in conjunction with your textbook at no additional cost to the user:

- Password-protected website
- Instructor's image CD/DVD and/or PowerPoint resource
- Student CD/DVD

All companions must contain instructions to users that the AAAS material may be used for non-commercial, classroom purposes only. Any other uses require the prior written permission from AAAS.

If your license is for the use of AAAS Figures/Tables, then the electronic rights granted herein permit use of the Licensed Material in any Custom Databases that you distribute the electronic versions of your textbook through, so long as the Licensed Material remains within the context of a chapter of the title identified in your request and cannot be downloaded by a user as an independent image file.

Rights also extend to copies/files of your Work (as described above) that you are required to provide for use by the visually and/or print disabled in compliance with state and federal laws.

This permission only covers a single edition of your work as identified in your request.

FOR NEWSLETTERS:
Permission covers print and/or electronic versions, provided the AAAS material reproduced as permitted herein remains in situ and is not exploited separately (for example, if permission covers the use of a full text article, the article may not be offered for access or for purchase as a stand-alone unit)

FOR ANNUAL REPORTS:
Permission covers print and electronic versions provided the AAAS material reproduced as permitted herein remains in situ and is not exploited separately (for example, if permission covers the use of a full text article, the article may not be offered for access or for purchase as a stand-alone unit)

FOR PROMOTIONAL/MARKETING USES:
Permission covers the use of AAAS material in promotional or marketing pieces such as information packets, media kits, product slide kits, brochures, or flyers limited to a single print run. The AAAS Material may not be used in any manner which implies endorsement or promotion by the American Association for the Advancement of Science (AAAS) or Science of any product or service. AAAS does not permit the reproduction of its name, logo or text on promotional literature.

If permission to use a full text article is permitted, The Science article covered by this permission must not be altered in any way. No additional printing may be set onto an article copy other than the copyright credit line required above. Any alterations must be approved in advance and in writing by AAAS. This includes, but is not limited to, the placement of

sponsorship identifiers, trademarks, logos, rubber stamping or self-adhesive stickers onto the article copies.

Additionally, article copies must be a freestanding part of any information package (i.e. media kit) into which they are inserted. They may not be physically attached to anything, such as an advertising insert, or have anything attached to them, such as a sample product. Article copies must be easily removable from any kits or informational packages in which they are used. The only exception is that article copies may be inserted into three-ring binders.

FOR CORPORATE INTERNAL USE:
The AAAS material covered by this permission may not be altered in any way. No additional printing may be set onto an article copy other than the required credit line. Any alterations must be approved in advance and in writing by AAAS. This includes, but is not limited to the placement of sponsorship identifiers, trademarks, logos, rubber stamping or self-adhesive stickers onto article copies.

If you are making article copies, copies are restricted to the number indicated in your request and must be distributed only to internal employees for internal use.

If you are using AAAS Material in Presentation Slides, the required credit line must be visible on the slide where the AAAS material will be reprinted

If you are using AAAS Material on a CD, DVD, Flash Drive, or the World Wide Web, you must include the following notice in any electronic versions, either adjacent to the reprinted AAAS material or in the terms and conditions for use of your electronic products: "Readers may view, browse, and/or download material for temporary copying purposes only, provided these uses are for noncommercial personal purposes. Except as provided by law, this material may not be further reproduced, distributed, transmitted, modified, adapted, performed, displayed, published, or sold in whole or in part, without prior written permission from the publisher." Access to any such CD, DVD, Flash Drive or Web page must be restricted to your organization's employees only.

FOR CME COURSE and SCIENTIFIC SOCIETY MEETINGS:
Permission is restricted to the particular Course, Seminar, Conference, or Meeting indicated in your request. If this license covers a text excerpt or a Full Text Article, access to the reprinted AAAS material must be restricted to attendees of your event only (if you have been granted electronic rights for use of a full text article on your website, your website must be password protected, or access restricted so that only attendees can access the content on your site).

If you are using AAAS Material on a CD, DVD, Flash Drive, or the World Wide Web, you must include the following notice in any electronic versions, either adjacent to the reprinted AAAS material or in the terms and conditions for use of your electronic products: "Readers may view, browse, and/or download material for temporary copying purposes only, provided these uses are for noncommercial personal purposes. Except as provided by law, this material may not be further reproduced, distributed, transmitted, modified, adapted, performed, displayed, published, or sold in whole or in part, without prior written permission from the publisher."

FOR POLICY REPORTS:
These rights are granted only to non-profit organizations and/or government agencies. Permission covers print and electronic versions of a report, provided the required credit line appears in both versions and provided the AAAS material reproduced as permitted herein

remains in situ and is not exploited separately.

FOR CLASSROOM PHOTOCOPIES:
Permission covers distribution in print copy format only. Article copies must be freestanding and not part of a course pack. They may not be physically attached to anything or have anything attached to them.

FOR COURSEPACKS OR COURSE WEBSITES:
These rights cover use of the AAAS material in one class at one institution. Permission is valid only for a single semester after which the AAAS material must be removed from the Electronic Course website, unless new permission is obtained for an additional semester. If the material is to be distributed online, access must be restricted to students and instructors enrolled in that particular course by some means of password or access control.

FOR WEBSITES:
You must include the following notice in any electronic versions, either adjacent to the reprinted AAAS material or in the terms and conditions for use of your electronic products: "Readers may view, browse, and/or download material for temporary copying purposes only, provided these uses are for noncommercial personal purposes. Except as provided by law, this material may not be further reproduced, distributed, transmitted, modified, adapted, performed, displayed, published, or sold in whole or in part, without prior written permission from the publisher."

Permissions for the use of Full Text articles on third party websites are granted on a case by case basis and only in cases where access to the AAAS Material is restricted by some means of password or access control. Alternately, an E-Print may be purchased through our reprints department (brocheleau@rockwaterinc.com).

REGARDING FULL TEXT ARTICLE USE ON THE WORLD WIDE WEB IF YOU ARE AN 'ORIGINAL AUTHOR' OF A SCIENCE PAPER

If you chose "Original Author" as the Requestor Type, you are warranting that you are one of authors listed on the License Agreement as a "Licensed content author" or that you are acting on that author's behalf to use the Licensed content in a new work that one of the authors listed on the License Agreement as a "Licensed content author" has written.

Original Authors may post the 'Accepted Version' of their full text article on their personal or on their University website and not on any other website. The 'Accepted Version' is the version of the paper accepted for publication by AAAS including changes resulting from peer review but prior to AAAS's copy editing and production (in other words not the AAAS published version).

FOR MOVIES / FILM / TELEVISION:
Permission is granted to use, record, film, photograph, and/or tape the AAAS material in connection with your program/film and in any medium your program/film may be shown or heard, including but not limited to broadcast and cable television, radio, print, world wide web, and videocassette.

The required credit line should run in the program/film's end credits.

FOR MUSEUM EXHIBITIONS:
Permission is granted to use the AAAS material as part of a single exhibition for the duration

of that exhibit. Permission for use of the material in promotional materials for the exhibit must be cleared separately with AAAS (please contact us at permissions@aaas.org).

FOR TRANSLATIONS:
Translation rights apply only to the language identified in your request summary above.

The following disclaimer must appear with your translation, on the first page of the article, after the credit line: "This translation is not an official translation by AAAS staff, nor is it endorsed by AAAS as accurate. In crucial matters, please refer to the official English-language version originally published by AAAS."

FOR USE ON A COVER:
Permission is granted to use the AAAS material on the cover of a journal issue, newsletter issue, book, textbook, or annual report in print and electronic formats provided the AAAS material reproduced as permitted herein remains in situ and is not exploited separately

By using the AAAS Material identified in your request, you agree to abide by all the terms and conditions herein.

Questions about these terms can be directed to the AAAS Permissions department permissions@aaas.org.

Other Terms and Conditions:

v 2

If you would like to pay for this license now, please remit this license along with your payment made payable to "COPYRIGHT CLEARANCE CENTER" otherwise you will be invoiced within 48 hours of the license date. Payment should be in the form of a check or money order referencing your account number and this invoice number RLNK501261797.
Once you receive your invoice for this order, you may pay your invoice by credit card. Please follow instructions provided at that time.

Make Payment To:
Copyright Clearance Center
Dept 001
P.O. Box 843006
Boston, MA 02284-3006

For suggestions or comments regarding this order, contact RightsLink Customer Support: customercare@copyright.com or +1-877-622-5543 (toll free in the US) or +1-978-646-2777.

Gratis licenses (referencing $0 in the Total field) are free. Please retain this printable license for your reference. No payment is required.

TABLE OF CONTENTS

Preface Acknowledgments……..iii

Abstract……...vi

Contributions……...….viii

Permissions…….ix

Table of Contents…….....xvi

List of Figures and Tables…….....xviii

Chapter 1 **An introduction: protein folding, misfolding and alternate conformations… 1**

References……8

Chapter 2 **Prions and [*PSI*$^+$] as a model system……..11**

References……..17

Chapter 3 **Strain conformation, primary structure and the propagation of the yeast prion [*PSI*$^+$]……...21**

PNM2 shows strain-specific effects on [*PSI*+] propagation…….26

PNM2 disrupts Sc37 growth rate and structural stability……..28

PNM2 does not affect growth, stability or structure of Sc4……..29

PNM2 does not affect Sc4-chaperone interactions……...30

PNM2 causes a defect in Sc4 propagon partitioning……..…33

Discussion……..34

Methods……...…37

Supplementary Information…….....49

References……..54

TABLE OF CONTENTS, *continued*

Chapter 4 Road to ruin: targeting proteins for degradation in the endoplasmic reticulum……...60

E3 ubiquitin ligases: central organizers…….64

How are substrates delivered to E3 complexes?.....68

Outlook……..…73

References……..80

Chapter 5 Binding of unfolded proteins by the lectin Yos9 induces aggregation……83

Experimental Procedures ……..88

Results……92

Discussion……..97

Supplemental Data……...106

References……109

Chapter 6 Defining the core regulators of protein homeostasis in the mammalian endoplasmic reticulum……...115

Results……..123

Discussion……125

Experimental Procedures…….128

References……136

LIST OF FIGURES AND TABLES

Chapter 3 **Strain conformation, primary structure and the propagation of the yeast prion [*PSI*$^{+}$]**

Figure 1 Characterization of *in vivo* prion phenotypes……41

Figure 2 Schematic of the prion propagation cycle…….42

Figure 3 Characterization of the physical properties of fibers formed *in vitro*……43

Figure 4 H/D exchange of wild-type and PNM2 SupNM fibers……..……45

Figure 5 PNM2 fibers in the Sc4 conformation interact with the *in vivo* chaperone machinery ……..46

Figure 6 PNM2 in the SC4 conformation shows a defect in partitioning……....48

Figure S1 The Hsp104ΔNTD variant is deficient in curing but propagates [*PSI*$^{+}$]^{Sc4} and maintains the PNM2 phenotype…….49

Figure S2 Overexpression of either *LSB3* or *ART5* suppresses the PNM2 phenotype……...50

Table S1 Yeast strains used in this study……..…51

Table S2 Plasmids used in this study……52

Chapter 4 **Road to ruin: targeting proteins for degradation in the endoplasmic Reticulum**

Figure 1 The events and components of ERAD……...76

Figure 2 Different paths substrates take to the E3 complexes…….77

Figure 3 Targeting glycoproteins for degradation……... 78

Chapter 5 **Binding of unfolded proteins by the lectin Yos9 induces aggregation**

Figure 1 A truncated variant of Yos9 is folded and functional……..101

Figure 2 $Yos9_{22-421}$ binds specific regions of CPY*……...102

Figure 3 Yos9 binds ΔEspP and Δ131Δ *in vitro*……..…..103

Figure 4 Yos9 forms aggregates in the presence of binding substrate……...104

Figure S1 Binding of Yos9 to mannotriose (man_3)-fluorescein……...106

Figure S2 Amino acid composition of peptides bound by Yos9……..107

Figure S3 Yos9 aggregates cooperatively in the presence of Δ131Δ……..…….107

Figure S4 Yos9 mutants do not affect aggregation……..108

Chapter 6 **Defining the core regulators of protein homeostasis in the mammalian endoplasmic reticulum**

Figure 1 Schematic of the loss of function screen to identify regulators of protein homeostasis in mammalian cells…….131

Figure 2 RNA binding proteins considered for use in the screen……..132

Figure 3 IP of PCP enriches for PP7 handle hairpin RNA……133

Figure 4 The presence of a proximal handle hairpin does not affect shRNA knockdown of GFP……..134

Figure 5 The UPRE reporter quantitatively responds to induction of ER protein folding stress……135

CHAPTER 1

An introduction: protein folding, misfolding and alternate conformations

The information required to make a protein is stored in the genome in the form of DNA and rendered accessible through conversion to mRNA, which is ultimately read out by the ribosome as a linear chain of amino acids. In order for the protein to be functional, this linear chain must convert into the correct three-dimensional structure termed the native state. As pivotal work by Anfinsen and colleagues showed, the chemistry of the amino acid sequence contains the requisite information to determine the native state[1]. Yet difficulty in reaching this structure is a common problem. Reliance on weak interactions, structural complexity, and the crowded nature of the cell all complicate the process of reaching the native state, or protein folding[2]. To retain functionally important conformational flexibility, the native state is often marginally stable: held together by multiple weak, noncovalent interactions. In addition, some proteins must assemble into multiprotein complexes in their native states. With these challenges, it is not surprising that proteins populate multiple non-native structures that do not lie along the most direct folding pathway. In fact one can argue that the formation of these off-pathway states, known as protein misfolding, is an intrinsic property of polypeptides.

Chaperones are a diverse set of cellular machinery dedicated to helping proteins navigate the complex process of folding and are largely responsible for maintenance of the cellular proteome, or proteostasis[3,4]. By regulating folding and handoff to transport machinery, chaperones ensure that the correct amount of active protein is present at the necessary location for optimal cellular function. To this end, the central role of chaperones is to counteract non-native interactions; especially those involved in aggregation, one form of off-pathway intermolecular association, which is enhanced by the macromolecular crowding intrinsic to the cellular environment. Insufficient chaperone activity results in the breakdown of proteostasis, which compromises cellular function and leads to aging or disease states[5]. An important

consequence of their central role in proteostasis is that chaperones facilitate evolution of protein function by buffering the affect of mutations that might otherwise preclude protein folding[6,7].

In order to maintain the entire proteome, chaperones must recognize a diverse range of clients in a multitude of conformations. To accomplish this impressive feat, chaperones employ a number of mechanisms. For example, Hsp90 exhibits extensive conformational flexibility that may be used to accommodate clients with different structural constraints[8], TRiC has different subunits with diverse binding specificities[9] and a single Hsp70 interacts with multiple Hsp40 co-chaperones to expand its client range[3]. Just as a single chaperone serves a variety of clients, an individual protein often uses multiple chaperones in order to maximize folding yield. These redundancies create a robust folding network that continually monitors proteostasis throughout the cell.

Specialization of chaperones to act at distinct times during protein biogenesis and to address different folding issues contributes to the robustness of the folding network[3]. As nascent a polypeptide emerges from the ribosome exit tunnel, it is greeted by ribosome-associated chaperones, such as NAC and RAC, that protect it from non-native interactions while the remainder of the polypeptide is synthesized. Once the complete polypeptide exits the ribosome and the long-range interactions needed for correct folding are possible, it is released for a first attempt at folding. If it remains unfolded off of the ribosome, Hsp70 chaperones prevent non-native client interactions by binding exposed hydrophobic regions. Recognition of these regions, which are normally buried within the core of a properly-folded protein, is a common mechanism employed by chaperones that permits recognition of an assortment of unfolded proteins. In addition to its role as a holdase in which it covers sticky hydrophobic patches, Hsp70 can mediate de novo folding, refolding or even aggregate solubilization through ATP-dependent, co-

chaperone-regulated cycles. If this initial assistance is insufficient, unfolded proteins are either transferred to chaperonins, which contain large chambers that promote folding via sequestration, steric confinement and forced unfolding of incorrect structures[10], or to Hsp90, which preferentially binds proteins that are approaching their native states[11]. For those proteins that are unable to fold correctly in spite of these efforts, chaperones interact with cellular protein degradation machinery to avoid transport of nonfunctional proteins as well as potentially harmful aggregation.

Under some circumstances, misfolded proteins can take the form of highly ordered aggregates rich in β-sheets termed amyloid fibers[12]. While these aggregates are generally detrimental to the cell and are associated with neurodegenerative diseases such as Alzheimer's, Huntington's, Parkinson's and amyotrophic lateral sclerosis (ALS), they also play a role in the normal biology of a number of organisms[13]. For example, in *Escherichia coli* amyloid takes on a structural role: the protein curlin forms extracellular amyloid fibers that facilitate surface adhesion and colony formation. In human melanocytes, amyloid formation by Pmel17 enhances the rate of melanin synthesis by accelerating polymerization of melanin precursors. Amyloid is also implicated in the formation of stress granules, which sequester, modify and/or degrade mRNA during the cellular stress response in order to regulate protein synthesis[14,15]. Many of the RNA binding proteins found in stress granules can self-associate through glycine-rich domains providing a possible mechanism for recruitment of mRNAs to these sites of mRNA metabolism. While stress granules normally subside with stress, this amyloid-forming pathway is also implicated in disease states. Abnormal aggregation of RNA binding proteins has been observed for TDP-43 and FUS in ALS as well as tau in Alzheimer's disease. It is not completely clear how

this aggregation deviates from normal stress granule formation, but mutated forms of TDP-43 seen in familial ALS can mislocalize and form irreversible aggregates.

Amyloid formation has been extensively studied in fungi, especially the yeast *Saccharomyces cerevisiae,* where it is thought to encode and transfer epigenetic information[16]. Yeast contain a number of proteins that form infectious and heritable forms of amyloid, called prions, of which [*PSI*$^{+}$] is the best characterized. While the role of prions in yeast is not exactly clear, they are hypothesized to be beneficial due to their high degree of conservation and their ability to confer a growth advantage under some conditions[17]. Lindquist and colleagues have posited that [*PSI*$^{+}$] functions as an evolutionary capacitor by causing stop-codon read through during protein translation[18]. Regardless of its function, [*PSI*$^{+}$] is a powerful model system that allows researchers to combine *in vitro* structural studies with an *in vivo* understanding of the cellular mechanisms used to regulate amyloid formation. The processes involved in [*PSI*$^{+}$] inheritance are the topic of chapters two and three of this thesis.

While misfolded proteins can occasionally play useful roles, more often than not they are an undesirable side effect of insufficient proteostasis and must be dealt with via cellular quality control. The complex chemistry and marginal stability of proteins not only makes misfolding of nascent proteins a prevalent issue, it also makes proteins prone to damage from environmental stressors such as heat shock, oxidation, chemical exposure and aging[5]. Whether proteins misfold de novo or only as a result of stress, adequate activation of quality control mechanisms is paramount for maintaining cellular function. If the load of defective molecules exceeds the cell's capacity to repair or degrade them the cell will undergo programmed cell death, or apoptosis. Since this is an undesirable outcome that consumes valuable resources, cells employ many cytoprotective strategies to mitigate damage. These quality control systems generally consist of

three parts: (1) detection of aberrant protein molecules, (2) local activation of repair or disposal machinery, and (3) global response to increase the cellular capacity to address the problem[19].

Detection of misfolded proteins is based on their deviation from the native state and involves many of the same challenges facing chaperones as they attempt to bind diverse clients. In fact, this step is often carried out by or in conjunction with chaperones. Importantly, the detection machinery must ignore those proteins that are in the process of folding along normal folding pathways as the cell must not waste resources by flagging these proteins for possible destruction. Once a misfolded protein has been detected, local machinery must either repair it via refolding or, if it is deemed terminally misfolded (beyond hope), dispose of it. This is predominantly a kinetic decision and there is increasing evidence for the spatial sequestration of misfolded molecules awaiting degradation[20]. As part of the ubiquitin-proteasome system (UPS), the proteasome, a complex of proteases that can be thought of as the cellular garbage disposal, degrades the majority of the unwanted proteins. Ubiquitin ligases specifically mark substrates with the small protein ubiquitin targeting them to the proteasome. Autophagy constitutes an alternate removal pathway which is intricately tied to the level of cellular stress and constitutes a powerful tool for both clearing the cell of aggregates that are too large to be fed into the proteasome as well as selectively disposing of specific targets via chaperone mediated autophagy (CMA)[21,22].

Global responses to misfolded proteins serve to both increase the folding capacity of the cell and decrease the load of new proteins via attenuation of protein synthesis. While these responses involve a change in whole cell physiology, they originate in a particular subcellular compartment. Misfolded proteins in the cytosol activate the heat shock response orchestrated by the transcription factor Hsf1[23]. In the endoplasmic reticulum (ER), they activate the unfolded

protein response (UPR)[24] and the multifaceted disposal pathway ER-associated degradation (ERAD) (reviewed in chapter four of this thesis)[25]. While less well understood, the mitochondrial UPR is conceptually similar to that in the ER, but uses distinct approaches to detect and signal the presence of misfolded proteins[26].

While protein quality control occurs in all cellular compartments, the secretory pathway is an especially rich place in which to study proteostasis. The ER is responsible for the biogenesis of all proteins destined for the extracellular space or insertion into the cellular membrane, which accounts for at least a third of cellular protein synthesis depending on the cell type. In order to prepare proteins for the harsh, oxidizing extracellular milieu, the ER maintains a specialized environment, which poses a number of distinct folding challenges such as the formation of disulfide bonds. Thus, how the ER attends to misfolded proteins is an important consideration for overall cellular homeostasis and is the topic of chapters four through six of this thesis. Chapter five addresses how the ERAD pathway recognizes terminally misfolded proteins for targeted degradation and chapter six introduces new tools for exploring the UPR and other stress pathways in mammalian cells.

References

1. Dobson, C. M., Šali, A. & Karplus, M. Protein Folding: A Perspective from Theory and Experiment. *Angew. Chem. Int. Ed.* **37,** 868–893 (1998).
2. Ellis, R. J. & Minton, A. P. Protein aggregation in crowded environments. *Biol. Chem.* **387,** 485–497 (2006).
3. Kim, Y. E., Hipp, M. S., Bracher, A., Hayer-Hartl, M. & Hartl, F. U. Molecular chaperone functions in protein folding and proteostasis. *Annu. Rev. Biochem.* **82,** 323–355 (2013).
4. Saibil, H. Chaperone machines for protein folding, unfolding and disaggregation. *Nat. Rev. Mol. Cell Biol.* **14,** 630–642 (2013).
5. Morimoto, R. I. The heat shock response: systems biology of proteotoxic stress in aging and disease. *Cold Spring Harb. Symp. Quant. Biol.* **76,** 91–99 (2011).
6. Tokuriki, N. & Tawfik, D. S. Chaperonin overexpression promotes genetic variation and enzyme evolution. *Nature* **459,** 668–673 (2009).
7. Sangster, T. A., Lindquist, S. & Queitsch, C. Under cover: causes, effects and implications of Hsp90-mediated genetic capacitance. *BioEssays News Rev. Mol. Cell. Dev. Biol.* **26,** 348–362 (2004).
8. Krukenberg, K. A., Förster, F., Rice, L. M., Sali, A. & Agard, D. A. Multiple conformations of E. coli Hsp90 in solution: insights into the conformational dynamics of Hsp90. *Struct. Lond. Engl. 1993* **16,** 755–765 (2008).
9. Spiess, C., Miller, E. J., McClellan, A. J. & Frydman, J. Identification of the TRiC/CCT substrate binding sites uncovers the function of subunit diversity in eukaryotic chaperonins. *Mol. Cell* **24,** 25–37 (2006).

10. Lin, Z., Madan, D. & Rye, H. S. GroEL stimulates protein folding through forced unfolding. *Nat. Struct. Mol. Biol.* **15,** 303–311 (2008).

11. Street, T. O., Lavery, L. A. & Agard, D. A. Substrate binding drives large-scale conformational changes in the Hsp90 molecular chaperone. *Mol. Cell* **42,** 96–105 (2011).

12. Chiti, F. & Dobson, C. M. Protein misfolding, functional amyloid, and human disease. *Annu. Rev. Biochem.* **75,** 333–366 (2006).

13. Fowler, D. M., Koulov, A. V., Balch, W. E. & Kelly, J. W. Functional amyloid--from bacteria to humans. *Trends Biochem. Sci.* **32,** 217–224 (2007).

14. Wolozin, B. Regulated protein aggregation: stress granules and neurodegeneration. *Mol. Neurodegener.* **7,** 56 (2012).

15. Li, Y. R., King, O. D., Shorter, J. & Gitler, A. D. Stress granules as crucibles of ALS pathogenesis. *J. Cell Biol.* **201,** 361–372 (2013).

16. Chien, P., Weissman, J. S. & DePace, A. H. Emerging principles of conformation-based prion inheritance. *Annu. Rev. Biochem.* **73,** 617–656 (2004).

17. True, H. L. & Lindquist, S. L. A yeast prion provides a mechanism for genetic variation and phenotypic diversity. *Nature* **407,** 477–483 (2000).

18. Tyedmers, J., Madariaga, M. L. & Lindquist, S. Prion switching in response to environmental stress. *PLoS Biol.* **6,** e294 (2008).

19. Stoecklin, G. & Bukau, B. Telling right from wrong in life - cellular quality control. *Nat. Rev. Mol. Cell Biol.* **14,** 613–615 (2013).

20. Tyedmers, J., Mogk, A. & Bukau, B. Cellular strategies for controlling protein aggregation. *Nat. Rev. Mol. Cell Biol.* **11,** 777–788 (2010).

21. Kroemer, G., Mariño, G. & Levine, B. Autophagy and the integrated stress response. *Mol. Cell* **40,** 280–293 (2010).

22. Arias, E. & Cuervo, A. M. Chaperone-mediated autophagy in protein quality control. *Curr. Opin. Cell Biol.* **23,** 184–189 (2011).

23. Anckar, J. & Sistonen, L. Regulation of HSF1 function in the heat stress response: implications in aging and disease. *Annu. Rev. Biochem.* **80,** 1089–1115 (2011).

24. Walter, P. & Ron, D. The unfolded protein response: from stress pathway to homeostatic regulation. *Science* **334,** 1081–1086 (2011).

25. Smith, M. H., Ploegh, H. L. & Weissman, J. S. Road to Ruin: Targeting Proteins for Degradation in the Endoplasmic Reticulum. *Science* **334,** 1086–1090 (2011).

26. Haynes, C. M., Fiorese, C. J. & Lin, Y.-F. Evaluating and responding to mitochondrial dysfunction: the mitochondrial unfolded-protein response and beyond. *Trends Cell Biol.* **23,** 311–318 (2013).

CHAPTER 2

Prions and [*PSI*$^{+}$] as a model system

Prions, named for proteinaceous infectious agents, are specific non-native protein conformations capable of self-replication and infection. Stanley Prusiner introduced the concept of prions in order to explain the propagation of a range of transmissible spongiform encephalopathies, one of which is the well-known bovine form commonly referred to as mad cow disease[1]. Prusiner posited that the prion protein alone, devoid of any nucleic acid, is the sole infectious agent in what was termed the "protein only" hypothesis. Animal studies by multiple groups subsequently validated this initially controversial hypothesis[2,3]. As Pruisner's ideas gained acceptance, researcher focused one general question: how do proteins produce the range of phenotypes and phenomena ascribed to prions?

All prion proteins can form ordered amyloid fibers through templated polymerization of β-sheet rich intermediates[4]. As mentioned in the previous chapter, amyloid fibers are extremely stable and have a variety of often deleterious affects on the cell as illustrated by amyloid-based diseases, which arise when different proteins assume the same highly-ordered structure[5]. For example, in Alzheimer's disease amyloid-β peptides polymerize into fibers that deposit predominantly in the extracellular space while in Parkinson's disease α-synuclein forms intracellular fibers. Thus, the formation of this common structure can have divergent affects depending on the protein involved and location of deposition. While amyloid fiber formation is often categorized as a phenomenon of protein misfolding, this is not strictly correct in all instances and instead one can broadly conceive of it as establishment of an alternate three-dimensional conformation. Inherent to all amyloid formed by different proteins is their ability to self-template, a reaction in which the fiber recruits soluble proteins and catalyzes their conversion into the alternate β-sheet conformation. This property is crucial to hallmarks that set prions apart frommost amyloid: they are both infectious and heritable.

During the time that the protein-only hypothesis was struggling to gain acceptance, Reed Wickner invoked the prion model to explain the inheritance of epigenetic traits exhibiting cytoplasmic inheritance in yeast[6,7]. Since yeast are easy to genetically manipulate, grow rapidly and do not confer the risk of human prion infection compared to mammalian cells, this observation of non-Mendelian elements in yeast provided a convenient model system in which to study multiple prion-related phenomena[8]. As the understanding of one of the prions identified by Wickner, [*PSI*$^+$], advanced, it became clear that many of the characteristics of mammalian prions were also true of their yeast counterparts. Both exist as multiple strains in which the polymerization of chemically identical proteins results in distinct phenotypes[9]. The development of a color readout for [*PSI*$^+$] in which a range of color phenotypes indicate different stably inherited strains helped show that strain differences are due to subtle, strain-specific variations in amyloid conformation and underscored the utility of yeast as a model system[10,11]. Additionally, prions in both yeast and mammals exhibit infection barriers between even highly related species[12–14]. This, like the phenomenon of strain variants, is an example of the specificity of self-propagating amyloid conformations. The formulation of a fiber infection protocol, which made it possible to deliver recombinant prion fibers created *in vitro* into [*psi*$^-$] yeast to convert them into the prion-carrying [*PSI*$^+$] form, greatly accelerated the structural understanding of both strain variants and species barriers[15–17]. Thus, [*PSI*$^+$] is uniquely suited to provide insight into multiple aspects of prion structure and biology.

Polymerization of the yeast translation termination factor Sup35 generates the [*PSI*$^+$] prion[18]. The amino (N) -terminus of Sup35 constitutes a modular amyloid-forming domain that is both necessary and sufficient for prion formation. Although this domain is dispensable for the normal function of Sup35, its high degree of conservation supports the hypothesis that prion

formation plays an important cellular role[19,20]. Conversion of the N-terminus to the amyloid form precludes the carboxy terminus from carrying out its function and causes stop-codon readthrough as one would expect in a loss-of-function mutant. Polymerization of the N-terminal domain occurs via tight face-to-face packing of parallel β-sheets such that their side chains interdigitate to form what has been termed a "steric zipper"[21]. While this arrangement was first observed in crystal structures of a Sup35 derived peptide, GNNQQNY, from the lab of David Eisenberg[21], peptides from many other amyloid-forming proteins also assemble into a "steric zipper"[22]. This packing of a portion of the amyloid-forming protein explains the stability of the fibers and hints at how cellular factors might interact with prions to regulate their formation and growth.

Yeast prions rely with a variety of chaperones, especially the AAA ATPase Hsp104, to ensure propagation during cell division[23]. The propagation of [*PSI*$^+$] requires the creation of propagons (defined as infectious oligomeric fiber seeds that can template Sup35 polymerization) and their distribution to daughter cells. Hsp104 creates propagons by severing long fibers into smaller seeds via a mechanism in which it extracts single Sup35 proteins out of the fiber by pulling them through its central pore[24,25]. The level of Hsp104 in the cell is crucial for prion propagation: either a deficiency, in which no seeds are made, or an excess, in which all fibers are dismantled, causes the loss of the prion state[10]. The central role of Hsp104 and the discovery that the small molecule guanidine hydrochloride (GuHCl) inhibits Hsp104 provided a convenient method for experimentally curing yeast of [*PSI*$^+$][26,27].

As mentioned previously, a single prion can exist as multiple strains that are the result of differences in amyloid conformation and manifest as unique phenotypes[9]. The powerful combination of *in vitro* creation of amyloid and *in vivo* characterization allowed researchers to control the formation of [*PSI*$^+$] strains[16,17]. *In vitro* polymerization of Sup35 under different

conditions, such as varied temperature, allows researchers to make fibrils with different biophysical properties and therefore control the formation of different [*PSI*$^{+}$] strains with distinct color phenotypes. Two well-defined strains of [*PSI*$^{+}$] Sc4 (white) and Sc37 (pink), named for their respective temperatures of polymerization, exhibit different growth rates as well as propensities to break to create new seeds[28] . Structural data explain these differences: Sc37 forms amyloid with a larger region of Sup35 than Sc4[29]. Thus, Sc37 fibers grow quickly, but are extremely stable and therefore have difficulty breaking to generate seeds. Conversely, the small region responsible for Sup35 polymerization in Sc4 limits the rate of fiber growth but facilitates fiber breakage, which promotes the formation of new seeds and more prion molecules.

One consequence of the structural variation between strains is that a given mutation can have divergent effects on different strains[16]. A mutation will have one effect if it falls within the "steric zipper" where it can easily disrupt side chain interdigitation and amyloid structure, but an entirely different effect if it falls outside of the prion-forming region and instead modulates interactions with chaperones or other cellular factors. One well-studied example of these effects is the mutation of glycine 58 to aspartate in Sup35 (termed PNM2[30]) that results in the loss of Sc4 but not Sc37.

Although the heritable nature of [*PSI*$^{+}$] was responsible for its initial detection, this aspect of [*PSI*$^{+}$] biology remains poorly understood. In order for daughter cells of [*PSI*$^{+}$] yeast to reliably inherit the prion, an entire cycle of prion propagation must occur. First, [*PSI*$^{+}$] must be capable of self-templated growth via the amyloid forming domain of Sup35. This is an intrinsic property of Sup35 as illustrated by *in vitro* polymerization experiments. Second, the prion fibers must divide in order to create new seeds for self-replication. While mechanical shearing can produce propagons *in vitro*, *in vivo* this requires chaperones such as Hsp104. Lastly, propagons

must be partitioned into daughter cells. Partitioning may occur through passive diffusion, but there is also likely to be an active component to this step involving specific host factors. In chapter three of this thesis, we use the PNM2 variant of Sup35, which causes loss of [*PSI*$^{+}$] in only certain strains, to gain insight into the steps of the propagation cycle and [*PSI*$^{+}$] inheritance.

References

1. Prusiner, S. B. Novel Proteinaceous Infectious Particles Cause Scrapie. *Science* **216,** 136–144 (1982).
2. Castilla, J., Saá, P., Hetz, C. & Soto, C. In vitro generation of infectious scrapie prions. *Cell* **121,** 195–206 (2005).
3. Deleault, N. R., Harris, B. T., Rees, J. R. & Supattapone, S. Formation of native prions from minimal components in vitro. *Proc. Natl. Acad. Sci. U. S. A.* **104,** 9741–9746 (2007).
4. Caughey, B., Baron, G. S., Chesebro, B. & Jeffrey, M. Getting a grip on prions: oligomers, amyloids, and pathological membrane interactions. *Annu. Rev. Biochem.* **78,** 177–204 (2009).
5. Chiti, F. & Dobson, C. M. Protein misfolding, functional amyloid, and human disease. *Annu. Rev. Biochem.* **75,** 333–366 (2006).
6. Wickner, R. B. [URE3] as an altered URE2 protein: evidence for a prion analog in Saccharomyces cerevisiae. *Science* **264,** 566–569 (1994).
7. Wickner, R. B., Masison, D. C. & Edskes, H. K. [PSI] and [URE3] as yeast prions. *Yeast Chichester Engl.* **11,** 1671–1685 (1995).
8. Tuite, M. F. & Cox, B. S. Propagation of yeast prions. *Nat. Rev. Mol. Cell Biol.* **4,** 878–890 (2003).
9. Chien, P., Weissman, J. S. & DePace, A. H. Emerging principles of conformation-based prion inheritance. *Annu. Rev. Biochem.* **73,** 617–656 (2004).

10. Chernoff, Y. O., Lindquist, S. L., Ono, B., Inge-Vechtomov, S. G. & Liebman, S. W. Role of the chaperone protein Hsp104 in propagation of the yeast prion-like factor [psi+]. *Science* **268,** 880–884 (1995).

11. Derkatch, I. L., Chernoff, Y. O., Kushnirov, V. V., Inge-Vechtomov, S. G. & Liebman, S. W. Genesis and variability of [PSI] prion factors in Saccharomyces cerevisiae. *Genetics* **144,** 1375–1386 (1996).

12. Santoso, A., Chien, P., Osherovich, L. Z. & Weissman, J. S. Molecular basis of a yeast prion species barrier. *Cell* **100,** 277–288 (2000).

13. Chernoff, Y. O. *et al.* Evolutionary conservation of prion-forming abilities of the yeast Sup35 protein. *Mol. Microbiol.* **35,** 865–876 (2000).

14. Kushnirov, V. V., Kochneva-Pervukhova, N. V., Chechenova, M. B., Frolova, N. S. & Ter-Avanesyan, M. D. Prion properties of the Sup35 protein of yeast Pichia methanolica. *EMBO J.* **19,** 324–331 (2000).

15. Sparrer, H. E., Santoso, A., Szoka, F. C., Jr & Weissman, J. S. Evidence for the prion hypothesis: induction of the yeast [PSI+] factor by in vitro- converted Sup35 protein. *Science* **289,** 595–599 (2000).

16. King, C.-Y. & Diaz-Avalos, R. Protein-only transmission of three yeast prion strains. *Nature* **428,** 319–323 (2004).

17. Tanaka, M., Chien, P., Naber, N., Cooke, R. & Weissman, J. S. Conformational variations in an infectious protein determine prion strain differences. *Nature* **428,** 323–328 (2004).

18. Tuite, M. F. & Cox, B. S. The [PSI+] prion of yeast: a problem of inheritance. *Methods San Diego Calif* **39,** 9–22 (2006).

19. Osherovich, L. Z. & Weissman, J. S. The utility of prions. *Dev. Cell* **2,** 143–151 (2002).

20. Halfmann, R. *et al.* Prions are a common mechanism for phenotypic inheritance in wild yeasts. *Nature* **482,** 363–368 (2012).

21. Nelson, R. *et al.* Structure of the cross-beta spine of amyloid-like fibrils. *Nature* **435,** 773–778 (2005).

22. Sawaya, M. R. *et al.* Atomic structures of amyloid cross-beta spines reveal varied steric zippers. *Nature* **447,** 453–457 (2007).

23. Jones, G. W. & Tuite, M. F. Chaperoning prions: the cellular machinery for propagating an infectious protein? *BioEssays News Rev. Mol. Cell. Dev. Biol.* **27,** 823–832 (2005).

24. Shorter, J. & Lindquist, S. Hsp104 catalyzes formation and elimination of self-replicating Sup35 prion conformers. *Science* **304,** 1793–1797 (2004).

25. Tessarz, P., Mogk, A. & Bukau, B. Substrate threading through the central pore of the Hsp104 chaperone as a common mechanism for protein disaggregation and prion propagation. *Mol. Microbiol.* **68,** 87–97 (2008).

26. Jung, G. & Masison, D. C. Guanidine hydrochloride inhibits Hsp104 activity in vivo: a possible explanation for its effect in curing yeast prions. *Curr. Microbiol.* **43,** 7–10 (2001).

27. Ferreira, P. C., Ness, F., Edwards, S. R., Cox, B. S. & Tuite, M. F. The elimination of the yeast [PSI+] prion by guanidine hydrochloride is the result of Hsp104 inactivation. *Mol. Microbiol.* **40,** 1357–1369 (2001).

28. Tanaka, M., Collins, S. R., Toyama, B. H. & Weissman, J. S. The physical basis of how prion conformations determine strain phenotypes. *Nature* **442,** 585–589 (2006).

29. Toyama, B. H., Kelly, M. J. S., Gross, J. D. & Weissman, J. S. The structural basis of yeast prion strain variants. *Nature* **449,** 233–237 (2007).

30. Doel, S. M., McCready, S. J., Nierras, C. R. & Cox, B. S. The dominant PNM2- mutation which eliminates the psi factor of Saccharomyces cerevisiae is the result of a missense mutation in the SUP35 gene. *Genetics* **137,** 659–670 (1994).

CHAPTER 3

Strain conformation, primary structure and the propagation of the yeast prion [*PSI*$^{+}$]

Strain conformation, primary structure and the propagation of the yeast prion [*PSI*$^+$]

Katherine J Verges[1,2,5], Melanie H Smith[1–3,5], Brandon H Toyama[1,2,4]

& Jonathan S Weissman[1,2]

[1]Department of Cellular and Molecular Pharmacology, University of California, San Francisco, California, USA. [2]Howard Hughes Medical Institute, University of California, San Francisco, California, USA. [3]Graduate Group in Biophysics, University of California, San Francisco, California, USA. [4]Present address: The Salk Institute for Biological Studies, La Jolla, California, USA.

[5]These authors contributed equally to this work.

Reproduced from *Nature Structure & Molecular Biology* **2011**, 18(4): 493-499.

doi:10.1038/nsmb.2030

Abstract

Prion proteins can adopt multiple infectious strain conformations. Here we investigate how the sequence of a prion protein affects its capacity to propagate specific conformations by exploiting our ability to create two distinct infectious conformations of the yeast [*PSI+*] prion protein Sup35, termed Sc4 and Sc37. PNM2, a G58D point mutant of Sup35 that was originally identified for its dominant interference with prion propagation, leads to rapid, recessive loss of Sc4 but does not interfere with propagation of Sc37. PNM2 destabilizes the amyloid core of Sc37 and causes compensatory effects that slow prion growth but aid prion division and result in robust propagation of Sc37. By contrast, PNM2 does not affect the structure or chaperone-mediated division of Sc4 but interferes with its delivery to daughter cells. Thus, effective delivery of infectious particles during cell division is a crucial and conformation-dependent step in prion inheritance.

Infectious proteins, or prions, are a form of conformation-based inheritance in which a prion protein aggregate binds to and catalyzes the conversion of newly made proteins to the prion form, thereby creating stably propagating states[1]. Such conformation-based inheritance underlies a range of transmissible spongiform encephalopathies in mammals as well as heritable epigenetic states in fungi, of which the yeast *Saccharomyces cerevisiae* prion [*PSI*+] is arguably the best characterized[2]. A common feature of prion proteins is that they misfold into ordered, β-sheet-rich amyloid fibers whose self-templating nature is thought to form the basis of prion propagation[1,3]. A single prion protein can adopt a spectrum of amyloid conformations that lead to different, heritable strain variants[4–11].

The yeast prion [*PSI*$^{+}$], which results from the aggregation of the translation termination factor Sup35, has emerged as a powerful system for studying strain variants. Sup35 can form different amyloid conformations *in vitro* when polymerized at 4 °C or at 37 °C (refs. 8,12,13). When introduced into yeast, these amyloid fibers form two distinct strains *in vivo* termed [*PSI*$^{+}$]^{Sc4} and [*PSI*$^{+}$]Sc37, respectively. (For clarity, we use [*PSI*$^{+}$]^{Sc4} to describe the *in vivo* strain and Sc4 to describe the fiber conformation.) These strains are distinguished by the degree of Sup35 aggregation: [*PSI*$^{+}$]^{Sc4} yeast show a strong prion phenotype, in which the large majority of Sup35 is aggregated, whereas [*PSI*$^{+}$]^{Sc37} yeast have a larger pool of soluble Sup35 and a weaker prion phenotype. Structural studies have shown that there is a marked expansion of the amyloid core in the Sc37 conformation relative to that found in Sc4 (refs. 14,15). The more extensive structure in Sc37 fibers increases fiber stability and decreases the rate of prion replication by the cell's chaperone system, which results in the weaker [*PSI*$^{+}$]^{Sc37} prion phenotype[16]. The ability to probe the biophysical properties of these defined strain variant conformations *in vitro* and to monitor their phenotypes *in vivo* makes [*PSI*$^{+}$] an excellent system for the study of prion strain

phenomena.

The precise amino acid sequence greatly biases the ability of a prion protein to adopt particular strain variants[7,17–19]. For example, the naturally occurring methionine-valine polymorphism at position 129 of the mammalian prion protein strongly influences disease susceptibility[20]. The Val129 allele does not interfere with the propagation of all prion strain variants and may even favor some, including certain iatrogenic forms of Creutzfeldt-Jakob disease[19]. However, the presence of even a single allele of Val129 seems to be highly protective against new variant Creutzfeldt-Jakob disease (nvCJD)[21], which is thought to result from the transmission of bovine spongiform encephalopathy (mad cow disease) to humans[22,23].

This strong relationship between strain variants and the sequence of the prion protein extends to the [*PSI*$^+$] prion system. A mutant of the Sup35 prion protein, which was originally identified in a screen for 'Psi no more' mutants that prevented propagation of [*PSI*$^+$], shows strain variant–specific effects. This mutant, termed PNM2, has a glycine-to-aspartate missense mutation at residue 58 (ref. 24). Originally, the effect of PNM2 was described as causing dominant inhibition of prion propagation when co-expressed with wild-type Sup35 (refs. 24,25). Later studies found that PNM2 does not interfere with the propagation of all [*PSI*$^+$] strain variants and might enhance the propagation of certain strain variants when overexpressed[17].

Here we used the PNM2 mutant and the well-defined prion strain conformations Sc4 and Sc37, together with in-depth biophysical and *in vivo* analyses, to investigate how point mutations can affect prion propagation in a manner that depends on the strain variant. Our systematic characterization of fiber structure, chaperone-mediated division of fibers into seeds and delivery of seeds to daughter cells revealed a PNM2-specific defect in seed partitioning for the [*PSI*$^+$]^{Sc4} strain variant. The findings indicate that the delivery of fiber seeds to daughter buds is a key step

in prion propagation.

RESULTS

PNM2 shows strain-specific effects on [*PSI*+] propagation

We began by characterizing the effect of the PNM2 mutation on prion propagation in [*PSI*+]^{Sc4} and [*PSI*+]^{Sc37} yeast. To allow rapid exchange of alleles, we used a yeast background in which the genomic copy of *SUP35* was deleted and replaced by a copy on a plasmid containing the counter-selectable *URA3* marker. We exchanged this plasmid with one that encoded wild-type Sup35 (WT) or Sup35 G58D (PNM2) and confirmed that the two proteins were expressed at similar levels (**Fig. 1a**). We assessed the prion phenotype with a red-white color readout that results from suppression of a nonsense mutation in an *ADE1* reporter (the *ade1–14* allele)[26]. When Sup35 is soluble ([*psi*$^-$]), translation of *ade1–14* terminates prematurely, and this results in the accumulation of a red metabolic intermediate. When Sup35 is aggregated ([*PSI*$^+$]), read-through of the nonsense mutation occurs and functional Ade1p is produced. Depending on the amount of soluble Sup35 present and perhaps on the nature of the aggregates, [*PSI*$^+$] strain variants have varying levels of functional Ade1p and have color phenotypes from pink ([*PSI*$^+$]^{Sc37}) to white ([*PSI*$^+$]^{Sc4}; **Fig. 1b**). This assay also indicates the stability of prion inheritance: when a cell in a growing colony loses [*PSI*$^+$], its progeny remain prion-free and form a red sector (**Fig. 1c**).

Using the [*PSI*$^+$]^{Sc4} and [*PSI*$^+$]^{Sc37} yeast backgrounds, we found that PNM2 has marked, strain variant–specific effects on prion propagation. When expressed as the sole copy of Sup35, PNM2 strongly compromised the propagation of [*PSI*$^+$]^{Sc4}, apparently by the continuous generation of prion-free ([*psi*$^-$]) states (**Fig. 1b–d**). This effect is similar to the originally

reported description of the PNM2 phenotype[24,25], although there are differences between studies: PNM2 is recessive in our strain background and thus does not strongly interfere with the propagation of $[PSI^+]^{Sc4}$ when co-expressed with the wild type (**Fig. 1b**). Thus, we focused on analyzing effects of prion propagation when PNM2 is expressed as the sole copy of Sup35.

In contrast to its marked effect on the propagation of $[PSI^+]^{Sc4}$, PNM2 had a much weaker effect on propagation of the $[PSI^+]^{Sc37}$ strain variant, with at most a mild darkening of the color phenotype and no discernable increase in prion loss (**Fig. 1b**,**d**). This result was unexpected because previous studies indicated that the PNM2 mutation was located in a region that is structured in Sc37 but not in Sc4 (ref. 15), leading us to expect that the PNM2 mutation would preferentially interfere with propagation of the Sc37 conformation.

We first investigated whether the defect in stable inheritance seen in $[PSI^+]^{Sc4}$ yeast could arise from the PNM2 mutation forcing an irreversible structural change that results in an amyloid conformation that is poorly propagated. We carried out a series of plasmid exchanges, replacing the wild-type plasmid with the PNM2 plasmid and then exchanging it back with the wild-type plasmid. Reintroduction of the wild-type plasmid fully restored the original $[PSI^+]^{Sc4}$ phenotype (**Fig. 1e**), indicating that the PNM2 Sc4 fibers retained the structural information necessary to template wild-type Sup35 to the characteristic Sc4 amyloid conformation.

To investigate what accounts for the negative impact of PNM2 on the propagation of $[PSI^+]^{Sc4}$ but not of $[PSI^+]^{Sc37}$, we systematically tested the parameters that affect each step in the prion replication cycle (**Fig. 2**): fiber growth; fiber division, of which fiber stability and ability to interact with the *in vivo* chaperone prion-replication machinery are key determinants; and the delivery of prion particles to daughter cells during cell division.

PNM2 disrupts Sc37 growth rate and structural stability

To determine whether changes in fiber growth rates account for the observed phenotypic differences, we compared the *in vitro* growth rates of wild-type and PNM2 fibers. Although earlier studies found that PNM2 fibers have a partial growth defect, the nature of the prion strain variants in these studies was not well defined[27]. We used a fragment of Sup35 (SupNM; residues 1–254, containing the Q/N-rich N-terminal and highly charged middle domains of Sup35) that is necessary and sufficient to support prion propagation[28,29]. We monitored the seeded polymerization rates of soluble SupNM by measuring the increase in fluorescence intensity of Thioflavin T. When seeded, PNM2 SupNM polymerized into the Sc37 conformation more slowly than did wild-type SupNM (**Fig. 3**). As this change in growth rate would be predicted to weaken the prion phenotype, other mechanisms must account for the similar phenotype of PNM2 and wild-type Sup35 in the Sc37 conformation.

A PNM2-induced change in amyloid structure could explain the change in Sc37 fiber growth rate as well as provide insight into prion division rates *in vivo*[16]. Therefore, we used a range of biophysical techniques, including hydrogen/deuterium (H/D) exchange NMR, fiber thermal denaturation and propensity for shearing to produce new fiber seeds, to analyze the structure and stability of PNM2 SupNM fibers. We measured shearing efficacy by the ability of long fibers fragmented by stirring to seed monomer growth as measured from the initial polymerization rates of such reactions.

For the H/D exchange experiments, we monitored the extent of backbone amide exchange for both wild-type and PNM2 fibers at two different time points: after a short exchange period of 2 min and after a more extensive exchange period of 1 day. Based on previous assignments[15], we measured exchange for 132 residues including extensive probes throughout

the amyloid core of both the Sc4 and Sc37 conformations.

The H/D exchange experiments revealed that the PNM2 mutation induced specific, localized structural defects in the Sc37 conformation. Specifically, we observed a region of increased exchange in residues proximal to the site of the PNM2 mutation for both early and late exchange time points (**Fig. 4a**,**b**). Consistent with this result, we observed a decrease in the thermal stability of PNM2 SupNM Sc37 fibers (T_m = 80 ± 2 °C) compared to wild-type SupNM Sc37 fibers (T_m = 86 ± 2 °C; **Fig. 3c**,**d**). In addition, when subjected to shearing forces, PNM2 SupNM Sc37 fibers fragmented more than wild-type SupNM Sc37 fibers (**Fig. 3e**). These results suggest that the PNM2 mutation in the Sc37 conformation causes a localized structural destabilization with a resulting decrease in fiber stability.

The effects of the PNM2 mutation on Sc37 fibers may have opposing consequences for prion propagation. The localized structural defect would be expected to enhance the rate of prion division *in vivo*, increasing the rate of generation of free fiber ends and subsequently strengthening the prion phenotype[15,16]. By contrast, the decrease in fiber growth would be expected to reduce monomer addition onto fibers and therefore to weaken the prion phenotype. Therefore, we hypothesize that the modest overall effect of the PNM2 mutation on the [*PSI*$^+$]^{Sc37} phenotype is the result of compensatory changes.

PNM2 does not affect growth, stability or structure of Sc4

To determine the mechanism by which the PNM2 mutation interferes with the propagation of [*PSI*$^+$]^{Sc4}, we carried out a set of experiments on Sc4 fibers analogous to those done on the Sc37 conformation. When seeded by Sc4, PNM2 SupNM polymerized into the Sc4 conformation at a rate similar to wild-type SupNM, which indicates that the negative effect of

the PNM2 mutation on [*PSI*$^{+}$]^{Sc4} propagation cannot be explained by a decrease in fiber growth rate (**Fig. 3a**,**b**). The Sc4 fiber structure was also unaffected by the PNM2 mutation: H/D exchange experiments showed no appreciable differences between wild-type SupNM and PNM2 SupNM fibers in the Sc4 conformation (**Fig. 4c**,**d**). Both the regions of protection and the extent of protection for all residues were virtually indistinguishable between the two samples for both short and long exchange times, suggesting that the structures were stable as well as very similar. Consistent with the above results, the melting temperatures of wild-type SupNM and PNM2 SupNM in the Sc4 conformation were comparable (77 ± 2 °C and 77 ± 5 °C, respectively; **Fig. 3c**,**d**). Last, when subjected to shearing forces, both PNM2 SupNM and wild-type SupNM fragmented to a similar extent (**Fig. 3e**).

Together, these results indicate that PNM2 SupNM can polymerize into fibers with growth, structure and stability that are indistinguishable from those of wild-type Sc4 fibers, and that the defect in [*PSI*$^{+}$]^{Sc4} propagation cannot be explained by the biophysical properties of the fibers.

PNM2 does not affect Sc4-chaperone interactions

Prion propagation depends crucially on the host chaperone machinery, and in particular on Hsp104 (ref. 26). There is growing evidence that Hsp104 acts with Ssa1 (Hsp70) and Sis1 (Hsp40) to divide prion particles and thereby to facilitate prion replication[30–33]. Specifically, Ssa1 and Sis1 bind to prion particles and deliver them to Hsp104, which is thought to extract prion particles from fibers in an ATP-dependent process that involves translocation of the extracted monomers through its axial pore[34]. In addition to its role in propagation, when expressed at high levels Hsp104 also causes curing of the prion (conversion from [*PSI*$^{+}$] to [*psi*$^{-}$]) through a

mechanism that is separate from fiber division. Therefore, the overall effect of Hsp104 is a balance between the fiber division that is necessary for propagation at low levels and curing at high levels[26]. As a fiber's differential susceptibility to fragmentation and curing by Hsp104 can directly affect its propagation, we investigated whether changes in chaperone-prion interactions caused the PNM2 phenotype.

One possible explanation for the ability of the PNM2 mutation to interfere with $[PSI^{+}]^{Sc4}$ propagation is that it causes loss of [*PSI*$^{+}$] through increased susceptibility to curing by Hsp104. To explore this possibility, we used a truncated variant of Hsp104 that is missing its N-terminal domain, termed Hsp104ΔNTD (ref. 35). When this variant is expressed from the endogenous *HSP104* locus in the genome, it is fully active in [*PSI*$^{+}$] propagation and can mediate thermotolerance but does not cure [*PSI*$^{+}$] when overexpressed35 (**Supplementary Fig. 1a**). We found the defect in [*PSI*$^{+}$] propagation in PNM2 even in the strain expressing Hsp104ΔNTD, which established that the sectoring seen in PNM2 was not due to curing by the mechanism that occurs when Hsp104 is overexpressed (**Fig. 5a**).

An alternate hypothesis is that the PNM2 mutation causes increased susceptibility to the fiber division activity of Hsp104 and that this leads to resolubilization of fibers. To test this, we expressed *HSP104* and *hsp104ΔNTD* from a low-copy (CEN/ARS) plasmid that leads to a 2–3-fold increase in expression. At this level of expression, wild-type Hsp104 destabilized [*PSI*$^{+}$] whereas Hsp104ΔNTD did not (**Fig. 5b**), which indicates that the destabilization must be due to the curing activity of Hsp104 and not to overfragmentation. Overexpression of Hsp104ΔNTD did not enhance PNM2 sectoring, which supports the idea that PNM2 fibers are not overly susceptible to fragmentation and resolubilization by Hsp104 (**Fig. 5b** and **Supplementary Fig. 1b**). These results are distinct from those of others[36], who found that the PNM2 mutation can

lead to fiber destabilization and enhanced Hsp104-mediated fiber dissolution. The differences between the two studies probably result from differences in the prion strain conformations that were examined; previous studies[36] found dominant curing of [*PSI*$^+$] when wild-type and PNM2 Sup35 were co-expressed whereas we found that the PNM2 phenotype was recessive in Sc4. In addition, the fact that the PNM2 mutation destabilized the fibers, as reported in ref. 36 suggests that residue 58 is within the amyloid core of their strain conformation. We have generated examples of prion strain conformation that, like the Sc4 conformation, lead to 'strong' prion phenotypes but nonetheless have amyloid cores that extend across residue 58 (unpublished data).

In an independent assay of Hsp104 activity, we used semi-denaturing detergent-agarose gel electrophoresis (SDD-AGE) to look at the size distribution of prion fibers. Changes in Hsp104 activity affect aggregate size[37] and Sc37 fibers, which are severed less efficiently by Hsp104 *in vivo*, are larger than those in the Sc4 conformation[16]. We examined the relative sizes of Sc37 and Sc4 fibers and found that PNM2 and wild-type Sc4 fibers have the same size distribution (**Fig. 5c**). This finding is consistent with our Hsp104ΔNTD data and indicates that PNM2 and wild-type Sc4 interact equally with Hsp104.

Finally, to look more directly at interactions between Hsp104 and Sc4 fibers, we used a system developed to monitor the flux of substrates through the axial pore of Hsp104 (**Fig. 5d**). The system uses derivatives of Hsp104 (HAP34 and 4BAP33) engineered to interact with ClpP, a bacterial protein that forms a proteolytic chamber. When used in conjunction with a catalytically dead mutant of ClpP (ClpPtrap), substrates of Hsp104 are translocated through HAP and trapped in the ClpP chamber. Thus, after inducing ClpPtrap in HAP-expressing yeast, we affinity purified ClpPtrap to identify Hsp104 substrates. Given that translocation through Hsp104 is likely to be the terminal event in an interaction between Sup35 and the chaperone machinery,

defects in any aspect of this interaction would be expected to yield changes in the flux of Sup35 through Hsp104.

Previous studies have shown that Sup35 is delivered to ClpPtrap in a HAP-dependent manner and that HAP translocates Sup35 into ClpPtrap only in [*PSI*$^+$] cells[33,34]. Moreover, substantially less Sup35 is trapped in the weak [*PSI*$^+$]^{Sc37} strain than in the strong and more efficiently divided16 [*PSI*$^+$]^{Sc4} strain[33]. We confirmed that wild-type Sup35 was trapped in a [*PSI*$^+$]-dependent manner (**Fig. 5e**) and found that the flux of PNM2 through Hsp104 was similar to that of the wild type when PNM2 was either expressed as the sole source of Sup35 or coexpressed with the wild type (**Fig. 5f**,**g**). Therefore, consistent with our Hsp104ΔNTD and SDD-AGE data, the HAP-ClpPtrap system shows that PNM2 Sc4 fibers interact normally with the Hsp104 chaperone machinery that is necessary for propagation.

PNM2 causes a defect in Sc4 propagon partitioning

We investigated whether the PNM2 mutation caused a defect in the delivery of [*PSI*$^+$]^{Sc4} infectious particles (propagons) to daughter cells during cell division using a published method[38]. Briefly, we separated corresponding pairs of mother and daughter cells and grew them in medium containing guanidine, which reversibly inhibits Hsp104 (refs. 39–41), so that the number of propagons remained fixed. As the cells divided, a point was reached at which there was no more than one propagon per cell. When we restored Hsp104 function by removing guanidine, the number of [*PSI*$^+$] colonies that arose from the mother versus the daughter reported on the relative number of propagons in each mother-daughter pair. Although this assay does not yield a quantitative measure of the absolute number of prion particles, it allows relative propagon numbers and loss of [*PSI*+] by one of the partners to be monitored.

Using the above assay for [*PSI*$^{+}$]^{Sc4} cells expressing wild-type or PNM2 Sup35, we found evidence of partitioning dysregulation in PNM2 [*PSI*$^{+}$]^{Sc4} cells (**Fig. 6a**,**b**). The mild bias in the distribution of propagons toward the mother and positive correlation between the number of propagons in the mother and daughter wild-type [*PSI*$^{+}$]^{Sc4} cells seen previously[38,42] were lost in PNM2 [*PSI*$^{+}$]^{Sc4} cells. For a subset of pairs, the mother contained a large number of propagons but the daughter did not inherit any. By contrast, we did not observe any pairs in which the daughter had propagons but the mother did not. The failure of propagons to partition into daughter cells accounts for the rapid appearance of red [*psi*$^{-}$] sectors in PNM2 [*PSI*$^{+}$]^{Sc4}.

DISCUSSION

Our studies point to a key role for prion conformation in modulating the effects of changes in the sequence of a prion protein on prion propagation. In the case of [*PSI*$^{+}$]^{Sc37}, the PNM2 mutation affects the structural and physical characteristics of the amyloid fibers in a manner that has compensatory effects on prion propagation, resulting in a mild effect on prion propagation *in vivo*. However, a different picture emerges from studying PNM2 in the context of [*PSI*$^{+}$]^{Sc4}, where the mutation does not affect the amyloid structure or chaperone-mediated fiber division but has a marked negative effect on propagation. The effect of PNM2 on [*PSI*$^{+}$]^{Sc4} points to a key role for the least understood step of [*PSI*$^{+}$] propagation - the partitioning of prion particles. In PNM2 [*PSI*$^{+}$]^{Sc4} yeast, we observed a pronounced defect in the delivery of aggregates to daughter cells. This finding highlights the question of how [*PSI*$^{+}$] prion particles are delivered to daughter cells.

Previous studies indicate that the mother bias in the allocation of [*PSI*$^{+}$] particles is roughly consistent with differences in cell volume between the mother and the daughter, suggestive of partitioning by passive diffusion[42]. Other studies point to the potential for more

active mechanisms in the segregation of protein aggregates, including the active recruitment of cytosolic aggregates to specific loci[43,44]. Because the PNM2 mutation lies outside the amyloid core of the Sc4 conformation, it could disrupt interactions between this region of the prion protein and host factors that are responsible for prion segregation.

Evidence that host factors have a role in the partitioning of prion particles came from an unbiased genetic screen for high-copy suppressors of the PNM2 phenotype, in which we identified multiple independent isolates of two genes, *LSB3* and *ART5*, that when overexpressed minimized sectoring in PNM2 [PSI^{+}]^{Sc4} yeast (**Supplementary Fig. 2a**,**b** and **Supplementary Methods**). Lsb3 interacts with Las17 and the Sla1–End3–Pan1 complex, both of which are involved in the regulation of actin dynamics[45–47]. The actin cytoskeleton has been implicated in both transport of general protein aggregates between mother and daughter cells43 and the regulation of prion formation[48,49]. Art5 is primarily uncharacterized but has been proposed to be active in the regulation of endocytosis[50,51]. Although full characterization of the role of these proteins in prion biology is beyond the scope of this study, it will be interesting to determine how prion particles are affected by actin-based transport and whether endocytic pathways are involved in prion delivery to daughter cells.

Recent studies have suggested that size selection has a vital role in the transmission of prion particles to daughter cells[52]. In this size-based model, the small prion particles, which are preferentially propagated to daughter cells, might be the species that are primarily affected by the PNM2 mutation; these transmission-competent particles are either not delivered to daughter buds or actively retained in the mother cell. These possibilities may be related to the more general mechanism in which the cell specifically recognizes and concentrates misfolded protein aggregates[43,44]. In the future, an understanding of the relationship between the cellular machinery

for segregation of general protein aggregates and prion transmission is essential.

Our studies illustrate the importance of the delivery of infectious proteins to daughter cells in the propagation cycle of [*PSI*$^+$]. In the future, we anticipate that the [*PSI*$^+$] system will be useful for studying how cells survey, partition and sequester protein aggregates. The PNM2 mutation in the Sc4 conformation should provide a key tool for such studies, as it shows a distinct partitioning defect that is not confounded by changes in amyloid structure or chaperone-mediated fiber division.

Acknowledgments

We thank B. Bukau, A. Mogk and P. Tessarz for reagents; M. Kelly for NMR assistance; D. Cameron, S. Collins, C. Gross, D. Mullins, G. Narlikar, M. Tanaka and K. Tipton for discussions; and O. Brandman, C. Foo, A. Frost, N. Ingolia, E. Oh, E. Quan and E. Rodriguez for critical reading of the manuscript. This work was funded by the Howard Hughes Medical Institute (J.S.W.), the National Science Foundation Graduate Research Fellowship program (K.J.V.), the Hertz Foundation Peter Strauss Fellowship (M.H.S.) and the US National Institutes of Health.

Author Contributions

K.J.V., M.H.S. and J.S.W. designed this study and wrote the manuscript. J.S.W. supervised this work. K.J.V. and M.H.S. conducted the majority of the experiments. B.H.T. designed the H/X NMR experiments and acquired and analyzed the NMR data.

METHODS

Strains and plasmids. All strains were converted to [*PSI*$^{+}$] by infection with *in vitro*–formed Sc4 or Sc37 fibers. See **Supplementary Tables 1** and **2** for full list of strains and plasmids.

Fiber preparation. Fibers were produced as described using bacterially produced pure SupNM proteins carboxy-terminally tagged with 7x histidine[53].

***In vivo* yeast prion propagation characterization.** YJW1110 and YJW1111 were transformed with a *LEU2*-marked plasmid expressing wild-type or PNM2 Sup35 from the endogenous promoter (pRS315 WT Sup35 or pRS315 PNM2 Sup35, respectively). The resulting transformants were selected on medium lacking uracil and leucine (SD–Ura–Leu), then subsequently passaged on YEPD, then 5-FOA, then 1/4 YEPD. For the swap-back experiment, the [*PSI*$^{+}$]^{Sc4} yeast background containing the pRS315 PNM2 Sup35 plasmid was transformed with the original pRS316 WT Sup35 plasmid. Resulting transformants were selected on SD–Ura–Leu. After passaging several times on SD–Ura, colonies that required leucine for growth were identified. The [*PSI*$^{+}$] phenotype was determined by observing the color on low-adenine medium (1/4 YEPD). The degree of sectoring or loss of [*PSI*$^{+}$] was determined by growing cultures in YEPD liquid medium for 24 h at 30 °C and plating onto 1/4 YEPD plates at a density of ~400 colonies per plate. The number of [*PSI*$^{+}$] and [*psi*$^{-}$] colonies were then counted.

***In vitro* analysis of the physical properties of strain conformations.** Fiber growth rates15, thermal stabilities[8] and susceptibility to shearing[16] were determined as described.

H/D exchange NMR. Uniformly 15N-labeled SupNM was expressed in *Escherichia coli* and purified as described[15]. 15N-SupNM seeded fibers of each strain were made as described[15] and concentrated to 1/25 of their original volume. The fibers were then diluted 1:10 into D2O buffer at pH 7.0 to begin the exchange. After the desired time, exchange was quenched by adjusting the pH to 2.5 and fibers were centrifuged at 100,000*g* for 25 min. The pellet was washed once with 5mM DCl in D2O then centrifuged again at 100,000*g* for 20 min. The pellet was frozen, freeze-dried and stored at −80 °C until NMR acquisition. The NMR spectra were acquired as described[15]. Estimated minimum peak intensity was calculated by averaging the intensity of a set of fully exchanged residues.

***In vivo* analysis of Hsp104 activity using the variant Hsp104ΔNTD.** The gene for the Hsp104 variant Hsp104ΔNTD35 has the nucleotides corresponding to the N-terminal 146 residues deleted. *hsp104ΔNTD* was amplified and fused to the NAT cassette by PCR, and inserted into the *HSP104* genomic locus of YJW1110 by homologous recombination, resulting in strain YJW1667. Plasmids pRS399 Hsp104 and pRS399 Hsp104ΔNTD35 were used to mildly (2–3-fold) overexpress Hsp104 or Hsp104ΔNTD. pRS399 is a pRS315 plasmid in which the *LEU2* marker has been replaced by a KanR cassette. Plasmids were transformed into YJW1110 and plated on 1/4 YEPD containing the antibiotic G418 for visualization of the [*PSI*$^{+}$] phenotype.

Semi-denaturing detergent-agarose gel electrophoresis (SDD-AGE). Relative aggregate size was determined by SDD-AGE as described[54,55]. Sup35 was probed for by western blotting using polyclonal anti-SupNM.

ClpPtrap affinity purification experiments. The ClpPtrap affinity purification experiments were conducted as described[34]. Briefly, YJW1112, YJW1113, YJW1114 or YJW1115 that had been transformed with pRS313 WT Sup35, pRS313 PNM2 Sup35, pRS313 WT Sup35HA or pRS313PNM2 Sup35HA were grown in s.d. medium with 50 μM CuSO4 from OD600 = 0.1 to 1 and lysed at 4 °C by bead beating in IP buffer (50 mM Tris/Cl pH 8.0, 1 M NaCl, 2 mM EDTA, 0.5% (v/v) Triton X-100, 5 mM β-mercaptoethanol + Roche Complete Protease Inhibitor Cocktail). The lysate was cleared by centrifugation at 15,000*g* for 15 min, incubated with Streptavidin Sepharose (GE Healthcare) at room temperature for 1 h, washed with 40 column volumes of IP buffer and eluted in IP buffer + 150 mM NaCl and 4 mM biotin. The eluate was subjected to SDS-PAGE and Sup35 was probed for by western blotting using polyclonal anti-SupNM.

Mother-daughter propagon counting. The propagons in mothers and daughters were counted as described38. Briefly, mothers and daughters of YJW1110 (containing pRS315 WT Sup35 or pRS315 PNM2 Sup35 as the sole source of Sup35) were separated by micromanipulation onto YEPD plates containing 3 mM Guanidine HCl. After growing at 30 °C for about 40 h, whole colonies were isolated using a cut pipette tip, resuspended in a small volume of H2O and plated onto SD–Ade + 5% (w/v) YEPD. After growing at 30 °C for 10–14 days, the number of [*PSI*$^+$] colonies was counted. For the wild-type samples, [*PSI*$^+$] colonies were easily distinguished from [*psi*$^-$] and Ade revertants by color. The PNM2 samples contained background that was indistinguishable from true [*PSI*$^+$] colonies by color. We estimated the average background by repeating the experiment using a [*psi*$^-$] PNM2 strain created by curing the [*PSI*$^+$]^{Sc4} PNM2 strain

by successive passaging on YEPD containing 3 mM guanidine HCl. The average background of ~25 colonies per sample was subtracted for all counted values.

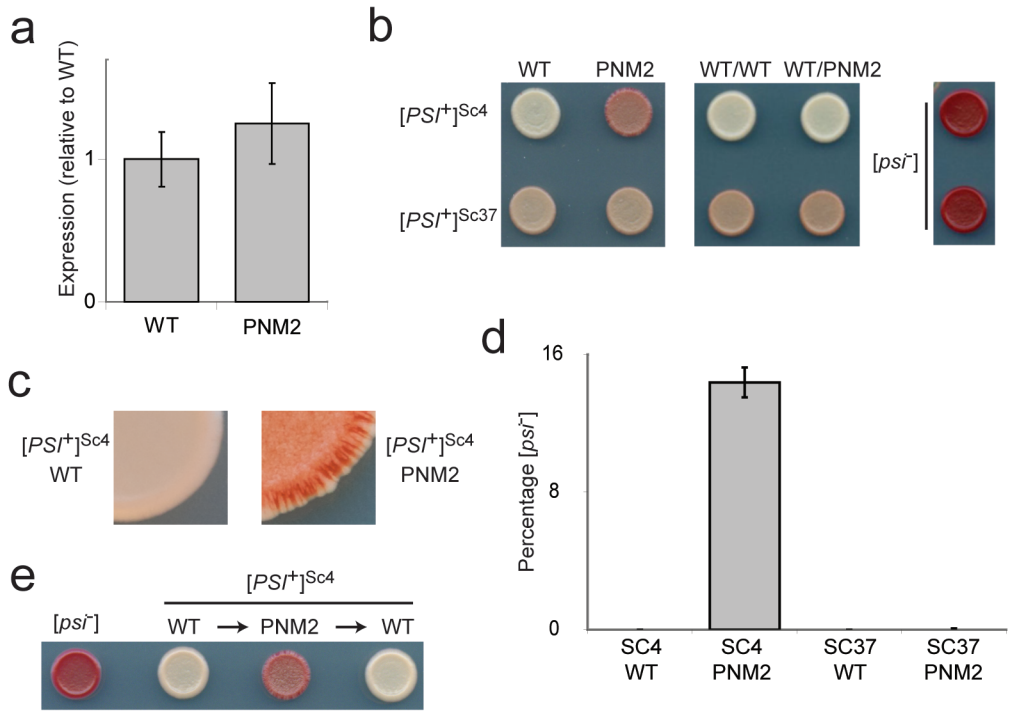


Figure 1 Characterization of *in vivo* prion phenotypes. (**a**) Expression levels of wild-type (WT) or PNM2 expressed from a plasmid in a [*PSI*+]Sc4 background. Expression was quantified by immunoblotting with a polyclonal antibody to SupNM. Values represent the mean ± s.d. for three experiments. (**b**) Representative *in vivo* prion phenotypes of yeast spotted on low adenine media. Wild-type Sup35 was replaced with (left) or was co-expressed with (middle) either WT or PNM2. (**c**) Enlarged view of the edge of the yeast spot. The presence of red sectors in [*PSI*+]Sc4 PNM2 indicates a loss of [*PSI*+]. (**d**) Quantification of loss of [*PSI*+] as determined by counting the number of [*psi*−] colonies after growing for 24 h in yeast extract peptone dextrose (YEPD) liquid medium. Values represent the mean ± s.d. for three experiments. (**e**) Representative *in vivo* prion phenotypes of yeast spotted on low-adenine medium. Wild-type Sup35 was replaced with PNM2, which was subsequently replaced with the WT through plasmid exchanges.

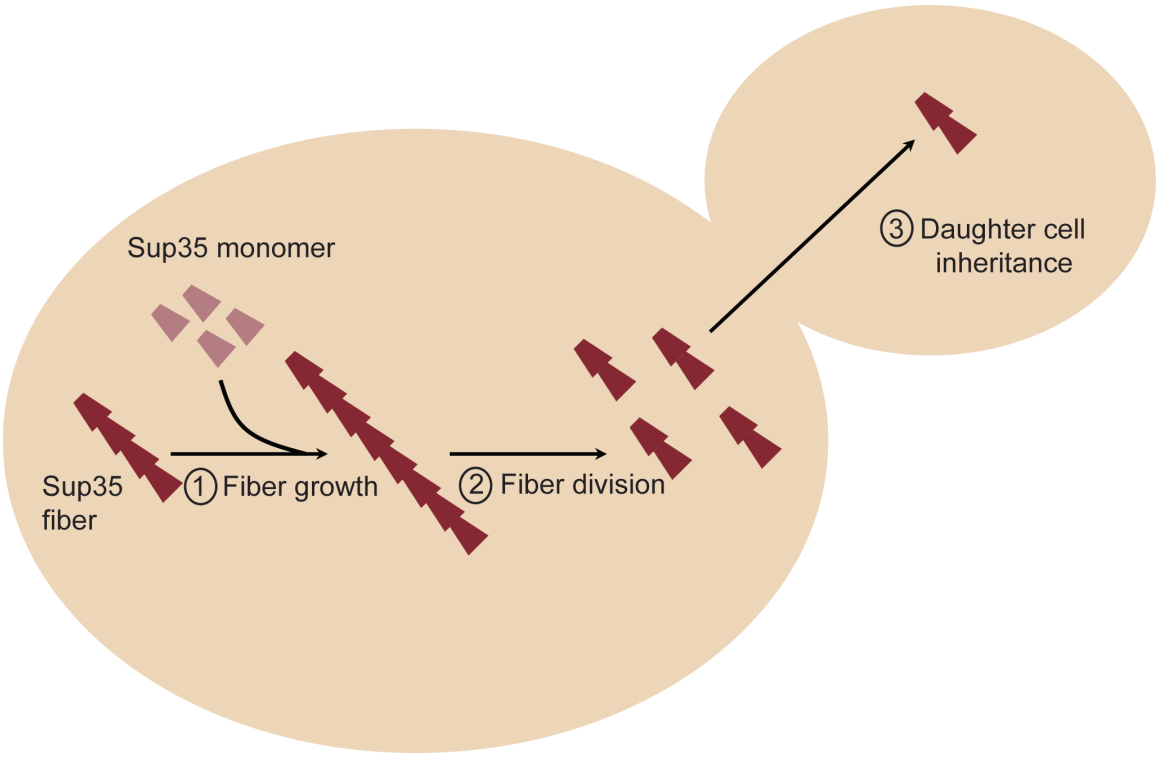


Figure 2 Schematic of the prion propagation cycle. (1) Fiber growth; (2) chaperone-mediated division; (3) partitioning to daughter cells.

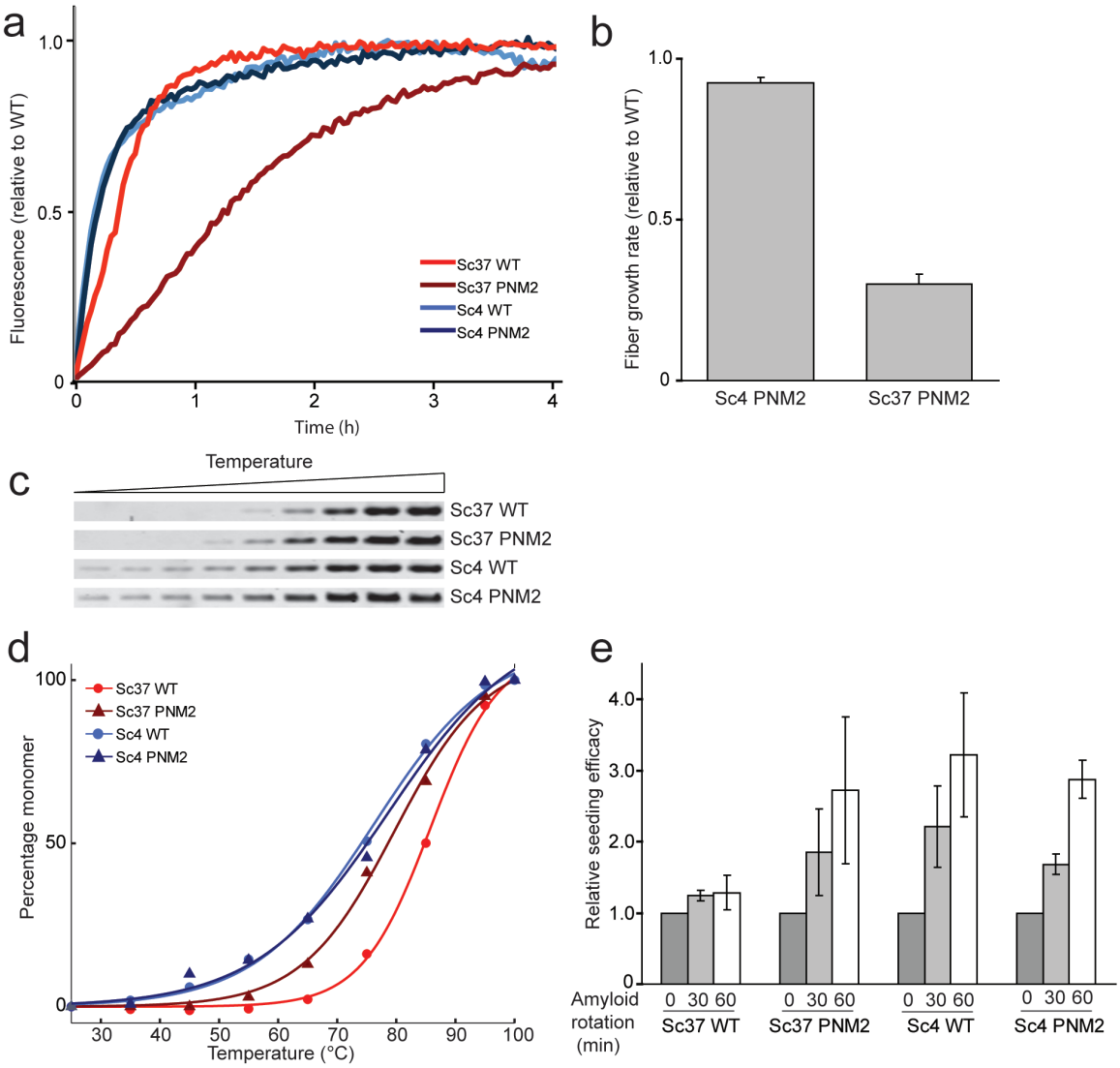


Figure 3 Characterization of the physical properties of fibers formed *in vitro*. (**a**) A representative experiment monitoring the relative growth rates of wild-type (WT) and PNM2 SupNM. Polymerization of SupNM was conducted with 5% (w/w) WT seed of the specified conformation, and the rate of addition of SupNM monomers was monitored by Thioflavin T fluorescence. Data were normalized to initial and final intensities. (**b**) Growth rates of Sc4 and Sc37 PNM2 SupNM normalized to those of WT SupNM polymerized on the relevant seed. Initial time points were fitted to a line and the slope (initial growth rate) was calculated. Values represent mean ± s.d. for three experiments. (**c**,**d**) Thermal stability of WT and PNM2 fibers in

Sc4 and Sc37 conformations. WT and PNM2 SupNM fibers in the Sc4 or Sc37 conformations were incubated at increasing temperatures, and samples were subjected to SDS-PAGE. Band intensities (susceptibility of aggregates to thermal solubilization) were plotted against temperature and fitted to a sigmoidal function. (**e**) Relative seeding efficacy of WT and PNM2 fibers in the Sc4 or Sc37 conformation before and after stirring for 30 or 60 min. Seeding efficacy was determined by monitoring the initial fiber growth rates of polymerization reactions using stirred samples as seeds. Values represent mean ± s.e.m. for three experiments.

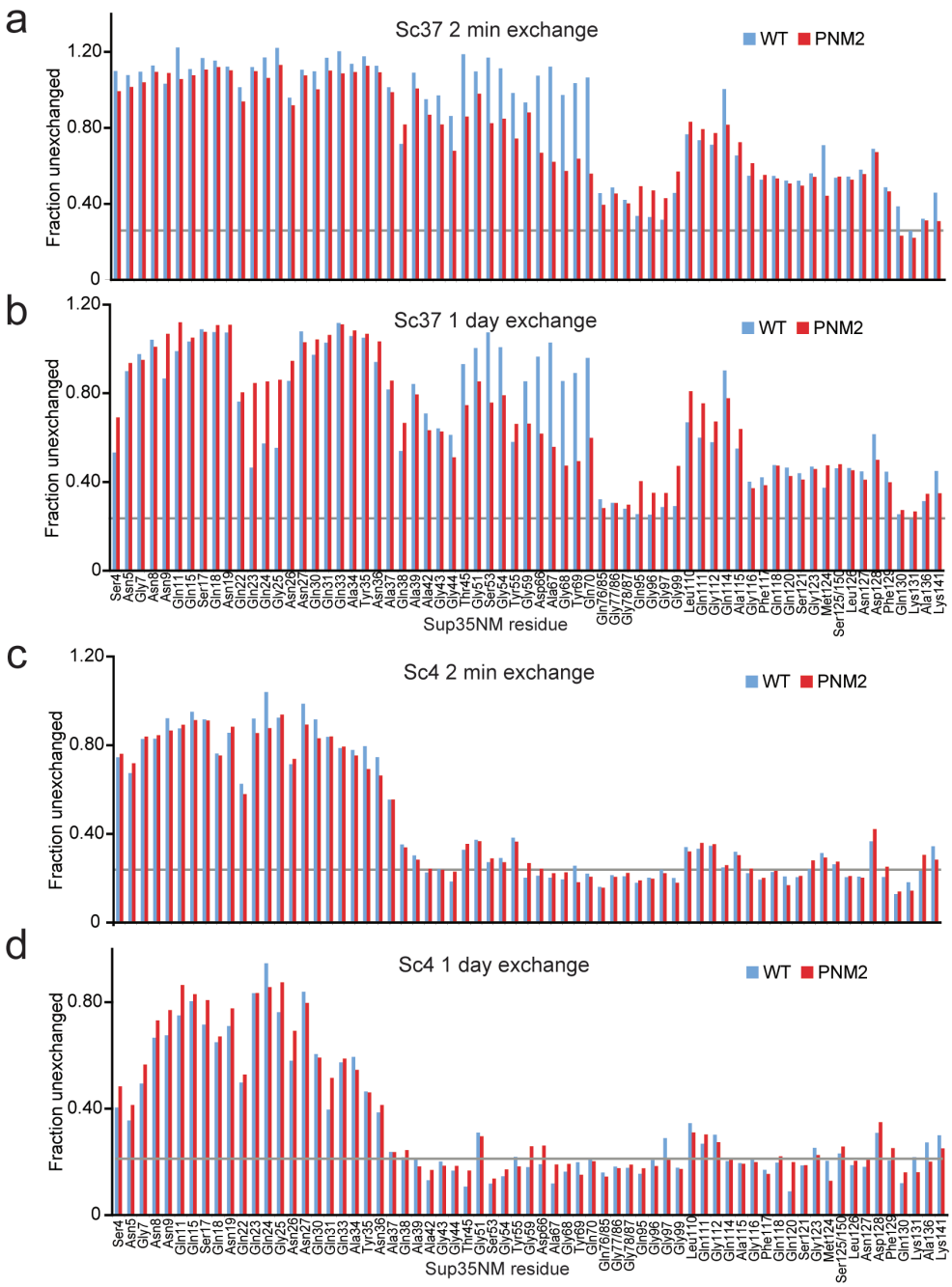


Figure 4 H/D exchange of wild-type (WT) and PNM2 SupNM fibers. (**a**–**d**) Intensities for assigned and unambiguous peaks corresponding to residues 1–141 were plotted as the fraction of the non-exchanged intensity after 2 min (**a**,**c**) and 1 day (**b**,**d**) of exchange for WT (blue) and PNM2 (red) fibers in the Sc37 (**a**,**b**) and Sc4 (**c**,**d**) conformations. Unassigned and ambiguous residues are not shown. Gray line, estimated minimum peak intensity after complete exchange.

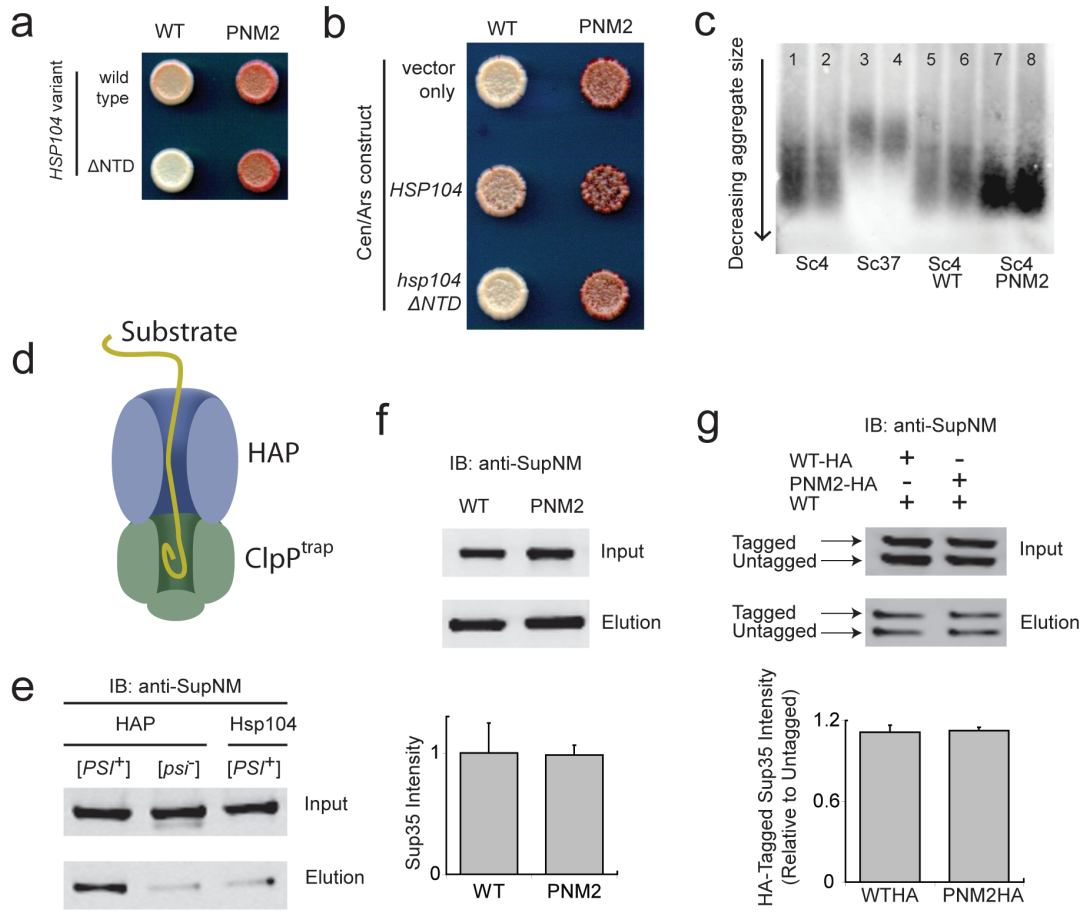


Figure 5 PNM2 fibers in the Sc4 conformation interact with the *in vivo* chaperone machinery. (**a**) *HSP104* (top) and *hsp104ΔNTD* (bottom) were expressed in [*PSI*$^{+}$]^{Sc4} yeast expressing wild-type (WT; left) or PNM2 (right) Sup35 and spotted onto low-adenine medium. (**b**) *HSP104* and *hsp104ΔNTD* were expressed at increased levels with endogenous Hsp104 in [*PSI*$^{+}$]^{Sc4} yeast expressing WT or PNM2 Sup35. 'Vector only' denotes transformation with an empty CEN/ARS plasmid. (**c**) SDD-AGE analysis of prion particle size in duplicate from lysates of [*PSI*$^{+}$]^{Sc4} (lanes 1,2 and 5,6), [*PSI*$^{+}$]^{Sc37} (lanes 3,4) and PNM2 [*PSI*$^{+}$]^{Sc4} (lanes 7,8). *SUP35* is genomic in lanes 1–4 and on a plasmid in lanes 5–8. Yeast express WT *HSP104* in all lanes. (**d**) Schematic of the *in vivo* HAP-ClpPtrap reaction. (**e**) Representative blot of ClpPtrap affinity purification. WT Sup35

and ClpPtrap were expressed in backgrounds that were [PSI^{+}]^{Sc4} or [psi^{-}] expressing HAP or Hsp104. (**f**) Monitoring the translocation of PNM2. HAP and ClpPtrap were expressed in [PSI^{+}]^{Sc4} cells that also expressed WT or PNM2 Sup35. Intensities of Sup35 elution signals from western blot (left) were normalized for input signal (right). (**g**) Monitoring translocation of PNM2 when co-expressed with WT. As in **f**, but untagged WT Sup35 also expressed in cells expressing HA-tagged WT or PNM2 Sup35. The higher-molecular-weight band corresponds to HA-tagged Sup35. Intensities of tagged-Sup35 elution signals were normalized for input signal and for untagged-Sup35 elution signal. For Sup35 intensity, values are mean ± s.e.m. for three experiments.

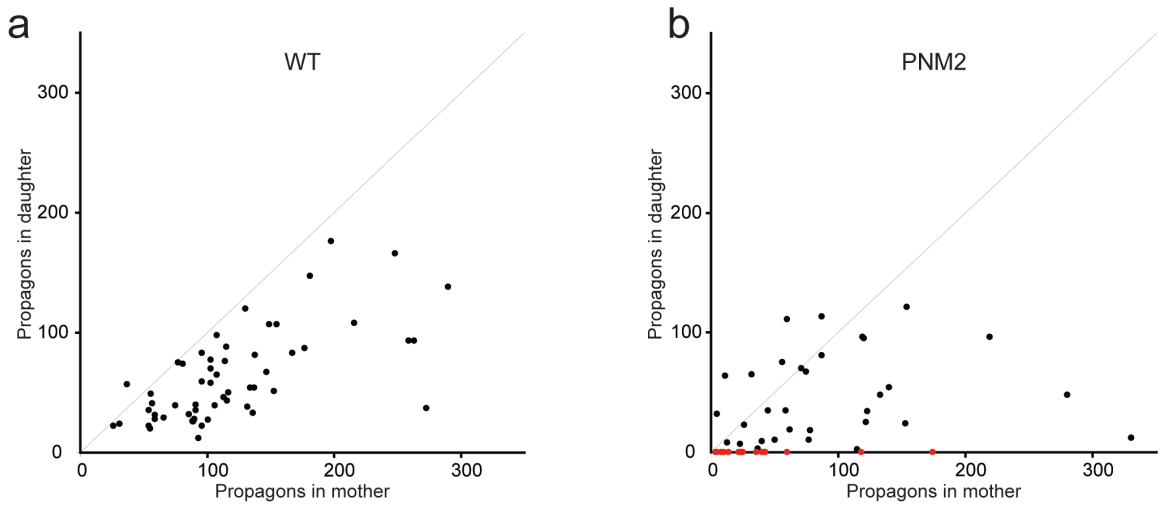
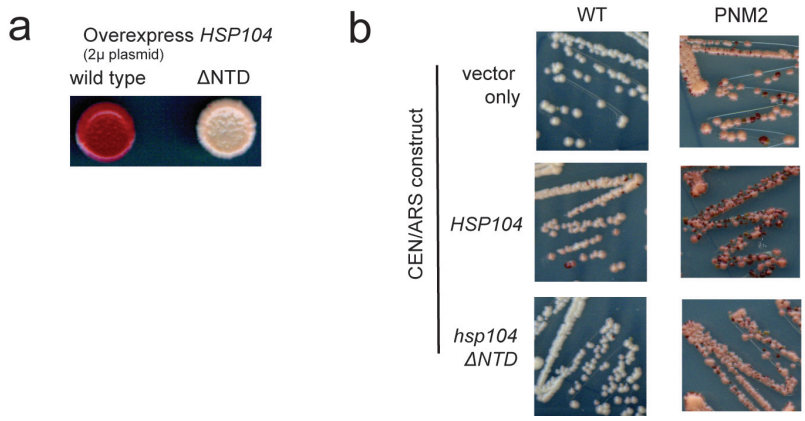
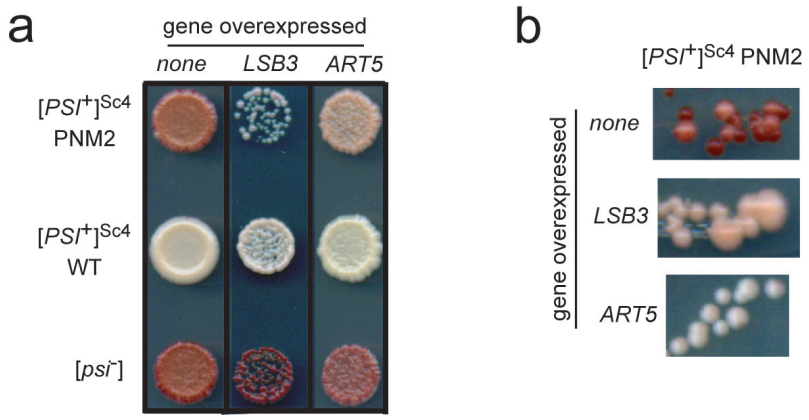


Figure 6 PNM2 in the Sc4 conformation shows a defect in partitioning. (**a**,**b**) The number of propagons in the daughters was plotted against the number of propagons in the mothers for WT (**a**) and PNM2 (**b**) [PSI^{+}]^{Sc4} backgrounds. Red dots represent mother-daughter pairs in which the mother contained propagons but the daughter did not.

SUPPLEMENTARY INFORMATION



Supplementary Figure 1. The Hsp104ΔNTD variant is deficient in curing but propagates [*PSI*$^{+}$]^{Sc4} and maintains the PNM2 phenotype. **(a)** *HSP104* or *hsp104ΔNTD* was expressed from a high copy (2μ) plasmid in [*PSI*$^{+}$]^{Sc4} yeast spotted onto low adenine media. **(b)** Streak out of yeast from Figure 5 on low adenine media for better visualization of phenotype. WT or PNM2 [*PSI*$^{+}$]^{Sc4} yeast that express: an empty CEN/ARS plasmid ("vector only"), a CEN/ARS plasmid containing *HSP104* or a CEN/ARS plasmid containing *hsp104ΔNTD*.



Supplementary Figure 2. Overexpression of either *LSB3* or *ART5* suppresses the PNM2 phenotype. **(a)** [*PSI*$^{+}$]^{Sc4} yeast with PNM2 (top row) or WT (middle row) Sup35p or WT cured to [*psi*$^{-}$] (bottom row) transformed with an overexpression (2μ) plasmid that contains: no gene (left column), *LSB3* (middle column) or *ART5* (right column). All yeast are spotted onto low adenine media. **(b)** Single colony photographs of PNM2 [*PSI*$^{+}$]^{Sc4} yeast with an overexpression (2μ) plasmid that contains: no gene (top), *LSB3* (middle) or *ART5* (bottom).

Supplementary Table 1: Strains

Sc Strain	Description	Genotype	Source
YJW1109	74D-694 [*psi*$^-$]	74D-694 *ade1-14 his3Δ200 leu2-3,112 trp1-289 ura3-52 sup35::TRP1*/pRS316 [*psi*$^-$]	this study
YJW1110	74D-694 [*PSI*$^+$]^{Sc4}	74D-694 *ade1-14 his3Δ200 leu2-3,112 trp1-289 ura3-52 sup35::TRP1*/pRS316 [*PSI*$^+$]^{Sc4}	this study
YJW1111	74D-694 [*PSI*$^+$]^{Sc37}	74D-694 *ade1-14 his3Δ200 leu2-3,112 trp1-289 ura3-52 sup35::TRP1*/pRS316 [*PSI*$^+$]^{Sc37}	this study
YJW1112	W303 [*psi*$^-$] HAP	W303 *ade1-14 leu2-3,112 his3-11,15 trp1-1 can1-100 ura3::nat hsp104::TRP1*/phs313HAP [*psi*$^-$]	this study
YJW1113	W303 [*PSI*$^+$]^{Sc4} HAP	W303 *ade1-14 leu2-3,112 his3-11,15 trp1-1 can1-100 ura3::nat hsp104::TRP1*/phs313HAP [*PSI*$^+$]^{Sc4}	this study
YJW1114	W303 [*PSI*$^+$]^{Sc4} Hsp104	W303 *ade1-14 leu2-3,112 his3-11,15 trp1-1 can1-100 ura3::nat hsp104::TRP1*/phs313*Hsp104* [*PSI*$^+$]^{Sc4}	this study
YJW1115	W303 [*PSI*$^+$]^{Sc4} HAP	W303 *ade1-14 leu2-3,112 his3-11,15 trp1-1 can1-100 ura3::kan hsp104::*HAP_*TRP1 Sup35::nat*/pRS316 WTSup35 [*PSI*$^+$]^{Sc4}	this study
YJW1667	74D-694 [*PSI*$^+$]^{Sc4} Hsp104ΔNTD	74D-694 *ade1-14 his3Δ200 leu2-3,112 trp1-289 ura3-52 sup35::TRP1*/pRS316 *hsp104*::*nat-hsp104ΔNTD (resi 1-146 deleted)* [*PSI*$^+$]^{Sc4}	this study; Hung and Masison[35]

Supplementary Table 2: Plasmids

Plasmid	Description	Source
pRS316 WT Sup35p	pRS316; *SUP35*	this study
pRS315 WT Sup35p	pRS315; *SUP35*	this study
pRS315 PNM2 Sup35p	pRS315; *SUP35 G58D*	this study
phs313 Hsp104p	phs313; *HSP104*	Tessarz et al.[34]
phs313 HAP	phs313; HAP	Tessarz et al.[34]
pmCUP425-ClpP^{trap}	pmCUP425; ClpP^{trap} (ClpPΔ1-13, S111A; SBP-tagged)	Tessarz et al.[34]
pRS313 WT Sup35p	pRS313; *SUP35*	this study
pRS313 PNM2 Sup35p	pRS313; *SUP35 G58D*	this study
pRS313 WT Sup35HA	pRS313; *SUP35* with 3HA inserted after amino acid 216	this study
pRS313 PNM2 Sup35HA	pRS313 *SUP35 G58D* with 3HA inserted after amino acid 216	this study
pRS399 WT Hsp104p	pRS399 (pRS315 backbone with *Leu*::*KanR*); *HSP104*	this study
pRS399 Hsp104ΔNTDp	pRS399 (pRS315 backbone with *Leu*::*KanR*); *hsp104ΔNTD*	this study; Hung and Masison[35]
pGP564	pGP564; empty vector	Jones et al.[56]
pGP564 Lsb3p	pGP564; *LSB3*	this study
pGP564 Art5p	pGP564; *ART5*	this study

Supplementary Methods:

High copy PNM2 suppression screen

Systematic overexpression of the full complement of yeast proteins was carried out using the Thermo Scientific Open Biosystems Yeast Genomic Tiling Collection[56]. The entire yeast genome was overexpressed in segments, each containing 4-5 genes, from 1588 clones using a pGP564 (2μ) vector in PNM2 $[PSI^{+}]^{Sc4}$ yeast. Colonies were visually screened for reduced sectoring and five were identified as meeting this criteria. Individual clones were recovered from these colonies and sequenced to determine the identity of the clone. Clone YGPM21g14 was recovered 2 times and clone YGPM34g01 was recovered 3 times. Individual genes from each clone were overexpressed using the pGP546 vector to determine the causative genes. Both *LSB3* (YFR024C) and *ART5* (YGR068C) were identified as high copy suppressors of the PNM2 $[PSI^{+}]^{Sc4}$ phenotype.

References

1. Caughey, B., Baron, G.S., Chesebro, B. & Jeffrey, M. Getting a grip on prions: oligomers, amyloids, and pathological membrane interactions. *Annu. Rev. Biochem.* **78**, 177–204 (2009).
2. Chiti, F. & Dobson, C.M. Protein misfolding, functional amyloid, and human disease. *Annu. Rev. Biochem.* **75**, 333–366 (2006).
3. Tuite, M.F. & Cox, B.S. Propagation of yeast prions. *Nat. Rev. Mol. Cell Biol.* **4**, 878–890 (2003).
4. Tessier, P.M. & Lindquist, S. Unraveling infectious structures, strain variants and species barriers for the yeast prion [PSI+]. *Nat. Struct. Mol. Biol.* **16**, 598–605 (2009).
5. Chien, P., Weissman, J.S. & DePace, A.H. Emerging principles of conformation-based prion inheritance. *Annu. Rev. Biochem.* **73**, 617–656 (2004).
6. Santoso, A., Chien, P., Osherovich, L.Z. & Weissman, J.S. Molecular basis of a yeast prion species barrier. *Cell* **100**, 277–288 (2000).
7. Morales, R., Abid, K. & Soto, C. The prion strain phenomenon: molecular basis and unprecedented features. *Biochim. Biophys. Acta* **1772**, 681–691 (2007).
8. Tanaka, M., Chien, P., Naber, N., Cooke, R. & Weissman, J.S. Conformational variations in an infectious protein determine prion strain differences. *Nature* **428**, 323–328 (2004).
9. Derkatch, I.L., Chernoff, Y.O., Kushnirov, V.V., Inge-Vechtomov, S.G. & Liebman, S.W. Genesis and variability of [PSI] prion factors in *Saccharomyces cerevisiae*. *Genetics* **144**, 1375–1386 (1996).
10. Bradley, M.E., Edskes, H.K., Hong, J.Y., Wickner, R.B. & Liebman, S.W. Interactions among prions and prion "strains" in yeast. *Proc. Natl. Acad. Sci. USA* **99** Suppl 4, 16392–

16399 (2002).

11. King, C.-Y. & Diaz-Avalos, R. Protein-only transmission of three yeast prion strains. *Nature* **428**, 319–323 (2004).
12. Chien, P. & Weissman, J. Conformational diversity in a yeast prion dictates its seeding specificity. *Nature* **410**, 223–227 (2001).
13. Sparrer, H.E., Santoso, A., Szoka, F.C. & Weissman, J.S. Evidence for the prion hypothesis: induction of the yeast [PSI+] factor by in vitro-converted Sup35 protein. *Science* **289**, 595–599 (2000).
14. Krishnan, R. & Lindquist, S.L. Structural insights into a yeast prion illuminate nucleation and strain diversity. *Nature* **435**, 765–772 (2005).
15. Toyama, B.H., Kelly, M.J., Gross, J.D. & Weissman, J.S. The structural basis of yeast prion strain variants. *Nature* **449**, 233–237 (2007).
16. Tanaka, M., Collins, S.R., Toyama, B.H. & Weissman, J.S. The physical basis of how prion conformations determine strain phenotypes. *Nature* **442**, 585–589 (2006).
17. Derkatch, I.L., Bradley, M.E., Zhou, P. & Liebman, S.W. The PNM2 mutation in the prion protein domain of SUP35 has distinct effects on different variants of the [PSI+] prion in yeast. *Curr. Genet.* **35**, 59–67 (1999).
18. Green, K.M. *et al.* The elk PRNP codon 132 polymorphism controls cervid and scrapie prion propagation. *J. Gen. Virol.* **89**, 598–608 (2008).
19. Takemura, K., Kahdre, M., Joseph, D., Yousef, A. & Sreevatsan, S. An overview of transmissible spongiform encephalopathies. *Anim. Health Res. Rev.* **5**, 103–124 (2004).
20. Zeidler, M., Stewart, G., Cousens, S.N., Estibeiro, K. & Will, R.G. Codon 129 genotype and new variant CJD. *Lancet* **350**, 668 (1997).

21. Mead, S. *et al.* Creutzfeldt-Jakob disease, prion protein gene codon 129VV, and a novel PrPSc type in a young British woman. *Arch. Neurol.* **64**, 1780–1784 (2007).

22. Collinge, J., Sidle, K.C., Meads, J., Ironside, J. & Hill, A.F. Molecular analysis of prion strain variation and the aetiology of 'new variant' CJD. *Nature* **383**, 685–690 (1996).

23. Hill, A.F. *et al.* The same prion strain causes vCJD and BSE. *Nature* **389**, 448–450 (1997).

24. Doel, S.M., McCready, S.J., Nierras, C.R. & Cox, B.S. The dominant PNM2- mutation which eliminates the psi factor of *Saccharomyces cerevisiae* is the result of a missense mutation in the SUP35 gene. *Genetics* **137**, 659–670 (1994).

25. Young, C.S.H. & Cox, B.S. Extrachromosomal elements in a super-suppression system of yeast: I. A nuclear gene controlling the inheritance of the extrachromosomal elements. *Heredity* **26**, 413–422 (1971).

26. Chernoff, Y., Lindquist, S., Ono, B., Inge-Vechtomov, S. & Liebman, S. Role of the chaperone protein Hsp104 in propagation of the yeast prion-like factor [psi+]. *Science* **268**, 880–884 (1995).

27. Kochneva-Pervukhova, N.V. *et al.* Mechanism of inhibition of Psi+ prion determinant propagation by a mutation of the N-terminus of the yeast Sup35 protein. *EMBO J.* **17**, 5805–5810 (1998).

28. Glover, J.R. *et al.* Self-seeded fibers formed by Sup35, the protein determinant of [PSI+], a heritable prion-like factor of *S. cerevisiae*. *Cell* **89**, 811–819 (1997).

29. King, C.Y. *et al.* Prion-inducing domain 2–114 of yeast Sup35 protein transforms in vitro into amyloid-like filaments. *Proc. Natl. Acad. Sci. USA* **94**, 6618–6622 (1997).

30. Higurashi, T., Hines, J.K., Sahi, C., Aron, R. & Craig, E.A. Specificity of the J-protein Sis1 in the propagation of 3 yeast prions. *Proc. Natl. Acad. Sci. USA* **105**, 16596–16601 (2008).

31. Jones, G.W. & Tuite, M.F. Chaperoning prions: the cellular machinery for propagating an infectious protein? *Bioessays* **27**, 823–832 (2005).

32. Shorter, J. & Lindquist, S. Hsp104, Hsp70 and Hsp40 interplay regulates formation, growth and elimination of Sup35 prions. *EMBO J.* **27**, 2712–2724 (2008).

33. Tipton, K.A., Verges, K.J. & Weissman, J.S. In vivo monitoring of the prion replication cycle reveals a critical role for Sis1 in delivering substrates to Hsp104. *Mol. Cell* **32**, 584–591 (2008).

34. Tessarz, P., Mogk, A. & Bukau, B. Substrate threading through the central pore of the Hsp104 chaperone as a common mechanism for protein disaggregation and prion propagation. *Mol. Microbiol.* **68**, 87–97 (2008).

35. Hung, G.-C. & Masison, D.C. N-terminal domain of yeast Hsp104 chaperone is dispensable for thermotolerance and prion propagation but necessary for curing prions by Hsp104 overexpression. *Genetics* **173**, 611–620 (2006).

36. Di Salvo, S., Derdowski, A., Pezza, J.A. & Serio, T.R. Dominant prion mutants induce curing through pathways that promote chaperone-mediated disaggregation. *Nat. Struct. Mol. Biol.* advance online publication, doi:10.1038/nsmb.2031 (20 March 2011).

37. Kryndushkin, D.S., Alexandrov, I.M., Ter-Avanesyan, M.D. & Kushnirov, V.V. Yeast [PSI+] prion aggregates are formed by small Sup35 polymers fragmented by Hsp104. *J. Biol. Chem.* **278**, 49636–49643 (2003).

38. Cox, B., Ness, F. & Tuite, M. Analysis of the generation and segregation of propagons: entities that propagate the [PSI+] prion in yeast. *Genetics* **165**, 23–33 (2003).

39. Ferreira, P.C., Ness, F., Edwards, S.R., Cox, B.S. & Tuite, M.F. The elimination of the yeast [PSI+] prion by guanidine hydrochloride is the result of Hsp104 inactivation. *Mol.*

Microbiol. **40**, 1357–1369 (2001).

40. Grimminger, V., Richter, K., Imhof, A., Buchner, J. & Walter, S. The prion curing agent guanidinium chloride specifically inhibits ATP hydrolysis by Hsp104. *J. Biol. Chem.* **279**, 7378–7383 (2004).
41. Jung, G. & Masison, D.C. Guanidine hydrochloride inhibits Hsp104 activity in vivo: a possible explanation for its effect in curing yeast prions. *Curr. Microbiol.* **43**, 7–10 (2001).
42. Byrne, L.J. *et al.* The number and transmission of [PSI] prion seeds (Propagons) in the yeast *Saccharomyces cerevisiae*. *PLoS ONE* **4**, e4670 (2009).
43. Liu, B. *et al.* The polarisome is required for segregation and retrograde transport of protein aggregates. *Cell* **140**, 257–267 (2010).
44. Kaganovich, D., Kopito, R. & Frydman, J. Misfolded proteins partition between two distinct quality control compartments. *Nature* **454**, 1088–1095 (2008).
45. Robertson, A.S. *et al.* The WASP homologue Las17 activates the novel actin-regulatory activity of Ysc84 to promote endocytosis in yeast. *Mol. Biol. Cell* **20**, 1618–1628 (2009).
46. Tonikian, R. *et al.* Bayesian modeling of the yeast SH3 domain interactome predicts spatiotemporal dynamics of endocytosis proteins. *PLoS Biol.* **7**, e1000218 (2009).
47. Madania, A. *et al.* The *Saccharomyces cerevisiae* homologue of human Wiskott-Aldrich syndrome protein Las17p interacts with the Arp2/3 complex. *Mol. Biol. Cell* **10**, 3521–3538 (1999).
48. Ganusova, E.E. *et al.* Modulation of prion formation, aggregation, and toxicity by the actin cytoskeleton in yeast. *Mol. Cell. Biol.* **26**, 617–629 (2006).
49. Bailleul, P., Newnam, G., Steenbergen, J. & Chernoff, Y. Genetic study of interactions between the cytoskeletal assembly protein Sla1 and prion-forming domain of the release

factor Sup35 (eRF3) in *Saccharomyces cerevisiae*. *Genetics* **153**, 81 (1999).

50. Lin, C.H., Macgurn, J.A., Chu, T., Stefan, C.J. & Emr, S.D. Arrestin-related ubiquitin-ligase adaptors regulate endocytosis and protein turnover at the cell surface. *Cell* **135**, 714–725 (2008).
51. Nikko, E. & Pelham, H.R.B. Arrestin-mediated endocytosis of yeast plasma membrane transporters. *Traffic* **10**, 1856–1867 (2009).
52. Derdowski, A., Sindi, S.S., Klaips, C.L., Disalvo, S. & Serio, T.R. A size threshold limits prion transmission and establishes phenotypic diversity. *Science* **330**, 680–683 (2010).
53. Tanaka, M., Chien, P., Yonekura, K. & Weissman, J.S. Mechanism of cross-species prion transmission: an infectious conformation compatible with two highly divergent yeast prion proteins. *Cell* **121**, 49–62 (2005).
54. Halfmann, R. & Lindquist, S. Screening for amyloid aggregation by semi-denaturing detergent-agarose gel electrophoresis. *J. Vis. Exp.* **16**, 838 (2008).
55. Bagriantsev, S.N., Kushnirov, V.V. & Liebman, S.W. Analysis of amyloid aggregates using agarose gel electrophoresis. *Methods Enzymol.* **412**, 33–48 (2006).
56. Jones, G. M., et al. A systematic library for comprehensive overexpression screens in Saccharomyces cerevisiae. *Nat Methods* **5**, 239-41 (2008).

CHAPTER 4

Road to ruin: targeting proteins for degradation in the endoplasmic reticulum

Road to Ruin: Targeting Proteins for Degradation in the Endoplasmic Reticulum

Melanie H. Smith[1], Hidde L. Ploegh[2] and Jonathan S. Weissman[1]

[1]Department of Cellular and Molecular Pharmacology, Graduate Group in Biophysics and Howard Hughes Medical Institute, University of California, San Francisco, 94158, California, USA. [2]Whitehead Institute for Biomedical Research, Massachusetts Institute of Technology, 9 Cambridge Center, Cambridge, 02142, Massachusetts, USA.

Reproduced with permission from AAAS from *Science* **2011**, 334(6059): 1056-1090. doi:10.1126/science.1209235.

Abstract

Some nascent proteins that fold within the endoplasmic reticulum (ER) never reach their native state. Misfolded proteins are removed from the folding machinery, dislocated from the ER into the cytosol, and degraded in a series of pathways collectively referred to as ER-associated degradation (ERAD). Distinct ERAD pathways centered on different E3 ubiquitin ligases survey the range of potential substrates. We now know many of the components of the ERAD machinery and pathways used to detect substrates and target them for degradation. Much less is known about the features used to identify terminally misfolded conformations and the broader role of these pathways in regulating protein half-lives.

Proteins destined for secretion or insertion into the membrane enter the endoplasmic reticulum (ER) in an unfolded form and generally leave only after they have reached their native states. Yet folding in the ER is often slow and inefficient, with a substantial fraction of polypeptides failing to reach the native state. Thus, the cell must continuously assess the pool of folding proteins and remove polypeptides that are terminally misfolded. This process of culling is critical to protect the cell from the toxic effects of misfolded proteins.

Remarkably, many proteins triaged as terminally misfolded are first removed from the ER via delivery (or dislocation) to the cytosol where they are then degraded by the ubiquitin-proteasome system (see review by Claessen et al[1]). This process is commonly referred to as ER-associated degradation (ERAD) - an umbrella term that covers a range of different mechanisms. Once terminally misfolded proteins are distinguished from what are likely to be structurally similar folding species, they are extracted from the pro-folding chaperone machinery, delivered to a transmembrane complex that coordinates their dislocation and, finally, escorted to the proteasome for degradation (Fig. 1A).

A convergence of genetic and biochemical studies, including work in the budding yeast *Saccharomyces cerevisiae* and in metazoan systems, has led to the identification of many of the key components involved in substrate recognition and degradation. Characterization of these components has uncovered distinct and well-conserved ERAD pathways, but for only a limited number of model substrates. We still do not know all of the endogenous targets of ERAD or the relative importance of ERAD in quality control of misfolded conformations versus a broader role in regulating the half-lives of proteins that have reached the native state.

E3 Ubiquitin Ligases: Central Organizers

At the center of all ERAD pathways are multi-protein transmembrane complexes formed around E3 ubiquitin ligases (*2-4*). The E3s have variable numbers of transmembrane domains and a cytosolic RING finger domain. They catalyze substrate ubiquitylation (*5*) and organize the complexes that coordinate events on both sides of and within the ER membrane. When overexpressed, the prototypical ERAD E3, the yeast Hrd1p protein, can autonomously carry out degradation of soluble substrates within the ER lumen (*6*). This ability implicates Hrd1p -and by inference other ERAD E3s- in the physical process of transporting substrates across the ER membrane. Yet this step remains mysterious and it is likely that other components also facilitate dislocation.

If the E3s can act alone, then why do they form large complexes? The E3s require a dynamic complement of adaptor proteins that facilitate substrate recognition and delivery, while also regulating E3 activity. In fact, overexpression of Hrd1p without its adaptors is toxic to cells, apparently due to uncontrolled and inappropriate degradation (*2*). Although we understand the role of these adaptors in specific systems, such as the delivery of glycoproteins to E3s, the broader role of adaptors in restricting E3 activity to legitimate substrates remains unclear.

Individual E3s can survey overlapping but distinct ranges of substrates with diverse topologies (i.e. those with misfolded domains in the ER lumen, membrane or cytosolic compartments) (*3*) (Fig. 1B). The E3s implicated in ERAD include two proteins with distinct topologies in yeast, Hrd1p (*5*) and Doa10p (*7*), and many more in metazoans, such as HRD1, gp78, RMA1(RNF5), TRC8, and TEB4(MARCH IV) (see review (*8*)). Here, we will focus on the complexes formed around the best-characterized class of E3s, the HRD ligases, which include Hrd1p in yeast as well as HRD1 and gp78 in metazoans (Fig. 1, C and D).

Adaptors control E3-substrate interactions

Adaptors are the peripheral components of the E3 complex that impart the rich substrate repertoire and stringent specificity of ERAD. Hrd3p in yeast and its metazoan counterpart SEL1L are the most thoroughly characterized adaptors (*9*). These proteins contain a single transmembrane domain, which, in the case of Hrd3p, is dispensable for function (*5*). Rather, the business end of the molecule is a large luminal domain composed of multiple tetratricopeptide repeats (TPR) thought to facilitate protein-protein interactions (*9*). Hrd3p can bind potential substrates directly on the basis of their misfolded character (*2, 9*) and thus recruits misfolded proteins to the E3 ligase. Hrd3p/SEL1L also recruit other adaptors such as the glycan-binding (lectin) proteins, Yos9p (*9*), in yeast, and OS-9 and XTP3-B (*10*), in mammals, to the E3 complex. These lectins broaden the E3 substrate repertoire; their absence leads to a specific defect in glycoprotein degradation, but does not affect degradation of other Hrd3p/SEL1L and HRD dependent substrates, such as Hmg-CoA reductase (*11*).

Housekeeping chaperones may serve as adaptors. The cytoplasmic Hsp70, Ssa1p, facilitates substrate interaction with Doa10p (*12*); the ER-resident Hsp70s, Kar2p in yeast and BiP in mammals, interact with Yos9p-Hrd3p (*2*) and OS-9/XTP3-B-SEL1L (*13*) in a stable manner, localizing them to the E3 complex. BiP may also help deliver substrates to E3s based on its interactions with other ERAD components (*14*) and with substrates (*15*).

How is the activity of the E3s tuned to meet the cells needs?

E3s are regulated by their intrinsic stability: for example, the Hrd1p E3 auto-ubiquitylates and thus triggers its own degradation (*5*). Hrd3p forms a stoichiometric complex with Hrd1p and

inhibits this auto-ubiquitylation. The dual activities of Hrd3p as an adaptor and a regulator ensure that Hrd1p is active only in the presence of controlled substrate delivery. While the ability to self-destruct appears to be conserved among E3s, their mechanisms of regulation may not be. In metazoans, SEL1L interacts with HRD1 but not gp78 (*13*), and HRD1 appears to stabilize SEL1L (in contrast to the relationship in yeast, where Hrd3p stabilizes Hrd1p) (*16*).

The oligomeric state of Hrd1p modulates its activity and is regulated by Usa1p (*6, 17*), another member of the complex. Although Hrd1p oligomerization may be essential for its activity (*6*), Usa1p is dispensable for degradation of some substrates (*3*) and other regulators of Hrd1p oligomerization have not been identified. The regulation and role of oligomerization, especially in metazoans, which (with the possible exception of Herp (*3*)) lack a clear Usa1p homolog, awaits clarification.

Changes in relative adaptor abundance and expression level can tune E3 activity. Turnover of a number of upstream adaptors, including two regulators of glycoprotein degradation, EDEMs and OS-9 (discussed in depth below), may help set ERAD activity (*18*). In response to stress, the unfolded protein response (UPR) orchestrates increased expression of key ERAD components and thus facilitates the upregulation of ERAD activity and capacity (see review (*19*)). In metazoans, different arms of the UPR upregulate distinct sets of ERAD components (*20, 21*), suggesting that cells can dynamically alter the specificity of ERAD, not just its overall activity.

The Derlins: crucial but mysterious components

Perhaps the most enigmatic members of E3 complexes are the Derlins, of which the yeast Der1p is the founding member. Der1p is a multi-pass transmembrane protein that interacts with

Hrd1p and Hrd3p (*4*) as well as with substrates (*6*). Although central members of the E3 complex, Derlins are dispensable for degradation of many substrates. At least part of their function is to act as adaptors.

Derlins contain a motif shared with rhomboid proteases, which recognize and cleave protein sequences within the membrane, using hydrophilic residues within their transmembrane domains (*22*). Although Derlins lack catalytic sites, their membrane-embedded hydrophilic residues resemble potential substrate binding residues in the rhomboids and could facilitate substrate interactions. Signal peptide peptidase may play a similar role in dislocation of major histocompatibility complex (MHC) class I products in cells that express the viral protein US2 (*23*).

Luminal ERAD substrates are typically more dependent on Derlins. Intramembrane binding to Derlin could thus help prime the initial passage of luminal substrates across the membrane, making them resemble misfolded transmembrane proteins that could proceed through Derlin-independent pathways. The connection between rhomboid-like motifs and ERAD is also apparent in another class of catalytically inactive transmembrane proteins, iRhoms, that promote ERAD of potential rhomboid substrates (*24*).

E3s connect luminal and cytosolic ERAD pathways

Although the cytosolic ubiquitylation of substrates commits them for degradation and is likely past the point of no return, substrates still require delivery to the proteasome. Ubiquitylated substrates can follow multiple dynamically-controlled pathways within the cytoplasm (see review (*1*)). A key cytosolic event is the extraction of substrates from the ER membrane, in which the AAA adenosine triphophatase (ATPase) Cdc48p (p97 in metazoans)

and in some cases the proteasome lid (*25*) play a central role. Once substrates are in the cytosol, p97 recruits peptide N-glycanase (PNGase) to the site of dislocation (*26*) to remove N-linked glycans from substrates before they enter the proteasome (*27*). In what may be an information-processing step involved in substrate targeting, p97 also recruits YOD1, a deubiquitylating enzyme involved in dislocation (*28*). Thus, degradation is tightly coupled to substrate dislocation in a complex manner.

How Are Substrates Delivered to E3 Complexes?

An early event in the decision to degrade a protein involves removing it from the folding machinery and delivering it to the E3 complex. We are now beginning to understand the mechanism of delivery for some substrates (Fig. 2).

Viral hijacking of the E3 machinery

Human cytomegalovirus (HCMV) downregulates MHC class I heavy chains (MHC-I HC) to avoid detection by the immune system. The HCMV proteins US11 and US2 directly deliver correctly folded MHC-I HC to E3s to effect their disposal (Fig. 2A). US11 and US2 employ different pathways, which require Derlin-1 (*29*) and signal peptide peptidase (*23*) respectively, to achieve the same goal. By hijacking the ERAD machinery, HCMV bypasses the requirement for substrate recognition and achieves degradation rates much faster than those of other ERAD substrates (*30*). The abbreviated pathway of HCMV-mediated ERAD has been a critical tool for characterizing events without the use of model misfolded substrates (*29, 31*) and underscores the utility of host-pathogen interactions in exploring ERAD pathways. Toxins such as ricin, cholera and Shiga toxins, which likely exploit ERAD machinery to reach the cytoplasm

after retrograde transport through the secretory pathway, are similarly useful investigative tools (see review (*32*)).

Regulated delivery of specific substrates

Degradation of yeast Hmg-CoA reductase (Hmg2p), the rate-limiting enzyme in cholesterol synthesis, is an elegant example of physiological regulation of protein abundance via ERAD. When cholesterol levels are high, Hmg2p undergoes a lipid-induced structural change so that it resembles a misfolded protein, which is then targeted for destruction (Fig. 2B) (*33*). Thus, when Hmg2p is not needed, it is constitutively degraded. This involves direct recognition of Hmg2p transmembrane domains by Hrd1p, circumventing the need for many of the known Hrd1p adaptor proteins including Der1p, Usa1p, and Yos9p.

Other components involved in sterol biosynthesis also employ ERAD-based mechanisms of regulation. Mammalian Hmg-CoA reductase is regulated via degradation, but is delivered to the E3 via specific adaptor proteins (Insig-1 and -2) (*34*). Apolipoprotein B (apoB), involved in delivery of cholesterol to tissues, is cotranslationally degraded if not adequately loaded with cargo (*35*) and Erg3p, a component of the sterol biosynthesis pathway in yeast, is an endogenous ERAD substrate (*36*).

Cyclooxygenase-2 (Cox-2), a key enzyme in prostaglandin biosynthesis, employs an alternative strategy to control stability via ERAD. The C terminus of Cox-2, but not Cox-1, contains a 19-amino-acid sequence necessary and sufficient for degradation (*37*). This element not only presents an appealing minimal ERAD substrate, but also hints at what could be a widespread mechanism for the control of protein turnover rates by a modular “degron” signal.

Glycans signal folding status

The most detailed and elaborate known mechanism for delivery of ERAD substrates is that for luminal glycoproteins (Fig. 2C). As nascent polypeptides are translocated into the ER, many are co-translationally modified on specific asparagine (N-X-T/S) residues with a three-branch, high-mannose glycan (Glc_3-Man_9-$GlcNAc_2$) (Fig. 3A). Immediately upon transfer of the glycan to a protein, it is dismantled, one saccharide at a time, to yield unique structures recognized by different glycan binding proteins. These modifications report on folding status and acts as flags for degradation

Soon after entry into the ER, proteins go through a deglucosylation/ reglucosylation cycle on the A branch. This drives release and binding, respectively, to the chaperone lectins calnexin (CNX) and calreticulin (CRT), which together promote ER retention and folding (Fig. 3B)(see review (*38*)). As a protein attempts to reach its native state, mannosidases carry out competing reactions that remove mannose residues from the B and C branches and so decrease the likelihood of entry into further folding cycles. Removal of a C branch mannose by EDEMs (Htm1p in yeast) exposes a terminal α1,6-linked mannose that acts as a key signal for degradation(*39-42*).

Delivery of the substrate to the E3 does not require the terminal α1,6 mannose linkage, but this glycan is necessary for degradation. Although SEL1L/Hrd3p, a core member of the HRD complex, and the lectins OS-9/XTP3-B/Yos9p can bind misfolded proteins in a glycan-independent manner (*2, 10, 21*), degradation requires an additional, poorly-characterized commitment step in which Yos9p/OS-9/XTP3-B recognizes the C branch α1,6 mannose linkage to effect degradation (*41, 43, 44*) (Fig. 3C). Thus, disposal of at least some unwanted glycoproteins requires both a misfolded conformation and the correct glycan signal.

Although the glycan-processing pathway can be conceived of as a linear pathway with multiple information processing steps, there are many possible branch points and detours that complicate this view. These include multiple glycan-independent roles for glycan processing and recognition factors (*2, 10, 21, 36, 45*). The fact that the α1,6-linked mannose may reside both on substrates and on the adaptor proteins SEL1L/Hrd3p adds a further layer of complexity and affords a possible mechanism for regulating the activity of the HRD complex. The interactions between SEL1L and OS-9 (*10*) as well as EDEMs (*45*) require mannosidase-processed glycans on SEL1L. Given these observations, one interesting but speculative model is that the HRD complex is inactive when OS-9/Yos9p binds SEL1L/Hrd3p glycans, but is activated in a hand-off mechanism when OS-9/Yos9p binds substrate glycans and releases SEL1L/Hrd3p.

Dismanteling structures upstream of E3s

Processing of substrates upstream of the E3s is essential both for the recognition of misfolded proteins and for dismantling the compact folds of disulfide-bonded substrates to facilitate dislocation. ERAD may require isomerization of *trans* peptidyl-prolyl bonds to eliminate turns (*46*) as well as the reduction of disulfide bonds to separate nonnative oligomers (*14*) or to recognize specific disulfide intermediates (*15*). ERdj5 interacts with EDEM1 and can reduce disulfide bonds of aberrantly linked proteins and accelerate ERAD when overexpressed (*14*) (Fig. 2D). Both its substrate-binding J domain and its disulfide-reactive thioredoxin domain are critical for ERdj5's activity. Other ER oxidoreductases also participate in ERAD, including the flavoprotein ERFAD (*47*) and protein disulfide isomerase (Pdi1p), underscoring the importance of disulfide modulation in this process. In yeast, Htm1p forms a disulfide-stabilized

complex with Pdi1p (*48*), necessary for both maximal Htm1p activity as well as its stability (*42*). The known chaperone roles of Pdi1p and ERdj5's binding partner, BiP, raise the possibility that these interactions may facilitate substrate recognition by EDEM1/Htm1p.

Other pathways to E3s

Substrates that are not glycosylated or that do not have misfolded domains within the ER lumen follow alternate pathways to E3s. Even though different pathways preferentially process certain substrates, the pathway and E3 used for a specific substrate likely depend on substrate load, adaptor availability and the overall stress level of the ER.

In mammalian cells, degradation of some non-glycosylated proteins requires an E3 complex composed of HRD1, Derlin-1 and Herp, a specialized adaptor for nonglycoproteins (*15*). Herp is a transmembrane protein with a large cytosolic domain that binds p97 as well as components of the 26S proteasome, suggesting a possible link between protein dislocation and degradation (*15*). Although its primarily cytosolic location raises the question as to how nonglycosylated-substrates are delivered to the E3 complex within the ER lumen, BiP might deliver misfolded substrates to E3s as well as serve as the primary folding chaperone for nonglycosylated proteins (*15*).

Via residues in its transmembrane domains, Hrd1p directly recognizes proteins that misfold within the ER membrane (*11*). Mutations within these Hrd1p intramembrane residues confer substrate-specific degradation defects (*11*). Given the hydrophilic character of some of these residues, they could act as sensors for misfolding within the hydrophobic environment of the membrane in a mechanism that could apply more generally to other E3s or to the Derlins.

Substrates with misfolded cytosolic domains prompt degradation via Doa10p, the only other ERAD-active E3 in yeast besides Hrd1p (*7*). Doa10p has broad substrate specificity, encompassing membrane proteins as well as soluble cytosolic and nuclear proteins and even exhibits some functional overlap with Hrd1p (*7*). Doa10p surveys this wide range of potential substrates without stably-associated adaptors; the only other members of the core Doa10p complex are the E2 ubiquitin conjugating enzymes Ubc6p and Ubc7p (along with Cue1p, the membrane anchor for Ubc7p) (*49*). Without defined substrate adaptors, Doa10p may directly bind improperly exposed hydrophobic surfaces on the cytosolic surface of the ER membrane (*49*) or general cytosolic chaperones could act as adaptors.

Outlook

Great progress has been made in characterizing key ERAD pathways used for specific substrates. A fundamental question going forward is what biophysical, chemical and structural properties characterize ERAD substrates. The absence of clear physico-chemical correlates of the misfolded state for any intracellular protein is a major impediment to experimental progress and optical approaches (ideally single molecule) that could accurately diagnose folding states of a given protein inside cells are needed. In both yeast and metazoan systems, the relatively slow rate of egress of dislocation substrates from the ER has hampered the establishment of robust in vitro assays for dislocation.

In addition to the physical properties of substrates, the time spent on folding and a substrate's precise position within the ER may be crucial determinants of ERAD recognition. Elucidating the basis of the slow degradation of soluble luminal substrates (~30 minutes in yeast and longer in mammalian systems) represents a critical technical and conceptual challenge in

understanding substrate recognition. Key factors may be glycan modifications, in particular those imposed by the slow-acting ER mannosidase I, proposed to create a time window for folding prior to surveillance by ERAD components (see review (*38*)). However, this is unlikely to be the full explanation because even if one bypasses the need for glycan processing, degradation remains slow (*41*).

The location of at least some of the degradation machinery may be distinct from the site of protein entry into the ER: substrates may have to migrate to specialized subregions of the ER to access their paths to destruction, causing delays. For example, class I MHC heavy chains that fail to fold are relegated to specialized tubulovesicular areas of the ER (*50*). If the rate of migration to these subregions depends on the folding status of a protein, the ER could potentially fractionate proteins based on conformation and allow different folding intermediates more or less time to reach the native state before encountering the ERAD machinery.

Finally, the folding and dislocation pathways are fascinating not just because of their inherent attraction, they may also afford the possibility of intervention, genetically or with small molecules, to affect the outcome of the entire biosynthetic process. Where mutations produce proteins with mild defects that target them for degradation, despite being able to execute their assigned function (for example, the case of the cystic fibrosis transmembrane conductance receptor (CFTR) (*51*)), interference in these pathways may help to restore the cell to relative health by pushing a larger fraction of the mutant protein into productive folding pathways.

Acknowledgements

We Thank D. G. Fujimori, C. Jan, M. Larson, Y. C. Liu, and E. Q. Toyama for critical readings of the manuscript. This work was supported by the Howard Hughes Medical Institute (J.S.W.), the Hertz Foundation Peter Strauss Fellowship (M.H.S.), and the National Institutes of Health (J.S.W. and H.L.P.).

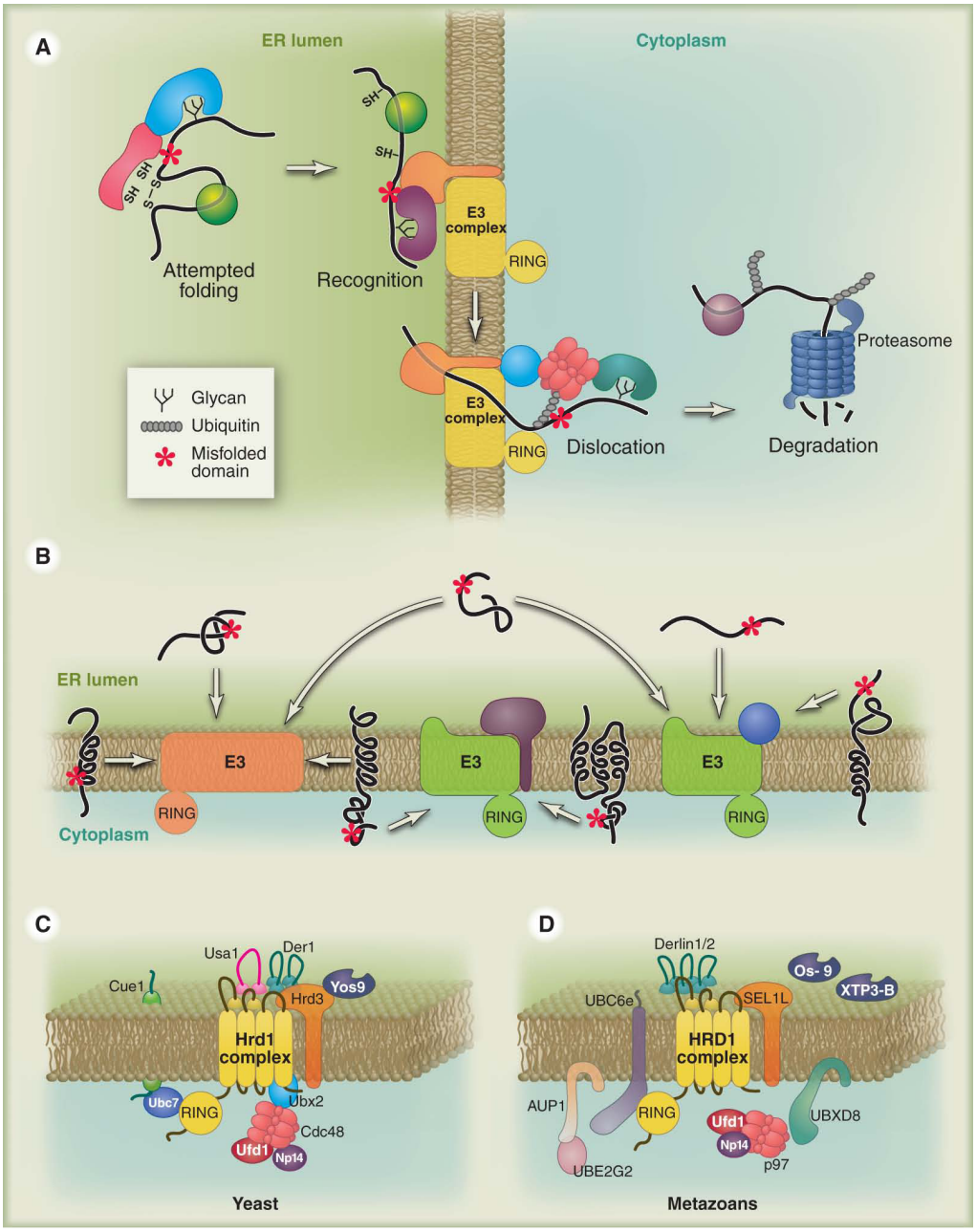


Figure 1. *The events and components of ERAD.* **(A)** The key steps of ERAD as shown for a luminal glycoprotein as apply to yeast or metazoans, and thus only the transmembrane E3 ubiquitin ligase complex is labeled along with its catalytic RING domain. **(B)** Overlapping substrate specificity of E3 ubiquitin ligases can be modulated by the presence of adaptors. The red asterisk denotes a misfolded domain. **(C)** The core Hrd1p complex in yeast. **(D)** The core HRD1 complex in metazoans.

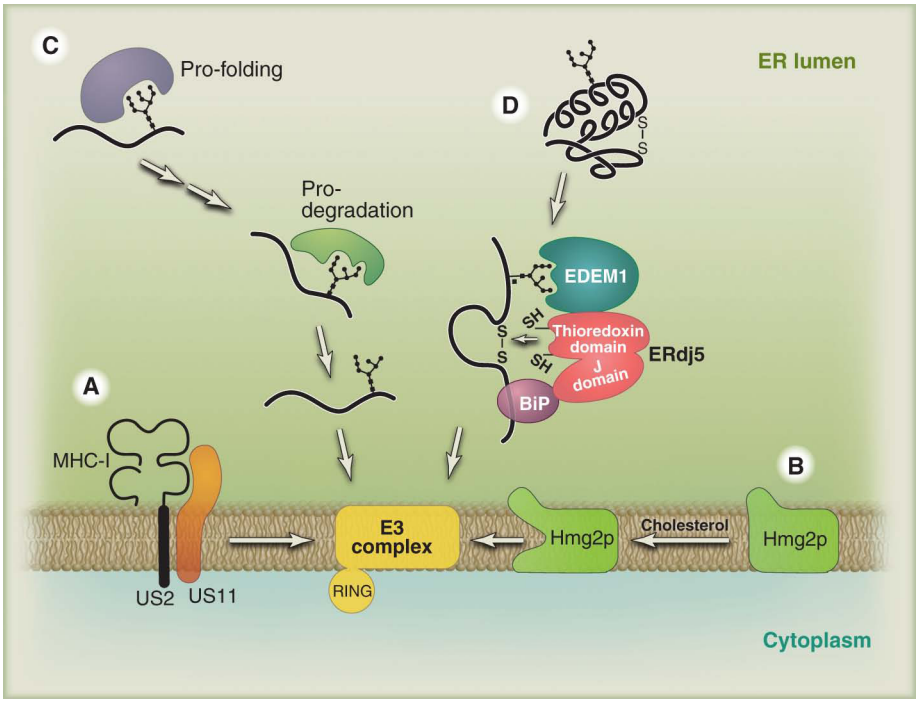


Figure 2. *Different paths substrates take to the E3 complexes.* **(A)** Delivery of correctly folded MHC class I molecules to the E3 by US11. **(B)** Cholesterol-regulated recognition of Hmg2p by the E3 complex. **(C)** Removal of a glycoprotein from the folding machinery and modification of the glycan followed by delivery to the E3 by pro-degradation factors. **(D)** Reduction of substrate disulfide bonds by the EDEM1-ERdj5-BiP complex in metazoans in preparation for translocation.

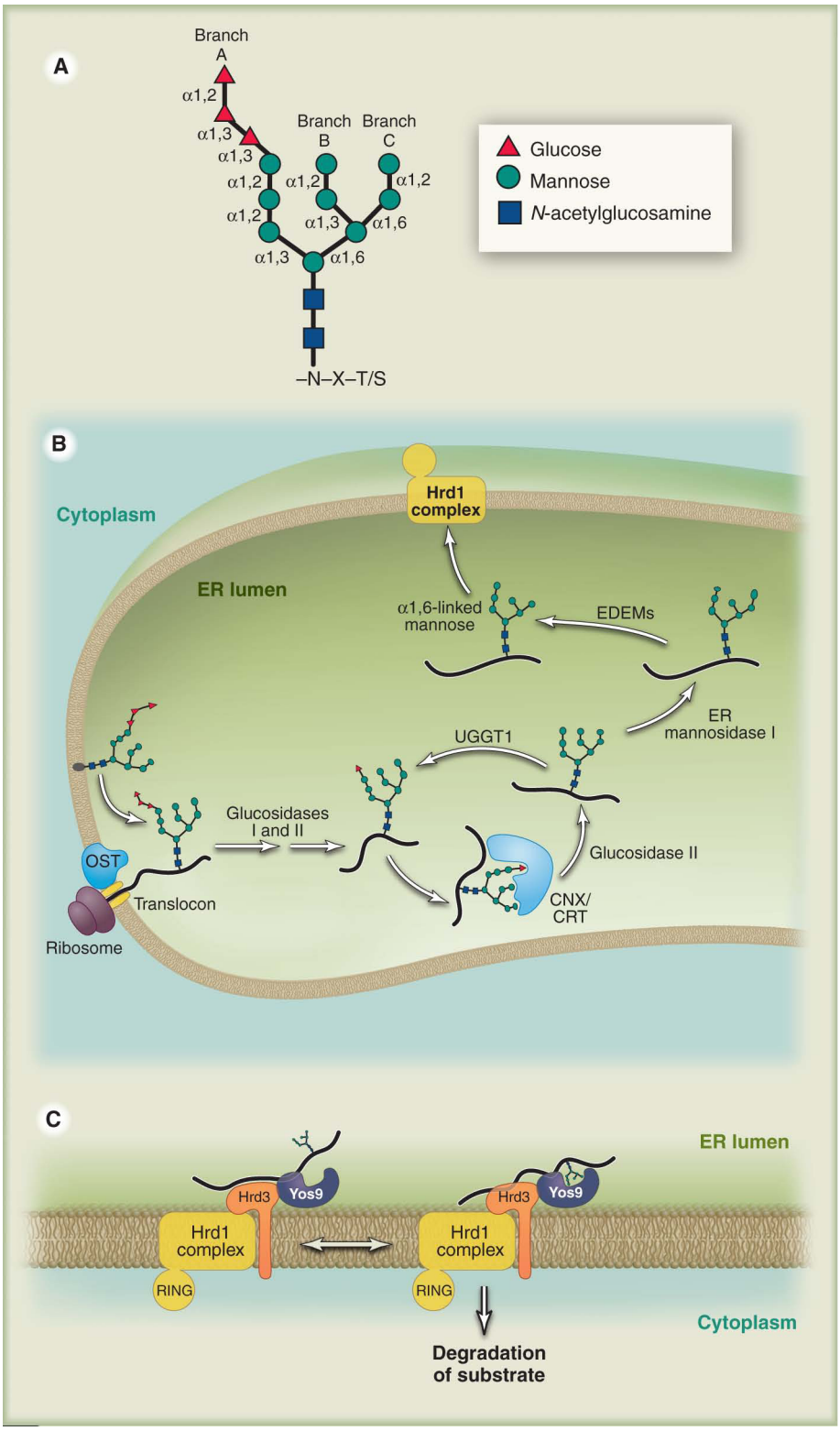


Figure 3. *Targeting glycoproteins for degradation*. **(A)** The initial high-mannose glycan appended to nascent polypeptides, Glc_3-Man_9-$GlcNAc_2$. **(B)** Metazoan glycan processing and

delivery to the HRD1-ligase complex. **(C)** Luminal glycoprotein recognition by the Hrd3p-Yos9p complex in yeast. Only the complex in which Yos9p binds the glycan with the terminal α1,6-mannose linkage is capable of degrading substrate. In metazoan systems it is thought that OS-9 may recognize glycans on SEL1L as opposed to those on ERAD substrates as discussed in the main text.

References

1. J. H. L. Claessen, L. Kundrat, H. L. Ploegh, *Trends Cell Biol* **22**, 22 (2012).
2. V. Denic, E. M. Quan, J. S. Weissman, *Cell* **126**, 349 (2006).
3. P. Carvalho, V. Goder, T. A. Rapoport, *Cell* **126**, 361 (2006).
4. R. Gauss, T. Sommer, E. Jarosch, *EMBO J* **25**, 1827 (2006).
5. R. G. Gardner *et al.*, *J Cell Biol* **151**, 69 (2000).
6. P. Carvalho, A. M. Stanley, T. A. Rapoport, *Cell* **143**, 579 (2010).
7. R. Swanson, M. Locher, M. Hochstrasser, *Genes Dev* **15**, 2660 (2001).
8. Z. Kostova, Y. C. Tsai, A. M. Weissman, *Semin Cell Dev Biol* **18**, 770 (2007).
9. R. Gauss, E. Jarosch, T. Sommer, C. Hirsch, *Nat Cell Biol* **8**, 849 (2006).
10. J. C. Christianson, T. A. Shaler, R. E. Tyler, R. R. Kopito, *Nat Cell Biol* **10**, 272 (2008).
11. B. K. Sato, D. Schulz, P. H. Do, R. Y. Hampton, *Mol Cell* **34**, 212 (2009).
12. K. Nakatsukasa, G. Huyer, S. Michaelis, J. L. Brodsky, *Cell* **132**, 101 (2008).
13. N. Hosokawa *et al.*, *J Biol Chem* **283**, 20914 (2008).
14. R. Ushioda *et al.*, *Science* **321**, 569 (2008).
15. Y. Okuda-Shimizu, L. M. Hendershot, *Mol Cell* **28**, 544 (2007).
16. Y. Iida *et al.*, *J Biol Chem* **286**, 16929 (2011).
17. S. C. Horn *et al.*, *Mol Cell* **36**, 782 (2009).
18. T. Calì, C. Galli, S. Olivari, M. Molinari, *Biochem Biophys Res Commun* **371**, 405 (2008).
19. P. Walter, D. Ron, *Science* **334**, 1081 (2011).
20. H. Yoshida *et al.*, *Dev Cell* **4**, 265 (2003).

21. R. Bernasconi, T. Pertel, J. Luban, M. Molinari, *J Biol Chem* **283**, 16446 (2008).

22. E. J. Greenblatt, J. A. Olzmann, R. R. Kopito, *Nat Struct Mol Biol* **18**, 1147 (2011).

23. J. Loureiro *et al.*, *Nature* **441**, 894 (2006).

24. M. Zettl, C. Adrain, K. Strisovsky, V. Lastun, M. Freeman, *Cell* **145**, 79 (2011).

25. R. J. Lee *et al.*, *EMBO J* **23**, 2206 (2004).

26. G. Li, G. Zhao, X. Zhou, H. Schindelin, W. J. Lennarz, *Proc Natl Acad Sci USA* **103**, 8348 (2006).

27. C. Hirsch, D. Blom, H. L. Ploegh, *EMBO J* **22**, 1036 (2003).

28. R. Ernst, B. Mueller, H. L. Ploegh, C. Schlieker, *Mol Cell* **36**, 28 (2009).

29. B. N. Lilley, H. L. Ploegh, *Nature* **429**, 834 (2004).

30. E. J. Wiertz *et al.*, *Cell* **84**, 769 (1996).

31. Y. Ye, Y. Shibata, C. Yun, D. Ron, T. A. Rapoport, *Nature* **429**, 841 (2004).

32. J. M. Lord, L. M. Roberts, W. I. Lencer, *Curr Top Microbiol Immunol* **300**, 149 (2005).

33. A. G. Shearer, R. Y. Hampton, *EMBO J* **24**, 149 (2005).

34. B.-L. Song, N. Sever, R. A. DeBose-Boyd, *Mol Cell* **19**, 829 (2005).

35. J. L. Brodsky, E. A. Fisher, *Trends Endocrinol Metab* **19**, 254 (2008).

36. L. A. Jaenicke, H. Brendebach, M. Selbach, C. Hirsch, *Molecular Biology of the Cell*, (2011).

37. U. R. Mbonye *et al.*, *J Biol Chem* **281**, 35770 (2006).

38. A. Helenius, M. Aebi, *Annu Rev Biochem* **73**, 1019 (2004).

39. M. Molinari, V. Calanca, C. Galli, P. Lucca, P. Paganetti, *Science* **299**, 1397 (2003).

40. Y. Oda, N. Hosokawa, I. Wada, K. Nagata, *Science* **299**, 1394 (2003).

41. S. Clerc *et al.*, *J Cell Biol* **184**, 159 (2009).

42. R. Gauss, K. Kanehara, P. Carvalho, D. T. W. Ng, M. Aebi, *Molecular Cell* **42**, 782 (2011).

43. E. M. Quan *et al.*, *Mol Cell* **32**, 870 (2008).

44. N. Hosokawa, Y. Kamiya, D. Kamiya, K. Kato, K. Nagata, *J Biol Chem* **284**, 17061 (2009).

45. J. H. Cormier, T. Tamura, J. C. Sunryd, D. N. Hebert, *Mol Cell* **34**, 627 (2009).

46. R. Bernasconi *et al.*, *PLoS ONE* **5**, (2010).

47. J. Riemer *et al.*, *Proc Natl Acad Sci USA* **106**, 14831 (2009).

48. M. Sakoh-Nakatogawa, S.-I. Nishikawa, T. Endo, *J Biol Chem* **284**, 11815 (2009).

49. T. Ravid, S. G. Kreft, M. Hochstrasser, *EMBO J* **25**, 533 (2006).

50. G. Raposo, H. M. van Santen, R. Leijendekker, H. J. Geuze, H. L. Ploegh, *J Cell Biol* **131**, 1403 (1995).

51. M. L. Drumm *et al.*, *Science* **254**, 1797 (1991).

CHAPTER 5

Binding of unfolded proteins by the lectin Yos9 induces aggregation

Binding of unfolded proteins by the lectin Yos9 induces aggregation

Melanie H. Smith[1], Edwin H. Rodriguez[1], and Jonathan S. Weissman[1]

[1]Department of Cellular and Molecular Pharmacology, Graduate Group in Biophysics, California Institute for Quantitative Biosciences, Center for RNA Systems Biology, and Howard Hughes Medical Institute, University of California, San Francisco, 94158, California, USA.

Abstract

A substantial fraction of nascent proteins delivered into the endoplasmic reticulum (ER) never reach their native conformations. Eukaryotes use a series of complementary pathways to efficiently recognize and dispose of these terminally misfolded proteins. In this process, collectively termed ER-associated degradation (ERAD), misfolded proteins are retrotranslocated to the cytosol, polyubiquitinated and degraded by the proteasome. While there has been great progress in identifying ERAD components, how these factors accurately identify substrates remains poorly understood. The targeting of misfolded glycoproteins in the ER lumen for ERAD requires the lectin Yos9, which recognizes the glycan species found on terminally misfolded proteins. In a role that remains poorly characterized, Yos9 also binds the protein component of ERAD substrates. Here, we identified a 45kDa domain of Yos9 comprising residues 22-421 that is proteolytically stable, highly structured and able to fully support ERAD *in vivo*. *In vitro* binding studies show that $Yos9_{22\text{-}421}$ exhibits sequence specific recognition of linear peptides from the ERAD substrate, CPY*, and binds a model unfolded peptide, ΔEspP, and protein, Δ131Δ, in solution. Binding of Yos9 to these substrates results in their cooperative aggregation. While the physiological consequences of this substrate-induced aggregation remain to be seen, it has the potential to play a role in the regulation of ERAD.

Nascent proteins destined for the secretory pathway enter the specialized environment of the endoplasmic reticulum (ER) as linear polypeptides that must fold into their native conformations. The complex topologies and numerous domains of many secreted proteins in conjunction with their high flux into the ER make folding of these proteins particularly challenging. Even with chaperone assistance, some of these proteins are not able to reach their native states and are considered terminally misfolded. To prevent transit of these nonfunctional proteins through the secretory system as well as formation of detrimental aggregates, eukaryotes efficiently eliminate them via a series of conserved pathways termed ER-associated degradation (ERAD). These pathways use multiple factors to recognize misfolded proteins and retrotranslocate them into the cytoplasm where they are ubiquitinated by the E3 ubiquitin ligase Hrd1 and degraded by the proteasome.

The ERAD machinery faces a challenging problem in specificity. Insufficient degradation causes accumulation of misfolded proteins, which is associated with disease, including neurodegenerative diseases such as Alzheimer's (1), while excessive degradation causes the loss of potentially functional proteins as in cystic fibrosis (2). To ensure efficient disposal of misfolded glycoproteins found in the ER lumen, cells employ a two-part commitment signal. These ERAD substrates must display glycans with a terminal α1,6-linked mannose (3–5) as well as unfolded protein determinants that remain poorly defined (6). These requirements have been primarily characterized for the model substrate CPY*, which is the G255R variant of budding yeast carboxypeptidase Y (CPY) that is misfolded and degraded via ERAD (7). CPY* has four glycans, of which the one closest to the carboxy (C)-terminus is necessary and sufficient to signal destruction of the full-length protein (4, 5). To effect ERAD of glycoproteins, the mannosidase Htm1 modifies substrate glycans (8), to reveal a terminal α1,6-linked mannose that

is subsequently recognized by the ER-resident lectin, Yos9 (3, 9–11). Yos9 binds this signal glycan via its well-conserved mannose receptor homology (MRH) domain, the selectivity of which was elucidated by the crystal structure of the MRH domain from the Yos9 human homolog, OS-9, in complex with α3,α6–mannopentaose (12). While the proper glycan is necessary for ERAD of glycoproteins, it is not sufficient; these ERAD substrates must also possess some misfolded character.

Members of a "luminal surveillance complex" recognize the protein determinant required for ERAD, recruit substrates to Hrd1-associated machinery, and activate downstream events that commit substrates for degradation (13, 14). These events are orchestrated by Kar2, an ER-localized Hsp70, Hrd3, a membrane-bound component of the Hrd1 complex, and Yos9. As a chaperone, Kar2 plays a crucial role in maintaining the solubility of ERAD substrates prior to retrotranslocation (15). Hrd3 binds CPY* (14, 16) and has been proposed to act as a substrate recruitment factor for the Hrd1 ligase given its role in stabilizing (17, 18) and activating (14) the Hrd1 ligase. Yos9 is also able to directly interact with CPY* and this binding is independent of its activity as a lectin. Previous work has shown that both wild type and a lectin mutant (R200A) of Yos9 immunoprecipitate CPY* with or without its glycans (9, 13, 19). Following from these findings, Yos9 has been proposed to have additional roles in which it retains misfolded proteins in the ER (19, 20) and facilitates degradation of non-glycosylated proteins (21).

Given that Yos9 can bind both the signal glycan as well as misfolded protein determinants, we hypothesized that Yos9 may contribute to the integration of both signals required for ERAD. In order to explore this possibility, we characterized the binding of misfolded proteins by Yos9 *in vitro*. Using both the full length protein as well as a proteolytically-derived variant of Yos9 that is functional *in vivo*, we show that Yos9 exhibits

sequence specific recognition of linear peptides from CPY* and that binding either a model unfolded protein or peptide *in vitro* results in the aggregation of Yos9 with its binding partner. This substrate-induced aggregation constitutes a novel property of Yos9 that has the potential to be biologically important for its function in ERAD.

EXPERIMENTAL PROCEDURES

Limited Proteolysis of Yos9 – Limited proteolysis was carried out by treating 100 µg of purified Yos9 with 0.005 units elastase (5 µL of 1 unit/mL where 1 unit is define by 9.6 units/mg) in a 250 µL reaction (10 mM Hepes, 150 mM NaCl, 1 mM $CaCl_2$, 10% glycerol, pH 7.4) for 2.5 hr at 23°C mixing continuously at 500 rpm. The reaction was quenched by the addition of guanidine chloride crystals until saturation and run on a gel, which was stained with Coomassie blue R250. Bands were cut out and mass spectrometry was performed by the lab of David King (UC Berkeley). The mass of the predominant cleavage product was confirmed to be 45401-45403 Da. For comparison $Yos9_{22\text{-}421}$ is calculated to be 45407 Da.

Yos9 Purification and Refolding – HIS-tagged Yos9 or $Yos9_{22\text{-}421}$ was purified as described previously (3) with the exception that the gel filtration was done in 10 mM HEPES, 150 mM NaCl, pH 7.4.

Circular Dichroism Spectroscopy – Measurements were conducted on a Jasco J-715 spectrometer in a 2 mm cuvette at 20°C. Samples contained 0.05 mg/mL $Yos9_{22\text{-}421}$ in 0.1 M sodium phosphate (pH 7.4). The spectrum was recorded over the range of 195-250 nm at a scanning speed of 5 nm/min and a bandwidth of 1.0 nm.

Size Exclusion Chromatography (SEC) Multi-Angle Light Scattering (MALS) - Molecular weight determination for purified Yos9 and $Yos9_{22\text{-}421}$ was done by SEC (Shodex KW-803

column) with an Ettan LC (GE Healthcare) and in-line DAWN HELEOS MALS and Optilab rEX differential refractive index detectors (Wyatt Technology Corporation). Data were analyzed by the ASTRA V software package. SEC was performed in 10 mM Hepes, 150 mM NaCl, pH 7.4.

Cycloheximide Degradation Assays – Cycloheximide chase degradation assays were performed as previously described (3, 13). The HA epitope (on CPY*) was detected using 12CA5 monoclonal antibody (Roche) used at 1:1000. Hexokinase was used as a loading control and was detected by an anti-hexokinase antibody (US Biologicals) used at 1:1200.

Peptide Array – The peptide array (W1007 B) was made by the MIT Biopolymers Laboratory for the lab of Peter Walter. The CPY* tiling arrays was composed of 18mer peptides that tiled through the CPY* sequence by 3 amino acids at a time. To calculate the affinity of Yos9 for different amino acids, a larger tiled peptide array was used that included sequences from CPY*, mouse insulin, myelin protein zero, protein 8ab from SARS-CoV virus and peptides known to bind BiP (22, 23).

The arrays were processed according to a protocol described previously (24) with some modifications. The array was incubated in methanol for 10 min, then washed three times in buffer (10 mM Hepes, 150 mM NaCl, 0.05% Tween20, pH 7.4) for 10 min. The array was then incubated for 1 hour at room temperature with 1.1 μM $Yos9_{22\text{-}421}$. The array was then washed again three times for 10 min in the buffer above. Using a semi-dry transfer apparatus, bound $Yos9_{22\text{-}421}$ was transferred to a nitrocellulose membrane and detected with an anti-6xHis tag antibody (Abcam 3H2201). The array was stripped before re-use (25).

Fluorescence Anisotropy – Synthetic peptides (Elim Biosciences) were purified to >90% purity and the identities were confirmed by mass spectrometry. Peptides were labeled with the

fluorophore fluorescein amidite (FAM). The following peptides were used in this study: ΔEspP-FAM (MKK HKR ILA LCF LGL LQS SYS FA K(5-FAM)-NH2); ΔEspP (MKK HKR ILA LCF LGL LQS SYS AAK KKK)

For binding of Yos9 to ΔEspP-FAM, changes in fluorescence anisotropy were measured on a Spectramax-M5 plate reader using a protocol described previously (24). Increasing concentrations of Yos9 were added to 50 nM FAM-labeled peptides in 20 μL reactions and after a 30 min incubation, readings were made with λ_{ex} = 485 nm and λ_{em} = 525 nm. Anisotropy values are reported as an average of 3 separate titrations.

For binding of Yos9 to Δ131Δ labeled with the fluorophore 5-((((2-iodoacetyl) amino) ethyl) amino) naphthalene-1-sulfonic acid (IAEDANS), changes in fluorescence anisotropy were measured on a Jobin Yvon fluorometer with excitation and emission monochromator slits both set to 7 nm, an integration time of 1 sec and with λ_{ex} = 340 nm and λ_{em} = 480 nm. Increasing concentrations of Yos9 were added to 1.25 μM Δ131Δ. Values are reported as an average of 4 readings. IAEDANS-labeled Δ131Δ was donated by the Agard Lab and made as described previously (26).

For both ΔEspP-FAM and IAEDANS-labeled Δ131Δ data sets, anisotropy (r) values were calculated from Equation 1,

$$r = \frac{I_{para} - I_{perp}}{I_{para} + (2 * I_{perp})} \quad (1)$$

where I_{para} and I_{perp} are the measured intensities when the excitation and emission polarizers are parallel or perpendicular, respectively. Binding constants were calculated by fitting the data to Equation 2,

$$r_{total} = r_{free} + (r_{bound} - r_{free}) \frac{[Yos9]^n}{[Yos9]^n + K_d} \quad (2)$$

where [Yos9] is the concentration of Yos9, n is the Hill coefficient (assumed to be 1 for the case of Yos9 at low concentrations) and K_d is the dissociation constant. The variables r_{free} and r_{bound} were fixed to the anisotropy of the peptide alone and the maximum anisotropy observed in the presence of Yos9, respectively.

Purification of ^{15}N-Labeled Δ131Δ and Nuclear Magnetic Resonance (NMR) Spectroscopy – The expression and purification of Δ131Δ from *Escherichia coli* were performed as described previously (27) with the following modifications for isotopic labeling. Δ131Δ was expressed beginning with a 20 mL overnight starter culture in LB that was spun down and resuspended in 1L of M9 minimal growth media supplemented with 1 g/L ^{15}N ammonium chloride and 0.5 g/L ISOGRO growth supplement (Sigma).

HSQC data of Δ131Δ in buffer (25 mM MES, 150 mM NaCl, pH6) were acquired on the UC Berkeley 900 MHz spectrometer with a cryoprobe using a fast HSQC pulse sequence from Mark Kelly (UCSF). An initial HSQC of 143 μM Δ131Δ was acquired followed by HSQC after serial additions of $Yos9_{22-421}$. Data was processed with NMRPipe (28) and peak height analysis was performed with the ccpn analysis software (http://www.ccpn.ac.uk/). Δ131Δ assignments were transferred from a previously published study (29).

Dynamic Light Scattering (DLS) – DLS measurements were done on a DynaPro MS/X light scattering instrument (Wyatt Technology). The laser is 55 mW laser and 826.6 nm; detection angle is 90°. Samples were prepared in 10 mM Hepes, 100 mM NaCl, 1 mM $CaCl_2$, 10 mM $MgCl_2$, pH 7.4 and solutions were filtered immediately prior to mixing. The laser power was 100%. Data was analyzed with Dynamics V6 software. Histograms represent the average of 3 independent data sets (except for $Yos9_{22-421}$ plus bovide serum albumin (BSA) for which there

was only a single measurement at the specified concentration) each with at least 10 measurements.

Aggregate Centrifugation Assay – Protein solutions were centrifuged for 15 min at 20,000 g after which the supernatant was separated from the pellet. SDS-loading buffer was added to samples and they were run on a 4-12% SDS-PAGE gel in MES buffer followed by staining with Coomassie blue R250.

RESULTS

A truncated variant of Yos9 is folded and functional in vivo – In order to assist in the biophysical characterization of Yos9, we sought to define a compact, stable domain that retained functionality *in vivo*. To this end, we carried out limited proteolysis of purified, recombinant Yos9. Using elastase, we identified a well-defined 45 kDa fragment that by mass spectrometry corresponded to residues 22-421 (Fig. 1A,B) and was similar to a truncation variant previously shown to be structured by circular dichroism (30). This fragment, $Yos9_{22\text{-}421}$, does not include the signal sequence or C-terminal residues that are part of a region predicted to be disordered by FoldIndex (31). Importantly, when integrated into the genome in place of the full-length protein, $Yos9_{22\text{-}421}$ facilitates CPY* degradation in a manner indistinguishable from full-length Yos9 (Fig. 1C). Thus, $Yos9_{22\text{-}421}$ represents a compact, folded domain that is sufficient to support Yos9-mediated degradation of a glycoprotein *in vivo*.

In vitro, $Yos9_{22\text{-}421}$ also behaved similarly to the full-length protein. Following renaturation, recombinant $Yos9_{22\text{-}421}$ appeared folded by circular dichroism in agreement with previous studies (3, 30) indicating secondary structure similar to that of the full-length protein (Fig. 1D). In addition, $Yos9_{22\text{-}421}$ binds fluorescently labeled mannotriose with an affinity similar

to that observed for Yos9 (supplemental Fig. S1). Currently there is no consensus in the literature regarding the oligomeric state of Yos9 (3, 30). Previous work hypothesized that Yos9 exists as a trimer (3), but this was based on its volume of elution from a size exclusion column, which may have overestimated the molecular weight due to the presence of disordered regions. In another study, the crystal structure of a portion of Yos9 ($Yos9_{266-424}$) showed that it could form a dimer (30). The authors confirmed this interaction via solution measurements *in vitro*, but could not detect the dimer or find evidence of its function *in vivo* (30). We determined the molecular weight of both full-length and $Yos9_{22-421}$ in solution using size exclusion chromatography multi-angle light scattering (SEC-MALS) and found that these weights were consistent with both species existing as monomers (Fig. 1E). While the molecular weights were constant over a range of concentrations (8 - 116 μM), it is possible that a low affinity dimer could dissociate within the SEC column producing the observed results.

$Yos9_{22-421}$ binds specific regions of CPY in vitro* – To determine if Yos9 specifically recognizes protein components of an ERAD substrate, we first identified binding sites for Yos9 along the sequence of CPY*. Using a peptide array created by tiling along the entire sequence of CPY*, we queried the binding of $Yos9_{22-421}$ to specific 18 amino acid segments of CPY* presented as linear epitopes (as they might be encountered in the context of an unfolded or misfolded protein) (Fig. 2A). We quantified the observed binding pattern by averaging Yos9 binding intensities for each amino acid along the sequence of CPY* and found that $Yos9_{22-421}$ exhibited a binding signature highlighting four regions of enhanced affinity (Fig. 2B). This signature also appears to be specific as Ire1, the luminal sensor for the unfolded protein response (UPR), shows a different binding signature with the same CPY* peptide array (24). Although none of the CPY* peptides were glycosylated, $Yos9_{22-421}$ bound to areas near the positions of the

second, third and fourth glycans as well as near the region that Ire1 binds most strongly (24). An analysis of the amino acid composition of the peptides bound suggested that $Yos9_{22\text{-}421}$ preferentially binds peptides rich in leucine, arginine and lysine (supplemental Fig. S2). The predilection for basic residues may be informative but should be interpreted with caution since the isoelectric point of Yos9 is 4.79.

Yos9 binds a model misfolded peptide and protein in solution – While we wanted to verify the binding of peptides from the CPY* array in solution, many of the peptides attached to the array were unlikely to be soluble. Therefore, we turned to two well-studied models of unfolded proteins, the peptide ΔEspP and the protein Δ131Δ, which are both soluble in spite of the fact that one is a peptide with hydrophobic character and the other exists in a predominantly unfolded state.

ΔEspP is a 24 amino acid peptide derived from a signal sequence that is "moderately hydrophobic but unusually basic" (32). The solubility imparted by the basic residues has made it useful for studying binding by both the signal recognition particle (32) and the UPR sensor Ire1 (24). We measured the affinity of Yos9 for ΔEspP modified with the fluorescein derivative FAM using fluorescence anisotropy. Yos9 bound ΔEspP-FAM with an affinity of $K_d = 0.94 \pm 0.26$ μM when fit to a noncooperative binding curve (Fig. 3A). The truncated version $Yos9_{22\text{-}421}$ also bound ΔEspP-FAM ($K_d = 2.27 \pm 0.58$ μM). The affinity of Yos9 for ΔEspP-FAM was greater than that of BSA for the peptide ($K_d = 3.53 \pm 1.25$ μM) and the latter interaction was weakened substantially by the addition of detergent indicating that it was likely due to nonspecific interactions.

In order to determine if ΔEspP bound Yos9 at a single saturable site, we attempted to compete fluorescently labeled ΔEspP-FAM off of Yos9 with unlabeled ΔEspP. When pre-

incubating either 1 or 10 μM Yos9 with 50 nM ΔEspP-FAM and titrating ΔEspP up to 250 μM, we did not observe the decrease in anisotropy expected if ΔEspP displaced ΔEspP-FAM on Yos9 (addressed further below). Therefore, we turned to another model misfolded substrate, Δ131Δ, to determine if Yos9 contains a unique site for substrate binding and if it binds a specific portion of the substrate.

Δ131Δ is a 131-residue fragment of staphylococcal nuclease (149 residues in full length) that is globally unfolded but compact (27, 29, 33). Its residual structure has been extensively characterized by NMR spectroscopy, and due to its well-dispersed HSQC spectrum, one can readily map regions of Δ131Δ that interact with binding partners. This was recently illustrated with the chaperone Hsp90, which recognizes Δ131Δ via a single region (26). We first determined if Yos9 bound Δ131Δ using fluorescence anisotropy. Full-length Yos9 bound Δ131Δ modified with the fluorophore IAEDANS with an apparent affinity of K_d = 38.8 ± 6.7 μM (Fig. 3B).

We next attempted to identify where Yos9 bound along the sequence of Δ131Δ. Using NMR, we acquired an HSQC titration series of Δ131Δ with increasing concentrations of $Yos9_{22-421}$ (Fig. 4A). As we added $Yos9_{22-421}$, peaks on the Δ131Δ spectrum uniformly lost intensity. Using 41 unambiguously assigned peaks, we calculated peak heights associated with Δ131Δ residues as increasing amounts of $Yos9_{22-421}$ were added (Fig. 4B). The simultaneous loss of peak intensity along the entire sequence of Δ131Δ is consistent with either multiple nonspecific contacts between $Yos9_{22-421}$ and Δ131Δ or increasing aggregation as they approached equimolar concentrations.

Yos9 forms aggregates in the presence of binding substrate - To directly assess if Yos9 formed aggregates with Δ131Δ, we used DLS, which can be used to derive the hydrodynamic radius of a species in solution. DLS measurements showed that Yos9, $Yos9_{22-421}$ and Δ131Δ did

not aggregate when alone in solution (Fig. 4C), but when mixed at or above concentrations of 1 μM they reproducibly formed large aggregates (Fig. 4D). The aggregation is highly cooperative, as we did not observe oligomers of intermediate sizes with a range of Yos9 and Δ131Δ concentrations (supplemental Fig. S3). Yos9 also aggregated in the presence of ΔEspP, which may explain the inability of ΔEspP to compete ΔEspP-FAM off of Yos9 in the anisotropy experiments. Of note, in some batches of ΔEspP, it formed oligomers on its own and DLS experiments with ΔEspP should be interpreted with caution. Importantly, Yos9 did not form aggregates in the presence of BSA (Fig. 4D).

While it appeared that Yos9 selectively aggregated in the presence of binding substrates, we were not able to identify conditions that attenuated this process; changes in solution conditions such as salt, pH, magnesium (which stabilizes Δ131Δ) and calcium (which stabilizes some ER resident proteins) did not impact aggregation. We also used available structural data for a portion of Yos9 to probe the affect of targeted mutations on aggregation. The crystal structure of $Yos9_{266-424}$ shows it arranged as a dimer in the asymmetric unit in which each monomer contains a hydrophobic groove that could potentially accommodate an extended polypeptide (30). We reasoned that either interactions with itself through the dimer interface or with substrate through the putative binding groove could drive aggregation. We recombinantly expressed two Yos9 variants with mutations in conserved residues in either the dimer interface (F383A/L393D) or the hydrophobic groove (Y318A/I377A/L329A) and found that both aggregated in a manner indistinguishable from wild type Yos9 (supplemental Fig. S4).

In an independent measure of aggregation propensity, we assessed the degree with which Yos9 and Δ131Δ form aggregates that can be cleared by centrifugation. Alone in solution, $Yos9_{22-421}$ and Δ131Δ stay in the supernatant when centrifuged, but upon mixing, some portion

of each comes down in the pellet (Fig. 4E). This was observed at concentrations as low as 1 μM. Of note, although the aggregates were composed of both proteins in all cases, Δ131Δ was more abundant than Yos9 in the pelleted fraction.

DISCUSSION

Yos9, an essential lectin in glycoprotein ERAD, binds glycans specifically found on terminally misfolded proteins in the ER. While this role has been characterized in a number of studies (3, 9–11), Yos9 also engages the protein component of misfolded proteins, whose unfolded character is necessary to effect ERAD (9, 13). Here we explore how Yos9 recognizes this protein determinant and the potential consequences of this interaction. In order to facilitate biophysical characterization of Yos9, we defined a truncated variant that is compact, ordered, and fully functional in the degradation of CPY*. Removal of the disordered C-terminus via limited proteolysis gave a remarkably well-defined fragment, $Yos9_{21\text{-}422}$, that contains both portions of Yos9 for which there are known structures: $Yos9_{266\text{-}424}$ (30) and the MRH domain of the human homolog OS-9 (12), which corresponds approximately to Yos9 residues 117-239. The truncated variant characterized here may facilitate further structural studies that address all functions of Yos9 without the potential issues incurred by the conformational flexibility of the C terminus.

Our studies show that Yos9 exhibits sequence specificity when recognizing polypeptides. Binding of $Yos9_{21\text{-}422}$ to an array of CPY*-derived peptides presented as linear epitopes revealed four regions of CPY* preferentially bound by Yos9. The existence of multiple binding sites is consistent with the previous finding that local perturbations near any of the four glycans on CPY* allows the glycan proximal to the defect to signal degradation via ERAD (6). These

purturbations may function to simply unfold CPY* sufficiently to expose linear polypeptides that are bound by Yos9 while it surveys the identity of the adjacent glycan. Since protein-glycan interactions are generally weak and involve multiple contacts to increase the avidity of binding (34), Yos9 may use unfolded protein determinants as handles with which to facilitate the interrogation of glycan structures.

$Yos9_{22\text{-}421}$ preferentially binds sequences rich in hydrophobic and basic amino acids. While unfolded proteins are often identified via exposed hydrophobic regions that are normally buried within the core of folded proteins, the role of basic residues may not be as readily apparent. Yet, the ER Hsp70 chaperone BiP (Kar2 in yeast) is known to bind regions rich in both basic and hydrophobic residues (22, 23, 35–37). Although work with a number of CPY/CPY* fusions has shown that Yos9 and BiP have different binding specificities (19), Kar2 has been shown to recognize regions of CPY* involved in ERAD (6). Thus, Yos9 and BiP/Kar2 may broadly share some of the same binding principles, which is consistent with studies showing that Yos9 retains misfolded proteins in the ER in addition to its role as a lectin (19, 20).

Solution studies complementary to those with the peptide array revealed an unexpected characteristic of Yos9. Binding of Yos9 to a peptide, ΔEspP, or a longer unfolded protein, Δ131Δ, resulted in the cooperative formation of large-scale aggregates.

While aggregation complicates the interpretation of the binding data, it is an interesting phenomenon with potential functional significance. Multiple studies indicate that the oligomerization of the Hrd1 complex may play a role in the regulation of ERAD. Endogenous Hrd1 forms high molecular weight complexes whose formation is regulated by the transmembrane protein Usa1 (38, 39). This oligomerization is required for ERAD of soluble glycoproteins in yeast (40) and appears to be conserved in the mammalian system in which the

protein Herp binds HRD1 oligomers (41). While it remains unclear exactly how Hrd1 oligomerization regulates ERAD activity, it is possible that Yos9 may modulate this process when bound to substrate. The interaction of Yos9 with Hrd3 (13, 16, 38), which interacts with and is essential for the stability of Hrd1 (17, 18), may facilitate transfer of information from Yos9 to the Hrd1 complex.

Oligomerization also plays a central role in the regulation of another key pathway involved in responding to misfolded proteins: the UPR. Ire1, the primary sensor in the yeast UPR, is a transmembrane protein whose oligomerization in response to unfolded proteins helps activate downstream signaling pathways central to the UPR (42–45). Recently, it was shown that direct binding of peptides *in vitro* induces Ire1 oligomerization through a specific interface that may become exposed as a result of a substrate-induced conformational change (24). Yos9 could employ a similar mechanism to facilitate downstream signaling to the Hrd1 complex.

In summary, Yos9 exhibits striking aggregation exclusively in the presence of its binding substrates. The physiologic consequences of this process and how it may be modulated by other ERAD components such as Hrd1 and Hrd3 remain to be seen, but the structural characterization of a compact, stable Yos9 variant, such as $Yos9_{22\text{-}421}$, is a potential starting place to elucidate its physiologic roles.

Acknowledgements

We thank D. King for performing the mass spectrometry on the Yos9 fragment; M. Kelly for NMR assistance; T. Street, D. Agard, B. Gardner, and P. Walter for reagents and advice; E.Q. Toyama for helpful discussions; and Y.C. Liu, E. Costa, and J. Dunn for critical reading of the manuscript. This work was supported by the Howard Hughes Medical Institute (to J.S.W.), the Structural Basis of Protein Homeostasis Grant U01 GM098254 (to J.S.W.), the Gilliam Fellowship for Advanced Studies (to E.H.R.) and the Hertz Foundation Peter Strauss Fellowship (to M.H.S.).

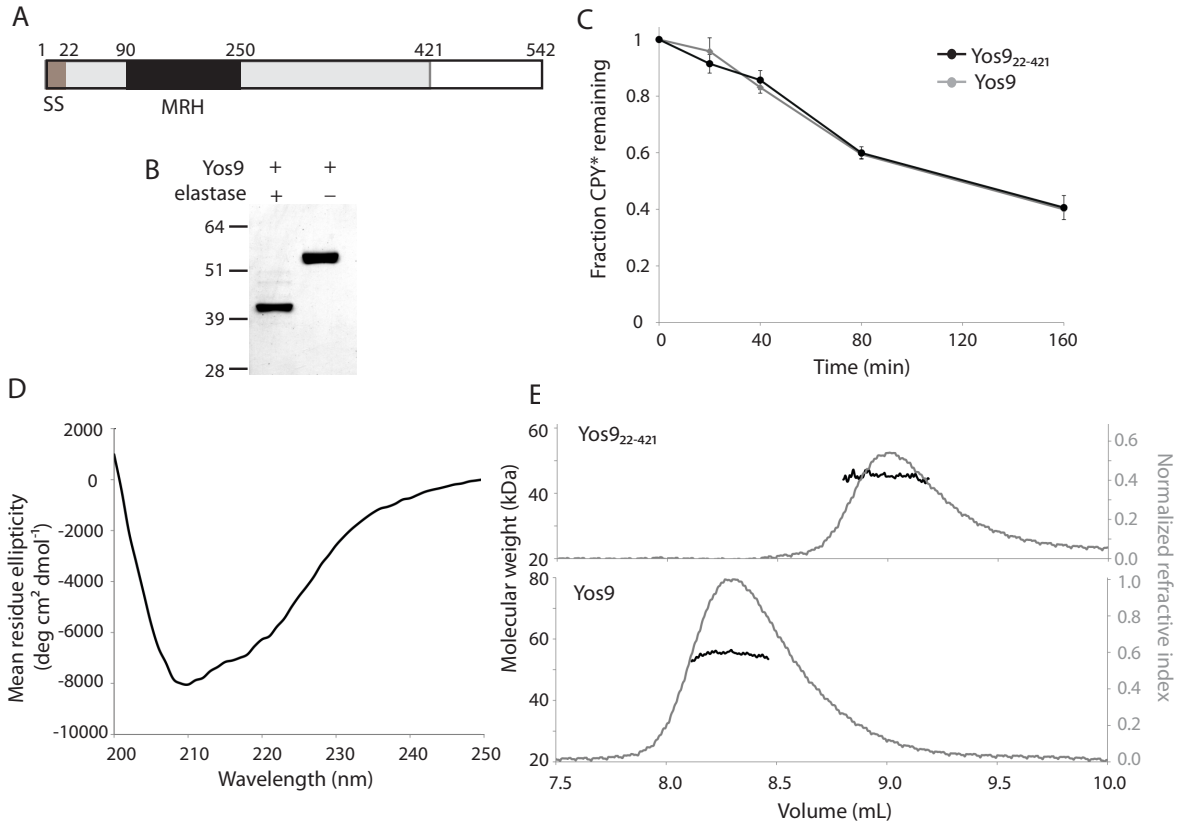


FIGURE 1. **A truncated variant of Yos9 is folded and functional.** *A*, a schematic of the Yos9 domain architecture. *Dark grey*, signal sequence (SS); *black*, mannose receptor homology (MRH) domain; *light grey*, truncated variant Yos9$_{22-421}$. *B,* limited proteolysis of Yos9 with elastase. *C,* degradation of CPY* after inhibition of translation with cycoheximide . *Grey*, wild type yeast ;*black*, genomic Yos9$_{22-421}$. *D,* circular dichroism spectra of Yos9$_{22-421}$. *E,* SEC-MALS of Yos9$_{22-421}$ (top) and Yos9 (bottom). *Black*, molecular weight; *grey*, normalized refractive index.

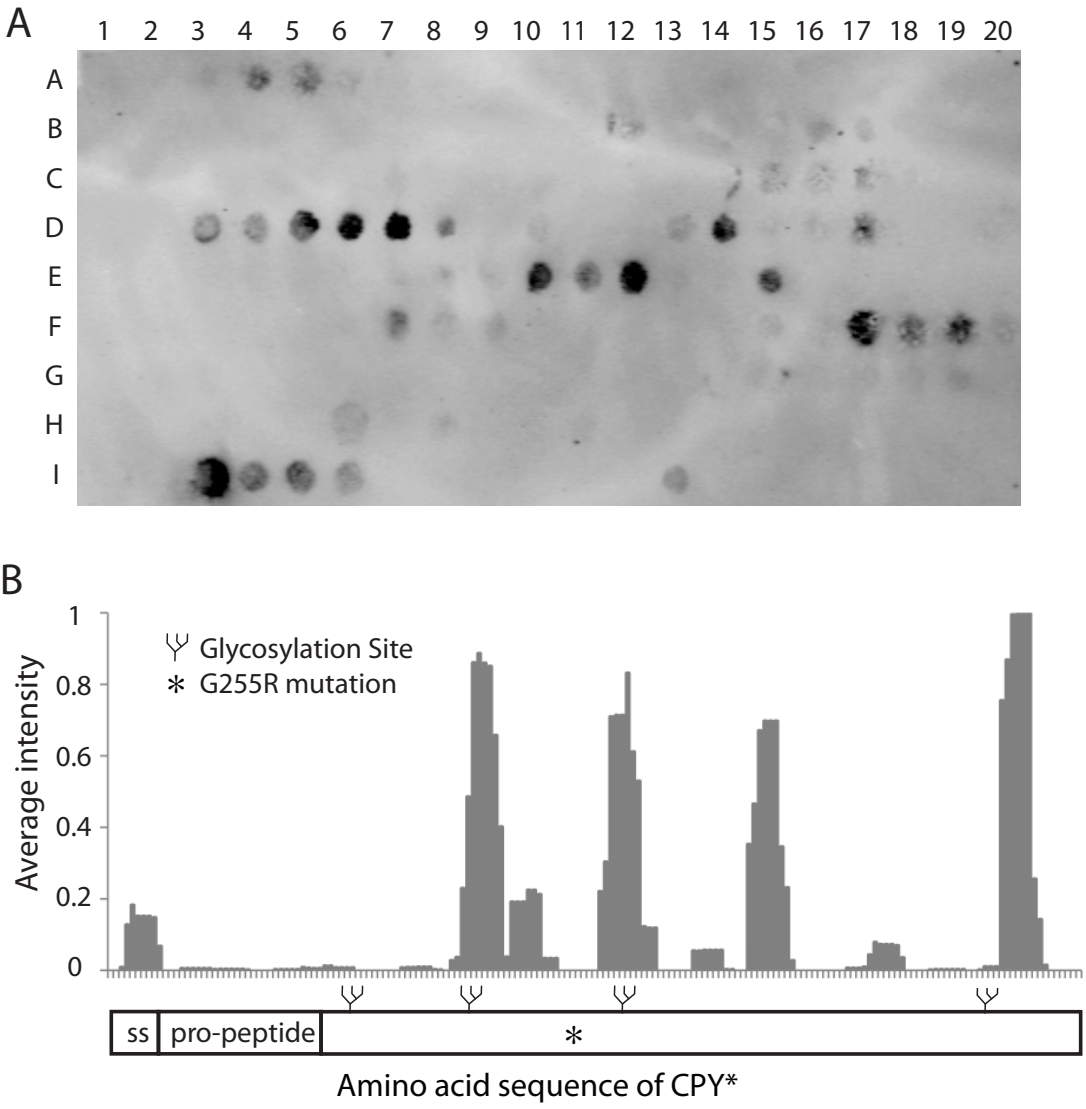


FIGURE 2. **Yos9$_{22\text{-}421}$ binds specific regions of CPY*.** *A,* binding of Yos9$_{22\text{-}421}$ to a peptide array tiling along the sequence of CPY* and detected with an anti-His antibody. *B,* quantification of Yos9$_{22\text{-}421}$ binding to each amino acid of CPY* by averaging the intensities of peptide spots containing a given amino acid. Ss, signal sequence.

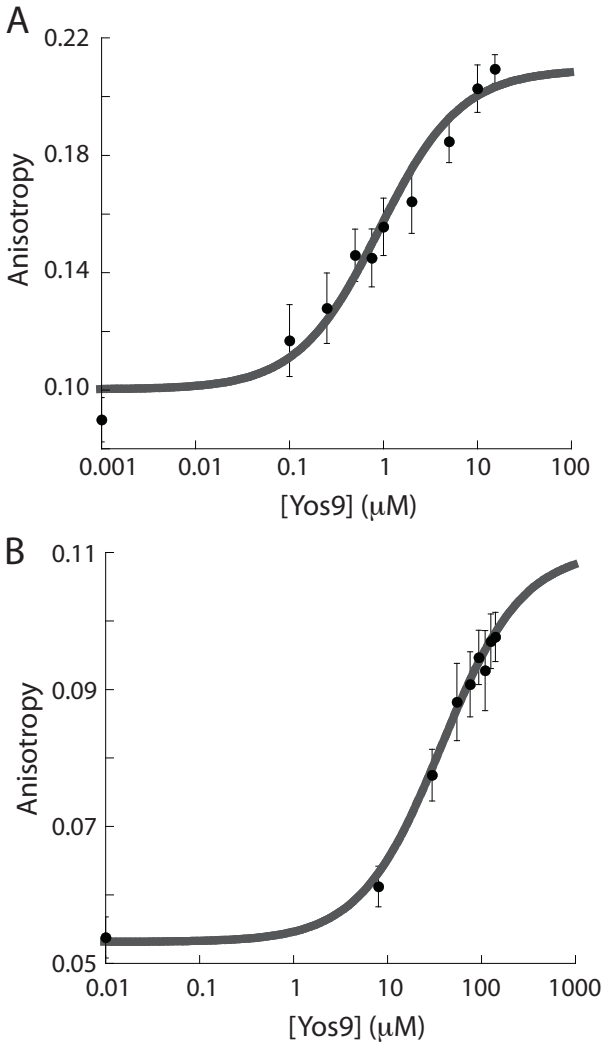


FIGURE 3. **Yos9 binds ΔEspP and Δ131Δ *in vitro*.** *A,* fluorescence anisotropy of 50 nM ΔEspP-FAM binding to Yos9. K_d is 0.94 ± 0.26 μM. *B,* fluorescence anisotropy of Yos9 titrated into 1.25 μM IAEDANS-labeled Δ131Δ. K_d is 38.8 ± 6.7 μM.

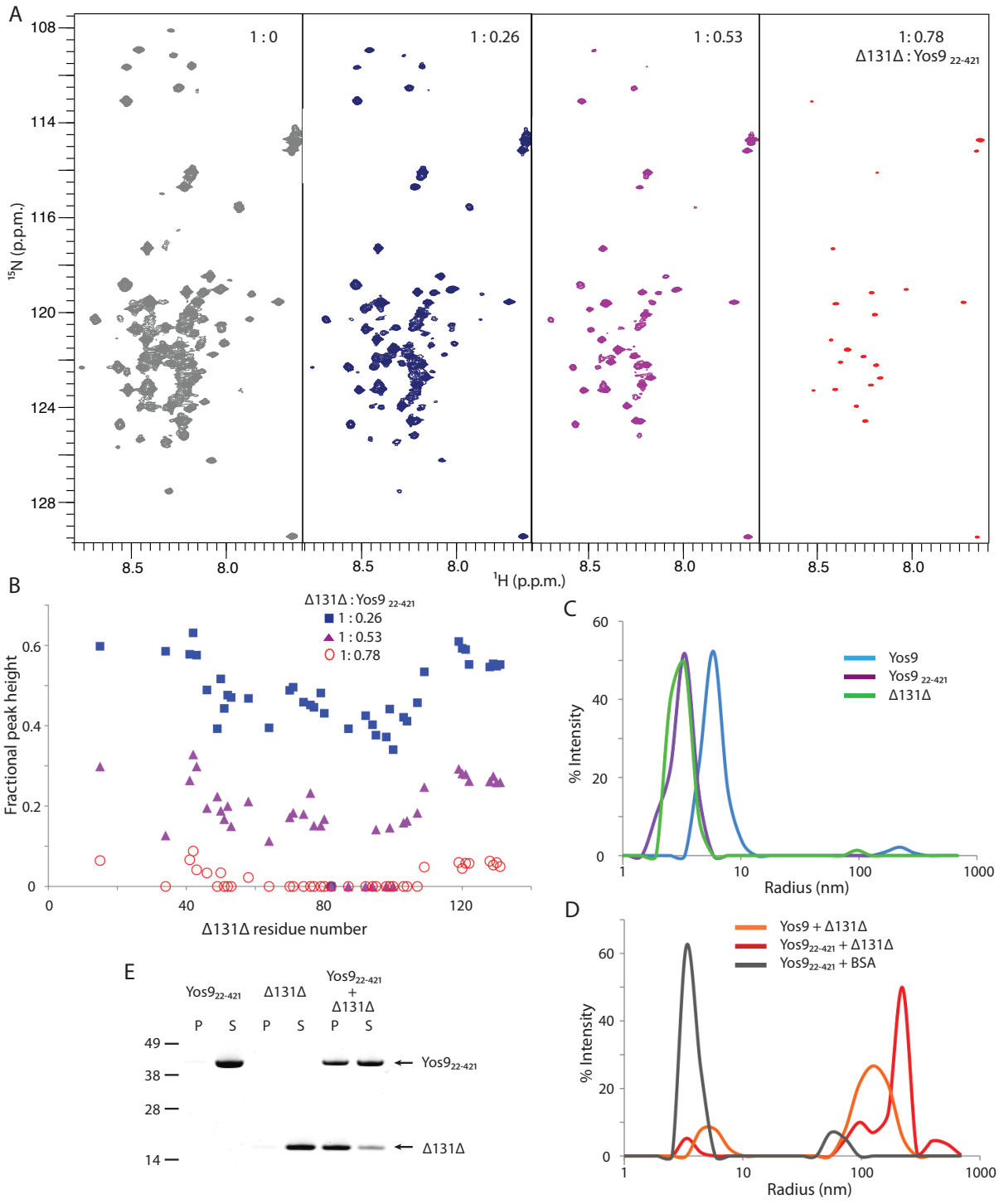


FIGURE 4. **Yos9 forms aggregates in the presence of binding substrate.** *A,* HSQC spectra of ^{15}N-Δ131Δ with the addition of increasing amounts of Yos9$_{22\text{-}421}$. Δ131Δ:Yos9$_{22\text{-}421}$ molar ratios are as follows: *grey*, 1:0; *navy*, 1:0.26; *purple*, 1:0.53; *red*, 1:0.78. *B,* intensity of Δ131Δ peak

height for each of the 41 assigned peaks after addition of $Yos9_{22\text{-}421}$. Peak height calculated as a fraction of that for Δ131Δ alone. *C and D,* DLS-derived values for the average hydrodynamic radius of the given species. *E,* samples of $Yos9_{22\text{-}421}$ and Δ131Δ alone or mixed were centrifuged and split into pellet (P) and supernatant (S) fractions.

SUPPLEMENTAL DATA

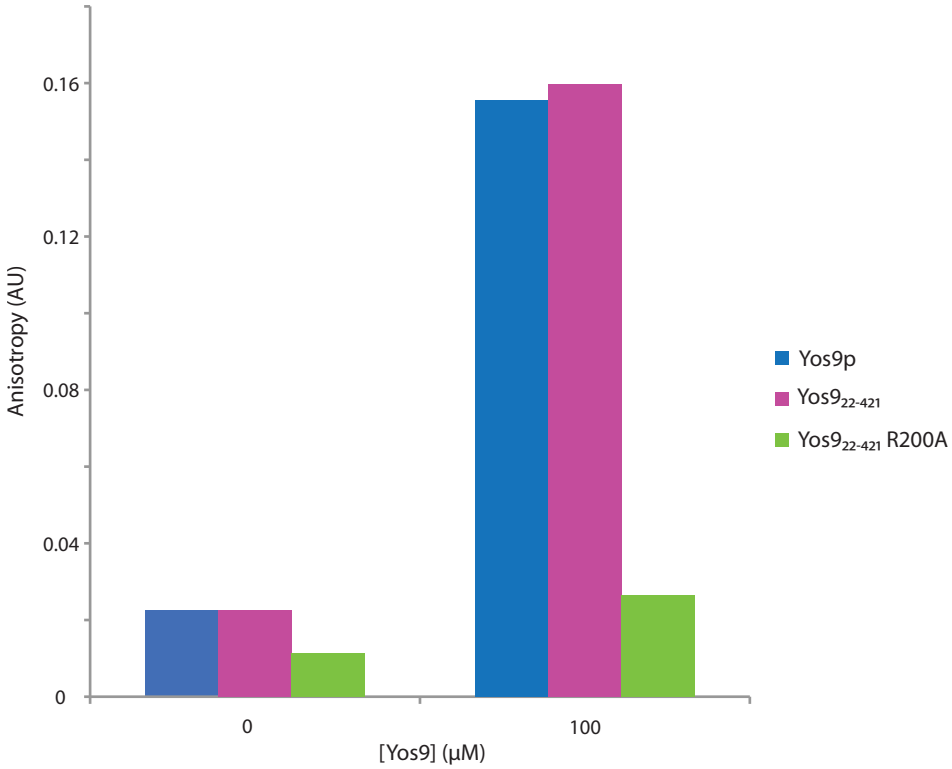


FIGURE S1. Binding of Yos9 to mannotriose (man_3)-fluorescein. Fluorescence anisotropy measurements with 50 nM man_3-fluorescein and 0.01 mg/mL BSA.

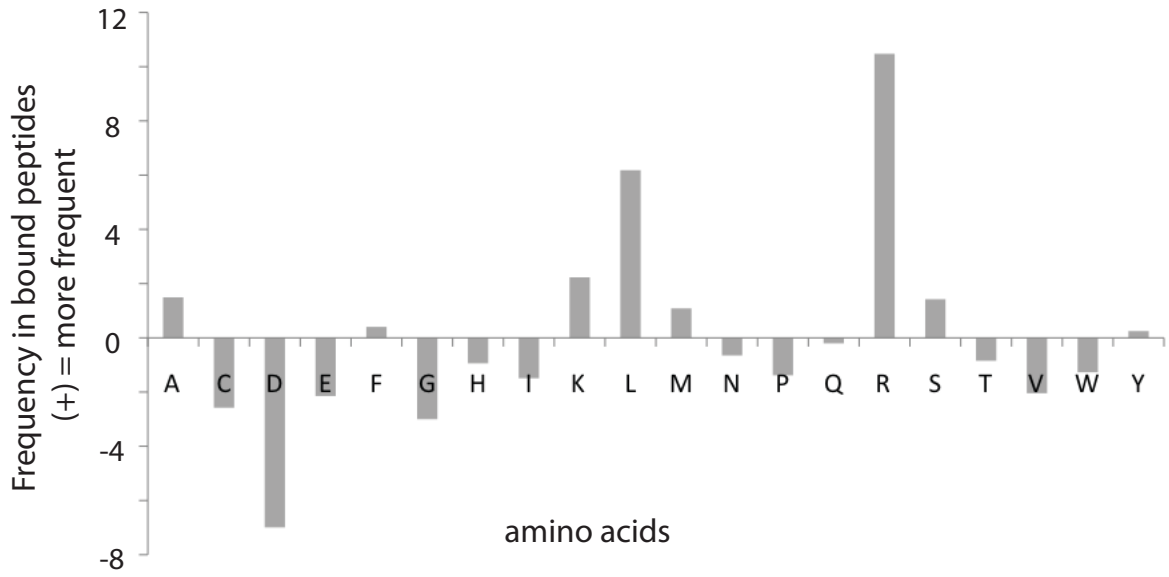


FIGURE S2. Amino acid composition of peptides bound by Yos9.

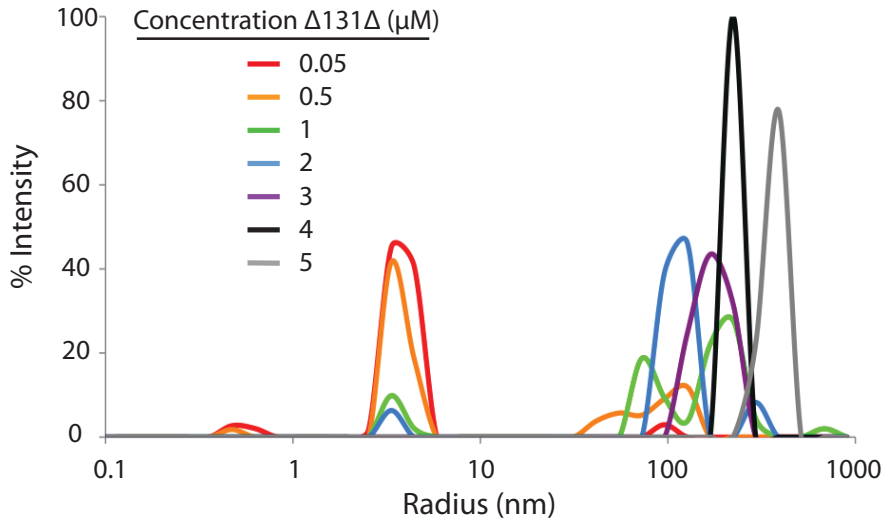


FIGURE S3. Yos9 aggregates cooperatively in the presence of Δ131Δ. DLS derived values for the average hydrodynamic radius of 5μM Yos9 with different concentrations of Δ131Δ as indicated in the figure.

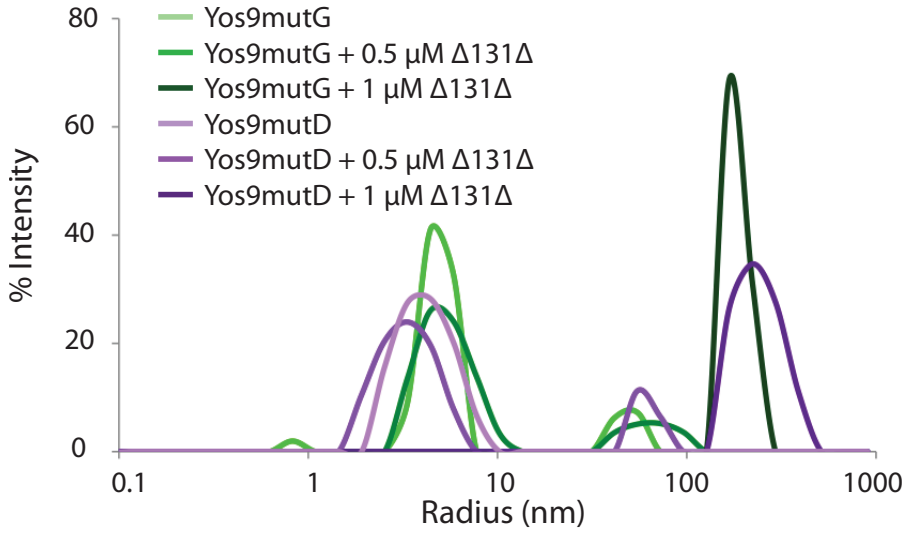


FIGURE S4. Yos9 mutants do not affect aggregation. DLS derived values for the average hydrodynamic radius of 5µM Yos9 mutants in the absence or presence of Δ131Δ as indicated in the figure. Yos9mutG, the Yos9 variant with mutations in the putative binding groove (Y318A/I377A/L329A); Yos9mutD, the Yos9 variant with mutations in the dimer interface (F383A/L393D).

References

1. Chiti, F. and Dobson, C.M. (2006) Protein misfolding, functional amyloid, and human disease. *Annu. Rev. Biochem.*, **75**, 333–366.

2. Younger, J.M., Chen, L., Ren, H.-Y., Rosser, M.F.N., Turnbull, E.L., Fan, C.-Y., Patterson, C. and Cyr, D.M. (2006) Sequential quality-control checkpoints triage misfolded cystic fibrosis transmembrane conductance regulator. *Cell*, **126**, 571–582.

3. Quan, E.M., Kamiya, Y., Kamiya, D., Denic, V., Weibezahn, J., Kato, K. and Weissman, J.S. (2008) Defining the glycan destruction signal for endoplasmic reticulum-associated degradation. *Mol. Cell*, **32**, 870–877.

4. Kostova, Z. and Wolf, D.H. (2005) Importance of carbohydrate positioning in the recognition of mutated CPY for ER-associated degradation. *J. Cell Sci.*, **118**, 1485–1492.

5. Spear, E.D. and Ng, D.T.W. (2005) Single, context-specific glycans can target misfolded glycoproteins for ER-associated degradation. *J. Cell Biol.*, **169**, 73–82.

6. Xie, W., Kanehara, K., Sayeed, A. and Ng, D.T.W. (2009) Intrinsic conformational determinants signal protein misfolding to the Hrd1/Htm1 endoplasmic reticulum-associated degradation system. *Mol. Biol. Cell*, **20**, 3317–3329.

7. Finger, A., Knop, M. and Wolf, D.H. (1993) Analysis of two mutated vacuolar proteins reveals a degradation pathway in the endoplasmic reticulum or a related compartment of yeast. *Eur. J. Biochem. FEBS*, **218**, 565–574.

8. Clerc, S., Hirsch, C., Oggier, D.M., Deprez, P., Jakob, C., Sommer, T. and Aebi, M. (2009) Htm1 protein generates the N-glycan signal for glycoprotein degradation in the endoplasmic reticulum. *J. Cell Biol.*, **184**, 159–172.

9. Bhamidipati, A., Denic, V., Quan, E.M. and Weissman, J.S. (2005) Exploration of the topological requirements of ERAD identifies Yos9p as a lectin sensor of misfolded glycoproteins in the ER lumen. *Mol. Cell*, **19**, 741–751.

10. Kim, W., Spear, E.D. and Ng, D.T.W. (2005) Yos9p detects and targets misfolded glycoproteins for ER-associated degradation. *Mol. Cell*, **19**, 753–764.

11. Szathmary, R., Bielmann, R., Nita-Lazar, M., Burda, P. and Jakob, C.A. (2005) Yos9 protein is essential for degradation of misfolded glycoproteins and may function as lectin in ERAD. *Mol. Cell*, **19**, 765–775.

12. Satoh, T., Chen, Y., Hu, D., Hanashima, S., Yamamoto, K. and Yamaguchi, Y. (2010) Structural basis for oligosaccharide recognition of misfolded glycoproteins by OS-9 in ER-associated degradation. *Mol. Cell*, **40**, 905–916.

13. Denic, V., Quan, E.M. and Weissman, J.S. (2006) A luminal surveillance complex that selects misfolded glycoproteins for ER-associated degradation. *Cell*, **126**, 349–359.

14. Gauss, R., Sommer, T. and Jarosch, E. (2006) The Hrd1p ligase complex forms a linchpin between ER-lumenal substrate selection and Cdc48p recruitment. *EMBO J.*, **25**, 1827–1835.

15. Nishikawa, S.I., Fewell, S.W., Kato, Y., Brodsky, J.L. and Endo, T. (2001) Molecular chaperones in the yeast endoplasmic reticulum maintain the solubility of proteins for retrotranslocation and degradation. *J. Cell Biol.*, **153**, 1061–1070.

16. Gauss, R., Jarosch, E., Sommer, T. and Hirsch, C. (2006) A complex of Yos9p and the HRD ligase integrates endoplasmic reticulum quality control into the degradation machinery. *Nat. Cell Biol.*, **8**, 849–854.

17. Gardner, R.G., Swarbrick, G.M., Bays, N.W., Cronin, S.R., Wilhovsky, S., Seelig, L., Kim, C. and Hampton, R.Y. (2000) Endoplasmic reticulum degradation requires lumen to cytosol signaling. Transmembrane control of Hrd1p by Hrd3p. *J. Cell Biol.*, **151**, 69–82.

18. Plemper, R.K., Bordallo, J., Deak, P.M., Taxis, C., Hitt, R. and Wolf, D.H. (1999) Genetic interactions of Hrd3p and Der3p/Hrd1p with Sec61p suggest a retro-translocation complex mediating protein transport for ER degradation. *J. Cell Sci.*, **112 (Pt 22)**, 4123–4134.

19. Izawa, T., Nagai, H., Endo, T. and Nishikawa, S. (2012) Yos9p and Hrd1p mediate ER retention of misfolded proteins for ER-associated degradation. *Mol. Biol. Cell*, **23**, 1283–1293.

20. Benitez, E.M., Stolz, A. and Wolf, D.H. (2011) Yos9, a control protein for misfolded glycosylated and non-glycosylated proteins in ERAD. *FEBS Lett.*, **585**, 3015–3019.

21. Jaenicke, L.A., Brendebach, H., Selbach, M. and Hirsch, C. (2011) Yos9p assists in the degradation of certain nonglycosylated proteins from the endoplasmic reticulum. *Mol. Biol. Cell*, **22**, 2937–2945.

22. Flynn, G.C., Chappell, T.G. and Rothman, J.E. (1989) Peptide binding and release by proteins implicated as catalysts of protein assembly. *Science*, **245**, 385–390.

23. Blond-Elguindi, S., Cwirla, S.E., Dower, W.J., Lipshutz, R.J., Sprang, S.R., Sambrook, J.F. and Gething, M.J. (1993) Affinity panning of a library of peptides displayed on bacteriophages reveals the binding specificity of BiP. *Cell*, **75**, 717–728.

24. Gardner, B.M. and Walter, P. (2011) Unfolded proteins are Ire1-activating ligands that directly induce the unfolded protein response. *Science*, **333**, 1891–1894.

25. Carter, J.M. and Loomis-Price, L. (2004) B cell epitope mapping using synthetic peptides. *Curr. Protoc. Immunol. Ed. John E Coligan Al*, **Chapter 9**, Unit 9.4.

26. Street, T.O., Lavery, L.A. and Agard, D.A. (2011) Substrate binding drives large-scale conformational changes in the Hsp90 molecular chaperone. *Mol. Cell*, **42**, 96–105.

27. Alexandrescu, A.T., Abeygunawardana, C. and Shortle, D. (1994) Structure and dynamics of a denatured 131-residue fragment of staphylococcal nuclease: a heteronuclear NMR study. *Biochemistry (Mosc.)*, **33**, 1063–1072.

28. Delaglio, F., Grzesiek, S., Vuister, G.W., Zhu, G., Pfeifer, J. and Bax, A. (1995) NMRPipe: a multidimensional spectral processing system based on UNIX pipes. *J. Biomol. NMR*, **6**, 277–293.

29. Alexandrescu, A.T. and Shortle, D. (1994) Backbone dynamics of a highly disordered 131 residue fragment of staphylococcal nuclease. *J. Mol. Biol.*, **242**, 527–546.

30. Hanna, J., Schütz, A., Zimmermann, F., Behlke, J., Sommer, T. and Heinemann, U. (2012) Structural and biochemical basis of Yos9 protein dimerization and possible contribution to self-association of 3-hydroxy-3-methylglutaryl-coenzyme A reductase degradation ubiquitin-ligase complex. *J. Biol. Chem.*, **287**, 8633–8640.

31. Prilusky, J., Felder, C.E., Zeev-Ben-Mordehai, T., Rydberg, E.H., Man, O., Beckmann, J.S., Silman, I. and Sussman, J.L. (2005) FoldIndex: a simple tool to predict whether a given protein sequence is intrinsically unfolded. *Bioinforma. Oxf. Engl.*, **21**, 3435–3438.

32. Peterson, J.H., Woolhead, C.A. and Bernstein, H.D. (2003) Basic amino acids in a distinct subset of signal peptides promote interaction with the signal recognition particle. *J. Biol. Chem.*, **278**, 46155–46162.

33. Wang, Y. and Shortle, D. (1995) The equilibrium folding pathway of staphylococcal nuclease: identification of the most stable chain-chain interactions by NMR and CD spectroscopy. *Biochemistry (Mosc.)*, **34**, 15895–15905.

34. Dam, T.K. and Brewer, C.F. (2004) Multivalent protein-carbohydrate interactions: isothermal titration microcalorimetry studies. *Methods Enzymol.*, **379**, 107–128.

35. Flynn, G.C., Pohl, J., Flocco, M.T. and Rothman, J.E. (1991) Peptide-binding specificity of the molecular chaperone BiP. *Nature*, **353**, 726–730.

36. De Crouy-Chanel, A., Kohiyama, M. and Richarme, G. (1996) Specificity of DnaK for arginine/lysine and effect of DnaJ on the amino acid specificity of DnaK. *J. Biol. Chem.*, **271**, 15486–15490.

37. Rüdiger, S., Germeroth, L., Schneider-Mergener, J. and Bukau, B. (1997) Substrate specificity of the DnaK chaperone determined by screening cellulose-bound peptide libraries. *EMBO J.*, **16**, 1501–1507.

38. Carvalho, P., Goder, V. and Rapoport, T.A. (2006) Distinct ubiquitin-ligase complexes define convergent pathways for the degradation of ER proteins. *Cell*, **126**, 361–373.

39. Horn, S.C., Hanna, J., Hirsch, C., Volkwein, C., Schütz, A., Heinemann, U., Sommer, T. and Jarosch, E. (2009) Usa1 functions as a scaffold of the HRD-ubiquitin ligase. *Mol. Cell*, **36**, 782–793.

40. Carvalho, P., Stanley, A.M. and Rapoport, T.A. (2010) Retrotranslocation of a misfolded luminal ER protein by the ubiquitin-ligase Hrd1p. *Cell*, **143**, 579–591.

41. Kny, M., Standera, S., Hartmann-Petersen, R., Kloetzel, P.-M. and Seeger, M. (2011) Herp regulates Hrd1-mediated ubiquitylation in a ubiquitin-like domain-dependent manner. *J. Biol. Chem.*, **286**, 5151–5156.

42. Shamu, C.E. and Walter, P. (1996) Oligomerization and phosphorylation of the Ire1p kinase during intracellular signaling from the endoplasmic reticulum to the nucleus. *EMBO J.*, **15**, 3028–3039.

43. Credle, J.J., Finer-Moore, J.S., Papa, F.R., Stroud, R.M. and Walter, P. (2005) On the mechanism of sensing unfolded protein in the endoplasmic reticulum. *Proc. Natl. Acad. Sci. U. S. A.*, **102**, 18773–18784.

44. Korennykh, A.V., Egea, P.F., Korostelev, A.A., Finer-Moore, J., Zhang, C., Shokat, K.M., Stroud, R.M. and Walter, P. (2009) The unfolded protein response signals through high-order assembly of Ire1. *Nature*, **457**, 687–693.

45. Li, H., Korennykh, A.V., Behrman, S.L. and Walter, P. (2010) Mammalian endoplasmic reticulum stress sensor IRE1 signals by dynamic clustering. *Proc. Natl. Acad. Sci. U. S. A.*, **107**, 16113–16118.

CHAPTER 6

Defining the core regulators of protein homeostasis in the mammalian endoplasmic reticulum

Defining the core regulators of protein homeostasis in the mammalian endoplasmic reticulum

Melanie H. Smith[1], Britt Adamson[1], Onn Brandman[2], and Jonathan S. Weissman[1]

[1]Department of Cellular and Molecular Pharmacology, and Howard Hughes Medical Institute, University of California, San Francisco, 94158, California, USA. [2]Department of Biochemistry, Stanford University, Stanford, 94305, California, USA

The endoplasmic reticulum (ER) is responsible for multiple cellular processes and plays a critical role in homeostasis. It is an important site of calcium storage, lipid synthesis, biogenesis of membranes for structures such as peroxisomes, autophagosomes and the nuclear envelope, as well as, regulation of proteins destined for the secretory pathway. All secreted and membrane proteins must traffic through the ER where they fold and acquire modifications, some of which facilitate sorting and delivery to the correct subcellular location. The ER is tuned to adapt to fluctuations in protein-folding requirements and responds to increased demand via two conserved pathways. One is ER-associated degradation (ERAD), discussed in chapters 4 and 5 of this thesis, which removes any folding-incompetent proteins from the ER to avoid congestion[1]. The other is the unfolded protein response (UPR), which both increases the folding capacity of the ER and decreases the load of imported proteins that require folding[2].

The UPR is a global cellular response best characterized in yeast through its activation in response to proteotoxic stress. In *Saccharomyces cerevisiae*, the UPR functions as a single linear pathway originating from the ER-resident sensor, Ire1p. Direct binding of unfolded proteins by Ire1p[3] results in activation of the transcription factor Hac1p, which subsequently translocates to the nucleus to activate target genes. A large-scale genetic screen using an UPR reporter identified the core regulators of ER protein homeostasis[4] and microarray analysis defined the transcriptional targets of the UPR[5]. These targets include a diverse set of genes involved in multiple processes, however, in aggregate, these studies illustrated that the yeast UPR can be understood through a relatively simple model of inputs and outputs explaining how the cell balances the folding capacity of the ER with the magnitude of the proteotoxic stress.

In metazoans, the UPR is greatly expanded into a complex network with three branches each employing its own ER-resident sensor and transcriptional regulator. The transmembrane

proteins, IRE1-α, PERK and ATF6-α, sense unfolded proteins and other markers of ER stress and activate separate cytosolic signaling pathways that result in distinct but overlapping programs of gene expression[6]. In the only branch homologous to the yeast UPR, unfolded proteins stimulate the kinase IRE1-α to oligomerize, autotransphosphorylate and activate its cytosolic RNase domain. This active nuclease splices a noncanonical intron from the *Xbp1* mRNA to produce a functional transcript that encodes the transcription factor XBP1, which targets genes involved in protein folding, ERAD and phospholipid synthesis (allowing for expansion of the ER). In addition, the nuclease also degrades mRNAs that encode membrane or secreted proteins in a process termed regulated IRE1-dependent decay (RIDD)[7]. In the second branch, the activated kinase PERK phosphorylates the eukaryotic translation initiation factor 2α (eIF2α) causing a global attenuation of protein synthesis. Phosphorylation of eIF2α also triggers the selective translation of mRNA encoding the transcription factor ATF4, which controls the levels of genes involved in antioxidant responses, amino acid metabolism, autophagy and apoptosis. Lastly, in the third branch, activation of ATF6 causes relocation to the Golgi where its cytosolic domain containing a basic leucine zipper (bZIP) transcription factor is released to upregulate genes primarily involved in ERAD as well as XBP1. Taken together, these pathways modify the cell so that it survives in conditions of excessive protein unfolding/misfolding or increased protein synthesis. Importantly, if these adaptive responses are insufficient, the UPR contains a safeguard to eliminate irreversibly damaged cells: it can trigger cell death via apoptosis[8].

The scenario created during the majority of UPR research, in which a harsh treatment activates all three branches, is likely to encompass only a subset of its cellular functions. The metazoan UPR is intricately linked to pathways outside of the realm of ER protein folding and

there is increasing evidence that it integrates many stimulating factors to effect diverse downstream responses[9]. The UPR is required in the course of normal physiology to meet the demands of diverse cell types and situations. For example, some secretory cells rely on sustained UPR signaling to perform their functions. In these cases, the UPR may alter folding capacity in anticipation of a future load as observed prior to the differentiation of secretory cells, which require a significant ER expansion[9]. Physiologic roles may also necessitate independent activation of specific branches: a scenario about which little is known given the dearth of sensor-specific UPR activators. While these physiological roles are likely to be important, there is no mechanistic understanding of how sustained, anticipatory or selective UPR activation might work.

Due to the complexities of the metazoan UPR and the difficulty of genetic manipulation of mammalian cells in comparison to yeast, the components that regulate ER protein folding as well as other processes central to ER homeostasis have not been systematically identified in mammalian organisms. While small-scale approaches have identified many key components (and especially those conserved from yeast), whole-genome screens similar to those carried out in yeast[4,10] have been largely avoided because of the size of the mammalian genome and the difficulty of scaling the available approaches. The fluorescent-based screening methods used in yeast do not transfer well to mammalian cells where the increased genome size makes a fluorescent readout extremely labor intensive. This is especially true when using small hairpin RNA (shRNA) libraries where multiple shRNAs per gene are required and the number of cells needed to assay knockdowns across the whole genome increases drastically. To accommodate these large numbers of cells, mammalian screens are ideally designed so that cells grow in a pooled format, which minimizes differences in the environments of cells with different genetic

perturbations. An approach that addresses these issues has the potential to greatly increase our understanding of the regulation of the UPR and, more generally, ER homeostasis in mammalian cells.

Using a new screening approach designed for use in mammalian cells, we seek to carry out a comprehensive characterization of the genetic networks that control mammalian ER protein homeostasis. More specifically, we will identify proteins that activate the UPR when depleted (known as UPR suppressors) through an unbiased loss-of-function screen. To do this, we will employ technologies recently developed to probe human pathways in cell culture on a whole-genome scale[11,12]. Researchers have created ultracomplex whole-genome shRNA libraries (~25 shRNAs per gene) that minimize the issues with false positives and negatives often associated with shRNA screens. These libraries can be used in pooled-format screens that when combined with a deep-sequencing-based readout allow maximal control over the cellular environmental and facilitate sample multiplexing[13]. In addition, this format allows rapid screening with the same shRNA library in different cell lines under a range of conditions. We set out to use this combination of ultracomplex shRNA libraries, pooled-format screening, and deep-sequencing readouts to create a new method in which we tie the activity of a pathway-specific reporter in a single cell to the knockdown of a single gene. As a first application of the method, we will use a well-established UPR reporter to establish a complete catalog of mammalian UPR suppressors.

Our method uses an RNA binding protein (RBP) with affinity for a specific RNA sequence to tie the activity of a UPR reporter to the identity of specific shRNAs in a whole genome shRNA library. In this screening approach, outlined in **Figure 1**, the RBP binding motif, known as its handle hairpin, is cloned next to the shRNA in a whole-genome library that is introduced into a mammalian cell line at a frequency of one copy per cell. The cell line features a

construction in which an XBP1-responsive promoter drives the expression of an affinity-tagged RBP such that the level of the RBP indicates the activity of the UPR and the co-immunoprecipitation (co-IP) of the RBP with its handle hairpin allows isolation of the shRNA. Therefore, the amount of a particular shRNA quantified through deep sequencing indicates the level of UPR activation resulting from the knockdown of the gene targeted by that specific shRNA. For example, an shRNA targeting BiP, the ER-resident Hsp70 chaperone, would expect to increase the load of unfolded protein in the ER of that cell and activate the UPR. The IP would isolate large amounts of the RBP as well as the associated shBiP RNA. In order to control for nonspecific changes in gene expression between cells, including those caused by shRNAs directly targeting factors involved in transcription or translation, we will introduce an RBP with a distinct affinity tag expressed under a constitutive promoter. We will do two IPs, one each for the induced and constitutively expressed RBPs, and calculate the level of RNA from the IP of the induced RBP as a ratio of that from the constitutively expressed RBP. This RBP-based methodology should allow increased efficiency and precision over the currently available reporter-based screens.

In designing the screening strategy, we considered three possible RNA binding proteins, the MS2 coat protein (MCP), the PP7 coat protein (PCP) and Csy4 (**Figure 2**). Csy4 is an endoribonuclease responsible for transcript processing in the CRISPR system involved in bacterial immunity in *Pseudomonas aeruginosa*[14]. It binds its substrate RNA with an extremely high affinity, the K_d is 50 pM[15], and a nuclease dead form (the mutant H29A) can be used to IP RNA of interest[16]. In addition to these attributes, Csy4 was an attractive candidate because the addition of imidazole rescues the RNase activity of the H29A mutant allowing a portion of the bound RNA to be selectively eluted[16]. In our system, this could have added a degree of

specificity beyond the IP and facilitated isolation of shRNAs for sequencing. Unfortunately, although it did not appear to be toxic to mammalian cells, the H29A variant of Csy4 was not well behaved *in vivo*. These issues prevented us from pursuing the use of Csy4 further.

Fluorescently tagged versions of MCP and PCP have been extensively used to visualize RNA in living cells and the binding of the coat proteins to their respective RNA handle hairpins has been well-characterized. The MCP/MS2 system has been the workhorse for microscopy of RNA in living cells since it was first used to visualize the localization of ASH1 mRNA in the yeast bud tip[17]. The MCP is a capsid protein from an RNA bacteriophage that infects *Escherichia coli* and binds the MS2 handle hairpin as a dimer[18]. This binding has endured much scrutiny and there exist a variety of mutants that modulate the affinity of the wild type protein-RNA pair, which is characterized by a dissociation constant of 3 nM[19]. In order to limit the assembly of the MCP into its native capsid structure, the dIFG mutant was created in which 13 residues were deleted from a 15 residue loop involved in the interaction between dimers in the virus particle[20]. In addition, the covalent linkage of two monomers ensures that the protein exists exclusively as a dimer. In this work, we use the forced-dimer V29I-dIFG MCP double mutant. The V29I-dIFG MCP monomer has a K_d of 0.4 nM with its handle hairpin[19].

The PCP is a viral coat protein analogous to MS2 derived from an RNA bacteriophage that infects *P. aeruginosa*. Binding of PCP to the PP7 handle hairpin involves interactions similar to those used by MCP to bind MS2, but the K_d of wild-type PCP for the PP7 RNA is 1 nM[21]. The crystal structure indicates that PCP binds its handle hairpin as a dimer and that dimers are covalently linked via disulfide bridges in the formation of the viral capsid[22]. The dimer can be fused to increase its stability[23] and the deletion of the loop containing the disulfide-forming

cysteines creates a mutant (ΔFG)[¶] that is deficient in capsid assembly[24]. Characterization of the PCP/PP7 interaction showed that the K_d is relatively invariant over a range of both pH and salt concentrations[25] and that there is maximal occupancy of PCP on the PP7 RNA[26]. These properties, the enhanced stability of the PCP dimer and its higher wild-type affinity for its handle hairpin may make PCP a better choice than MCP for both RNA labeling[26]. Although it is unclear if these properties will also make PCP superior to MCP for our purposes, we chose to focus on PCP for a number of our initial experiments.

Results

We began the development of our screening methodology by performing a number of important controls. We verified that the handle hairpin RNA could be pulled down via IP of the coat proteins. When PCP is used to visualize RNA *in vivo* via microscopy, the target RNA is expressed with 24 consecutive PP7 handle hairpins in the 3' UTR so that multiple fluorescently tagged PCP molecules bind to a single RNA and enhance the fluorescent signal. Since we will co-express two differently tagged PCP molecules per cell (to allow for a ratiometric readout), we would like the PCP to bind its RNA in a 1:1 ratio. Thus, we plan to use a single PP7 handle hairpin in our constructs. We co-expressed either 1x PP7 or 24x PP7 with PCP-Flag in 293T cells, performed a Flag IP and extracted RNA from the PCP sample eluted from the Flag affinity beads. We were able to selectively enrich for the handle hairpin RNA with both the 1x and 24x PP7, but we obtained 14 times more RNA with 24x PP7 handle hairpins as measured by qPCR (**Figure 3**). One important caveat in the interpretation of the 1xPP7 data is that we inadvertently incorporated a strong stem loop adjacent to the PP7 sequence in this construct that could

¶ Note: we did not use the ΔFG mutant in this work.

interfere with PCP binding. If the corrected 1x PP7 construct does not perform equivalently to the 24x PP7 one, we will determine the least number of PP7 handle hairpins needed to maximize enrichment of the target RNA while only engaging a single PCP.

Next, we showed that the presence of the handle hairpin near the shRNA did not affect the efficiency of shRNA-mediated gene knockdown. We made a series of constructs with the MS2 or PP7 handle hairpin either 3' or 5' of an shRNA against GFP (shGFP) and introduced them into a K562 cell line stabling expressing GFP (**Figure 4**). When compared to cells expressing an shRNA against GFP without an adjacent handle hairpin, the handle hairpins had no affect on GFP knockdown by the shGFP.

Another essential control is to determine if the coat proteins hold onto their handle hairpins during cell lysis and IP. If the coat proteins come off their RNAs and rebind to those from other cells during the IP, then the amount of the coat protein in a given cell will not be correctly related to the identity of the shRNA in that cell during the screen. To test for this possibility, we will express PCP-Flag and PCP-Strep each with the PP7 handle hairpin fused to a different barcode (BC1 or BC2) in two different cell cultures such that PCP-Flag will bind PP7-BC1 and PCP-Strep will bind PP7-BC2. We will then mix the two cell cultures, lyse the cells and do both a Strep and Flag IP. If we detect BC1 in the Strep IP or BC2 in the Flag IP, we will know that there is mixing of the coat proteins and their handle hairpins *in vitro*. We may be able to minimize this mixing by either modifications to the IP protocol or the addition of a cross-linking step prior to cell lysis.

In parallel to these controls, we characterized the UPR reporter that we will use in the screen. The unfolded protein response element (UPRE) promoter is a transcriptional target of the UPR and was originally termed 5xATF6 as it was thought to have a number of ATF6 binding

sites[27]. Work by a separate group showed that XBP1 preferentially binds to the promoter and renamed it the UPRE[28]. To determine the dynamic range of the UPRE, we made a K562 cell line expressing the fluorescent protein mCherry under the control of the UPRE promoter. By treating these cells with thapsigargin, a small molecule that interferes with protein folding through the disruption of calcium homeostasis in the ER, we could activate the UPRE and drive mCherry expression (**Figure 5**). A titration of thapsigargin demonstrated that the reporter activity corresponds to the load of unfolded proteins in the ER and that mCherry production as a result of UPRE activation peaked at around 12 hours. By mCherry fluorescence, we measured a 40 fold UPRE induction and when we used qPCR of mCherry to verify this measurement, we found an ~70 fold induction. We verified that thapsigargin activates the UPR in our cell line by measuring *xbp1* splicing.

We will create a cell line containing the UPRE reporter in which to perform the screen. By making a stable integration of the UPRE-RBP construct and selecting for a single clone, we will be able to maximize the dynamic range of the reporter and reduce heterogeneity. A large dynamic range will be especially important given that the shRNA-mediated knockdowns are unlikely to induce the UPR as strongly as treatment with thapsigargin. Since some aspects of mammalian ER homeostasis are well known, we can test shRNA-mediate depletion of known UPR suppressors or activators to verify the function of the UPR in our reporter cell line.

Discussion

Through the implementation of this unbiased screening approach, we can obtain information on multiple pathways that affect ER homeostasis in mammalian cells. In addition to identifying factors that have not previously been implicated in protein biogenesis, we will gain

insight into additional mechanisms of UPR activation. For example, the transmembrane domain of IRE1-α can sense abnormalities in membrane composition[29] and the membrane stress response can feed into the UPR[30]. Our screen will detect the key regulators of this and other aspects of cellular homeostasis sensed by IRE1-α.

While our initial screen will focus on the IRE1-α branch of the UPR, it can easily be extended to other branches through the use of different reporters. The UPR has predominantly been studied as a single entity, through the simultaneous activation of all three branches. Yet, to better understand the regulation of the metazoan UPR imparted by its expansion from that in yeast, we need to know how the branches work independently either in response to specific unfolded substrates or folding-independent stimuli. This is especially true for the ATF6-α and PERK branches where, given the lack of yeast homologs, it is unclear what issues they address. Broadening our understanding of the mammalian UPR through our XBP1 reporter as well as ATF6 and ATF4 reporters is likely to uncover branch-specific regulators that could become novel drug targets. Protein homeostasis is implicated in a growing number of prevalent diseases such as diabetes and cancer and targeting this network has the potential to yield a significant therapeutic affect[31].

The screening methodology described here is also well suited to the genetic dissection of any pathway of interest. The creation of reporter cell lines in which pathway-specific promoters drive the RBP allows efficient, high-throughput analysis of multiple pathways with a single shRNA library. This method is not limited to use with shRNAs and could be adapted for use with new gene repression technologies such as CRISPRi, which may even augment its efficacy[32,33]. Our screening methodology is versatile platform that will allow us to answer questions in mammalian cells that we could previously only address in yeast.

Acknowledgments

We thank Michael Bassik for the UPRE construct and helpful discussions about UPR reporters; Martin Kampmann and Max Horlbeck for shRNA constructs, advice on using the shRNA libraries, and the K562-GFP cell line; Marvin Tanenbaum in the lab of Ron Vale at UCSF for MCP/MS2 and PCP/PP7 constructs; Jacqueline Villalta for the RNA extraction protocol; Diego Acosta-Alvear for the *xbp1* splice detection protocol; and Samuel Sternberg in the lab of Jennifer Doudna at UC Berkeley for advice on using Csy4. This work was supported by the Howard Hughes Medical Institute (JSW), the Hertz Foundation Peter Strauss Fellowship (MHS) and the Damon Runyon Cancer Research Foundation (BA).

Experimental Procedures

RBP Immunoprecipitation

The IP protocol was modified from that previously described for IP of MCP with its bound RNAs[34]. Cell culture of either 293T or K562 were grown in mid-log phase and harvested by centrifugation. Cell pellets were washed with cold PBS and frozen at -80 °C prior to further use. Cells were lysed with cold lysis buffer (50 mM Tris–HCl pH 7.5, 150 mM KCl, 0.5% Igepol CA-630, 5% Glycerol, 1 mM EDTA, 5 mM $MgCl_2$, 1X protease inhibitors (Roche), and RNasin Ribonuclease Inhibitor (Promega)) for 10 min on ice. Lysate was cleared of cell debris by centrifugation at 10,000 x g for 15 minutes at 4 °C to yield the whole cell extract. To immunoprecipitate the FLAG-tagged construct, 40 μL pre-equilibrated anti-FLAG M2 magnetic beads (Sigma M8823) was added to 300 μL of the whole cell extract and incubated at 4°C for 1 hour with nutation. Beads were pelleted with a magnetic separator and the immunoprecipitates were washed once with 500 μL wash buffer (50 mM Tris–HCl pH 7.5, 150 mM KCl, 0.5% Igepol CA-630, 5% Glycerol, and 1 mM EDTA), twice with 500 μL wash buffer with 500 mM KCl, and once more with 500 μL low salt wash buffer. The bound protein was eluted by the addition of 1 mg/mL 3XFlag peptide (Sigma F4799) at 5X packed bead volume (100 μL) in two batches. For each addition, 50 μL of 1 mg/ml 3XFLAG peptide was added and the slurry was put on ice for 20 min stirring every 10 minutes with gel-loading pipette. The two eluants were mixed and the success of the IP was assayed via anti-FLAG western blot (mouse monoclonal M2 anti-FLAG antibody - Sigma F3165).

RNA Extraction

TRlzol Reagent (Life Technologies, 15596-026) was added to the cell lysate or FLAG IP samples to bring the volume to 1 mL. These were incubated for 5 min prior to loading into pre-spun 15 ml, Heavy Phase Lock Gel tubes (5 PRIME, 2302850). 200 µL of chloroform was added and the samples were centrifuged at 1500 g for 10 min. The aqueous phase (above the Phase Lock Gel) was transferred to fresh tubes and the RNA was precipitated by adding 500 µL of isopropanol, mixing well and incubating for 1 hour at ambient temperature. Samples were centrifuged for 15 min at 12,000 g at 4 °C to recover the RNA. The RNA pellet was washed twice with 1 mL of cold 80% ethanol. After the second wash, allow pellets to air-dry and then dissolve RNA in 30 µL 10 mM Tris pH 7.0. The RNA was treated with TURBO DNase (Life Technologies AM1907) as per instructions in the kit.

Reverse Transcription (RT) and qPCR

For each reaction, we usee 10 pg - 5 µg of total RNA or 10 pg - 500 ng of mRNA. RT was performed using the SuperScript III Reverse Transcriptase kit (Invitrogen, 18080-051) with gene-specific RT primers: MS371 (5'-GGCATTAAAGCAGCGTATCC, T_m = 63.7 °C) and BA81 (5'-CTGCTGTCACCTTCACCGTTCC, T_m = 60.3 °C), that anneal to the target handle hairpin mRNA and *ACTB*. The sample cDNA was then quantified relative to that of *ACTB* by qPCR in 20 µL reactions using GoTaq DNA Polymerase (Promega M300) with the associated clear PCR buffer and SYBR Green I Nucleic Acid Gel Stain (Life Technologies S7563).

PCR detection of XBP1 Splice Variants

Total RNA was isolated from thapsigargin-treated K562 cells containing the UPRE-mCherry construct as described above. RT was performed on 500 ng of RNA in 20 μL reactions using the SuperScript III Reverse Transcriptase kit (Invitrogen, 18080-051) and the supplied random hexamers RT primer. The volume of the RT reaction was brought up to 200 μL with 10 mM Tris pH 8.0 before 1% was used as a template for semi-quantitative PCR. The PCR reaction was run using Taq DNA polymerase (New England BioLabs M0270) and the primers: For: 5'-AGCTTTTACGAGAGAAAACTCAT and Rev: 5'-ACTGGGTCCAAGTTGTCCAG (T_m = 60.5 °C). Reaction products were visualized on a 2.8% agarose gel.

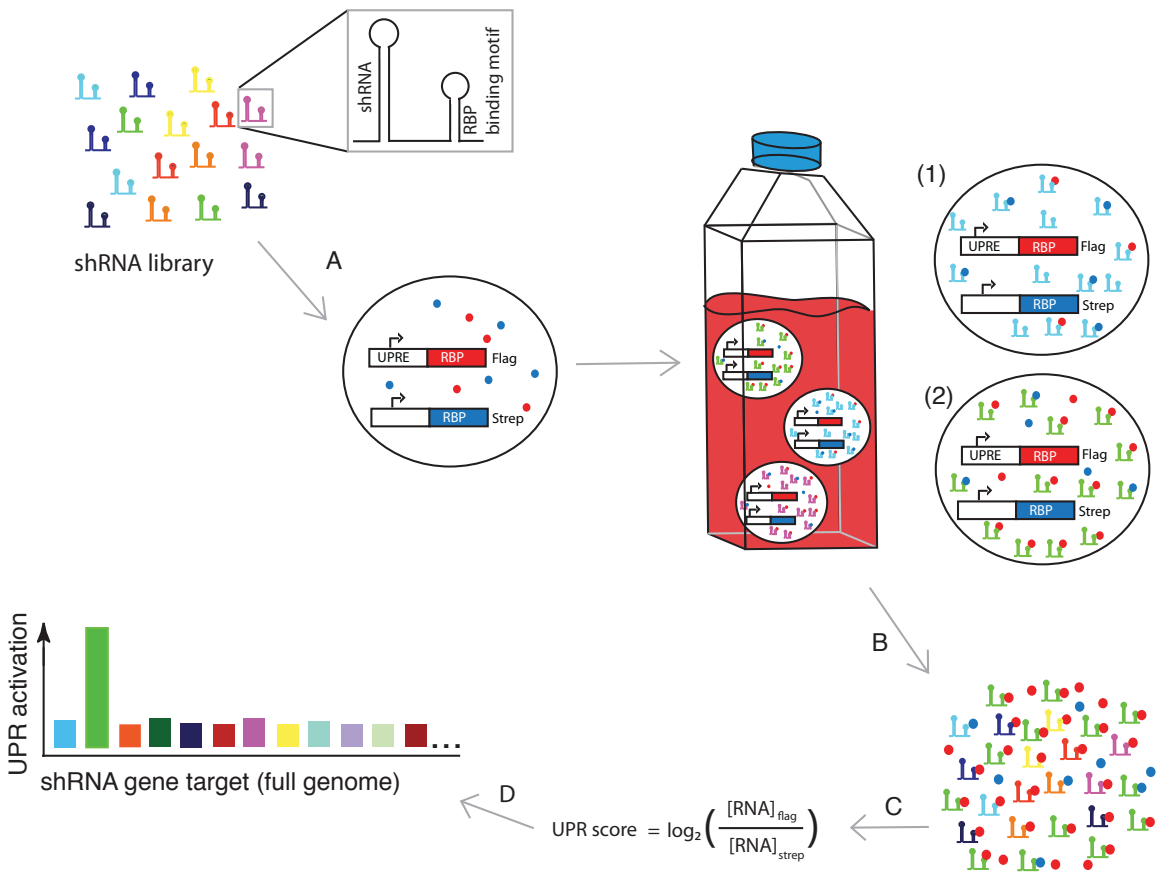


Figure 1. *Schematic of the loss of function screen to identify regulators of protein homeostasis in mammalian cells.* **(A)** Reporter cell lines containing a UPR reporter (UPRE) driving the expression of an RBP-Flag and a constitutively expressed RBP-strep control will be infected with a pooled library in which the shRNA is adjacent to the RBP handle hairpin. Possible outcomes depend on the affect of the shRNA. For example, (1) the shRNA has no affect on ER homeostasis, or (2) the shRNA causes an increase in unfolded proteins in the ER. **(B)** The cells are lysed and the RBPs are immunoprecipitated. **(C)** RNA is isolated and shRNAs are identified by reverse transcription of the RNA followed by deep sequencing. **(D)** To identify genes that activate or dampen the UPR when knocked down, a UPR score will be calculated from the abundance of each shRNA from the IP of the UPRE driven RBP relative to that from the IP of the control RBP.

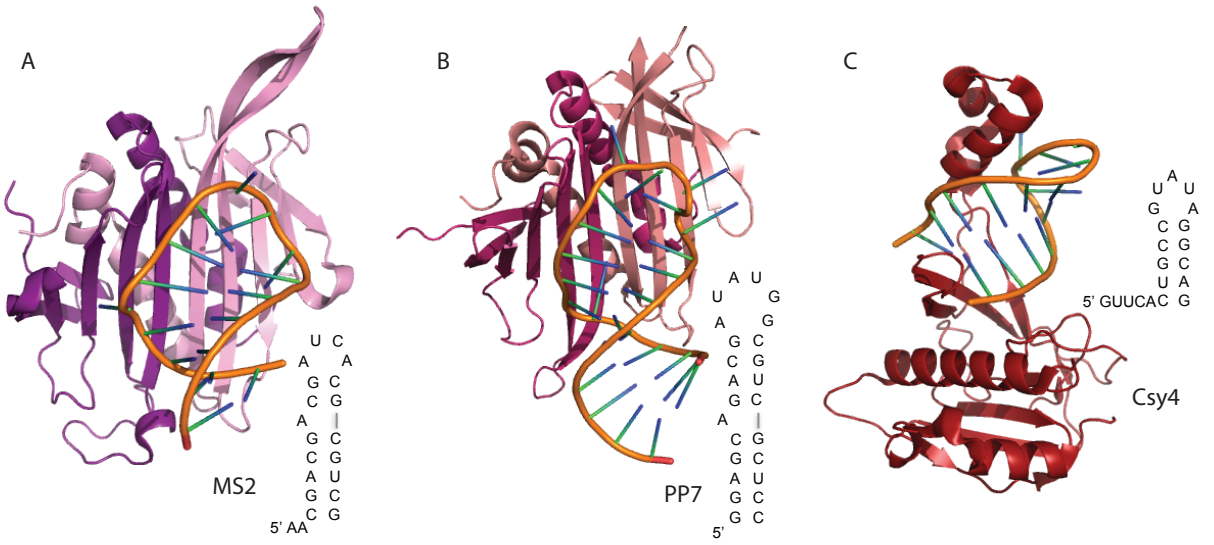


Figure 2. *RNA binding proteins considered for use in the screen.* **(A)** MCP with MS2 RNA. PDB: 2BU1. **(B)** PCP with PP7 RNA. PDB: 2QUX. **(C)** Csy4 with the hairpin it binds. PDB: 4AL5.

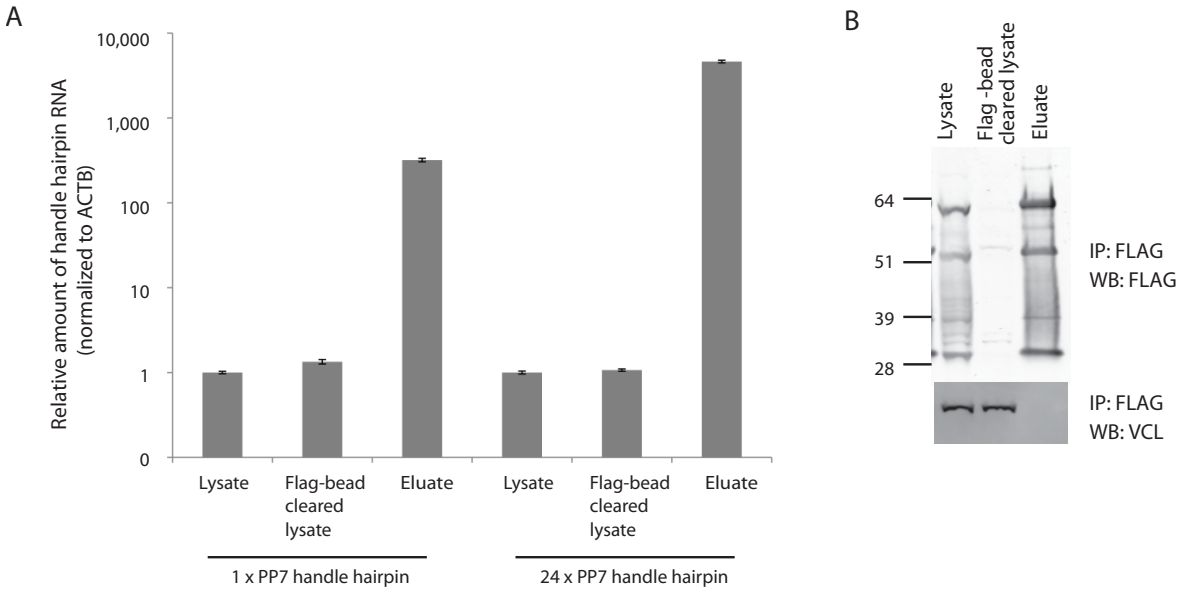


Figure 3. *IP of PCP enriches for PP7 handle hairpin RNA.* **(A)** RNA was extracted from 293T cell lysate, the lysate after it had incubated with FLAG magnetic beads and the eluate from the FLAG beads. The amount of handle hairpin RNA was quantified relative to that from the ACTB gene using qPCR. **(B)** A representative western blot from the FLAG IP where 1% of the lysate, 1% of the Flag-bead cleared lysate and 5% of the eluate were loaded. Vinculin (VCL) is shown as a loading control. The three primary bands are likely to be: 2xPCP-mCherry-FLAG (60 kDa), 1xPCP-mCherry-FLAG (46 kDa), and mCherr-FLAG (30 kDa).

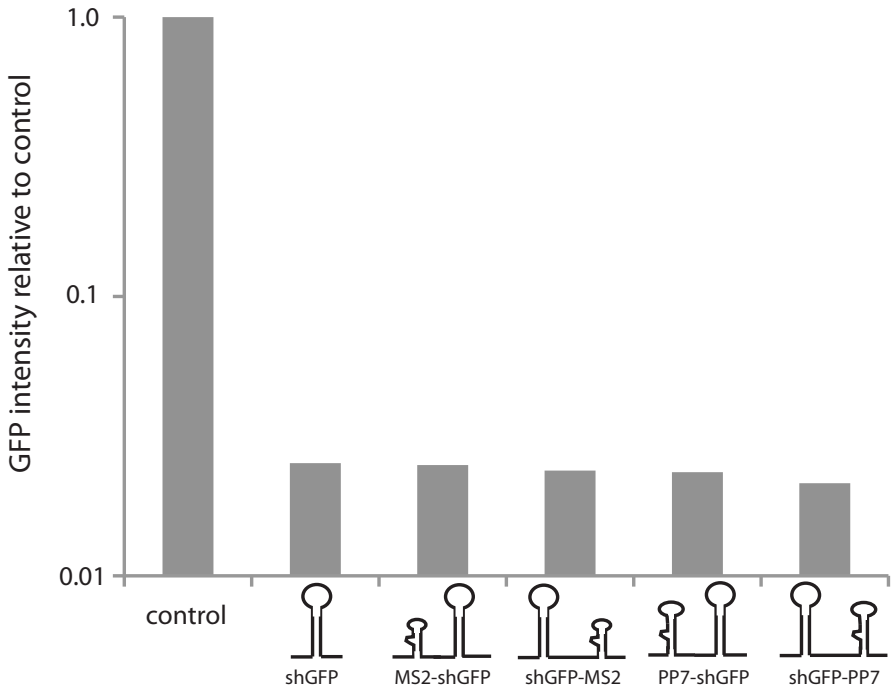


Figure 4. *The presence of a proximal handle hairpin does not affect shRNA knockdown of GFP.* A K562 cell line expressing GFP was stably infected with constructs containing an shRNA against GFP (shGFP) with or without a proximal handle hairpin.

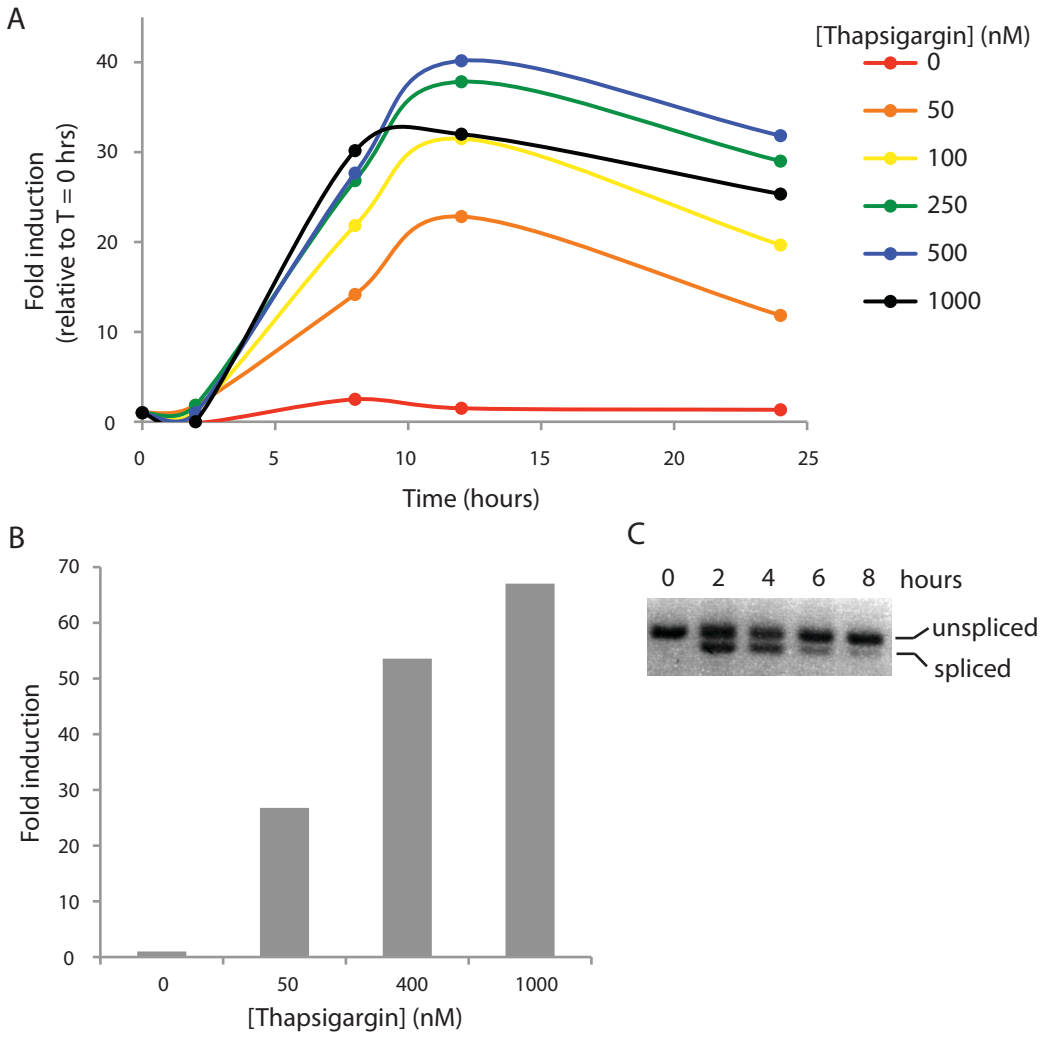


Figure 5. *The UPRE reporter quantitatively responds to induction of ER protein folding stress.* **(A)** K562 cells with the UPRE driving mCherry expression were treated with different concentrations of thapsigargin and monitored over the course of 24 hours. The intensity of mCherry fluorescence was background subtracted and fold induction was calculated relative to the level at the time of treatment (0 hours). **(B)** UPRE induction was verified by qPCR of mCherry. Samples were taken after 15 hours of thapsigargin treatment. The fold induction was normalized to 0 nM thapsigargin. **(C)** UPR activation was verified in this cell line by treatment with 1000 nM thapsigargin, RNA extraction and PCR over the *xbp1* splice site. The spliced form can be seen as early as 2 hours post treatment.

References

1. Smith, M. H., Ploegh, H. L. & Weissman, J. S. Road to Ruin: Targeting Proteins for Degradation in the Endoplasmic Reticulum. *Science* **334,** 1086–1090 (2011).
2. Walter, P. & Ron, D. The unfolded protein response: from stress pathway to homeostatic regulation. *Science* **334,** 1081–1086 (2011).
3. Gardner, B. M. & Walter, P. Unfolded proteins are Ire1-activating ligands that directly induce the unfolded protein response. *Science* **333,** 1891–1894 (2011).
4. Jonikas, M. C. *et al.* Comprehensive characterization of genes required for protein folding in the endoplasmic reticulum. *Science* **323,** 1693–1697 (2009).
5. Travers, K. J. *et al.* Functional and genomic analyses reveal an essential coordination between the unfolded protein response and ER-associated degradation. *Cell* **101,** 249–258 (2000).
6. Hetz, C. The unfolded protein response: controlling cell fate decisions under ER stress and beyond. *Nat. Rev. Mol. Cell Biol.* **13,** 89–102 (2012).
7. Hollien, J. & Weissman, J. S. Decay of endoplasmic reticulum-localized mRNAs during the unfolded protein response. *Science* **313,** 104–107 (2006).
8. Shore, G. C., Papa, F. R. & Oakes, S. A. Signaling cell death from the endoplasmic reticulum stress response. *Curr. Opin. Cell Biol.* **23,** 143–149 (2011).
9. Rutkowski, D. T. & Hegde, R. S. Regulation of basal cellular physiology by the homeostatic unfolded protein response. *J. Cell Biol.* **189,** 783–794 (2010).
10. Brandman, O. *et al.* A ribosome-bound quality control complex triggers degradation of nascent peptides and signals translation stress. *Cell* **151,** 1042–1054 (2012).

11. Bassik, M. C. *et al.* A systematic mammalian genetic interaction map reveals pathways underlying ricin susceptibility. *Cell* **152,** 909–922 (2013).

12. Kampmann, M., Bassik, M. C. & Weissman, J. S. Integrated platform for genome-wide screening and construction of high-density genetic interaction maps in mammalian cells. *Proc. Natl. Acad. Sci. U. S. A.* **110,** E2317–2326 (2013).

13. Bassik, M. C. *et al.* Rapid creation and quantitative monitoring of high coverage shRNA libraries. *Nat. Methods* **6,** 443–445 (2009).

14. Haurwitz, R. E., Jinek, M., Wiedenheft, B., Zhou, K. & Doudna, J. A. Sequence- and structure-specific RNA processing by a CRISPR endonuclease. *Science* **329,** 1355–1358 (2010).

15. Sternberg, S. H., Haurwitz, R. E. & Doudna, J. A. Mechanism of substrate selection by a highly specific CRISPR endoribonuclease. *RNA N. Y. N* **18,** 661–672 (2012).

16. Lee, H. Y. *et al.* RNA-protein analysis using a conditional CRISPR nuclease. *Proc. Natl. Acad. Sci. U. S. A.* **110,** 5416–5421 (2013).

17. Bertrand, E. *et al.* Localization of ASH1 mRNA particles in living yeast. *Mol. Cell* **2,** 437–445 (1998).

18. Valegård, K., Murray, J. B., Stockley, P. G., Stonehouse, N. J. & Liljas, L. Crystal structure of an RNA bacteriophage coat protein-operator complex. *Nature* **371,** 623–626 (1994).

19. Lim, F. & Peabody, D. S. Mutations that increase the affinity of a translational repressor for RNA. *Nucleic Acids Res.* **22,** 3748–3752 (1994).

20. Valegård, K., Liljas, L., Fridborg, K. & Unge, T. The three-dimensional structure of the bacterial virus MS2. *Nature* **345,** 36–41 (1990).

21. Lim, F. & Peabody, D. S. RNA recognition site of PP7 coat protein. *Nucleic Acids Res.* **30,** 4138–4144 (2002).

22. Tars, K., Fridborg, K., Bundule, M. & Liljas, L. The three-dimensional structure of bacteriophage PP7 from Pseudomonas aeruginosa at 3.7-A resolution. *Virology* **272,** 331–337 (2000).

23. Caldeira, J. C. & Peabody, D. S. Stability and assembly in vitro of bacteriophage PP7 virus-like particles. *J. Nanobiotechnology* **5,** 10 (2007).

24. Chao, J. A., Patskovsky, Y., Almo, S. C. & Singer, R. H. Structural basis for the coevolution of a viral RNA-protein complex. *Nat. Struct. Mol. Biol.* **15,** 103–105 (2008).

25. Lim, F., Downey, T. P. & Peabody, D. S. Translational repression and specific RNA binding by the coat protein of the Pseudomonas phage PP7. *J. Biol. Chem.* **276,** 22507–22513 (2001).

26. Wu, B., Chao, J. A. & Singer, R. H. Fluorescence fluctuation spectroscopy enables quantitative imaging of single mRNAs in living cells. *Biophys. J.* **102,** 2936–2944 (2012).

27. Wang, Y. *et al.* Activation of ATF6 and an ATF6 DNA binding site by the endoplasmic reticulum stress response. *J. Biol. Chem.* **275,** 27013–27020 (2000).

28. Yoshida, H., Matsui, T., Yamamoto, A., Okada, T. & Mori, K. XBP1 mRNA is induced by ATF6 and spliced by IRE1 in response to ER stress to produce a highly active transcription factor. *Cell* **107,** 881–891 (2001).

29. Promlek, T. *et al.* Membrane aberrancy and unfolded proteins activate the endoplasmic reticulum stress sensor Ire1 in different ways. *Mol. Biol. Cell* **22,** 3520–3532 (2011).

30. Thibault, G. *et al.* The membrane stress response buffers lethal effects of lipid disequilibrium by reprogramming the protein homeostasis network. *Mol. Cell* **48,** 16–27 (2012).

31. Zhao, L. & Ackerman, S. L. Endoplasmic reticulum stress in health and disease. *Curr. Opin. Cell Biol.* **18,** 444–452 (2006).

32. Gilbert, L. A. *et al.* CRISPR-mediated modular RNA-guided regulation of transcription in eukaryotes. *Cell* **154,** 442–451 (2013).

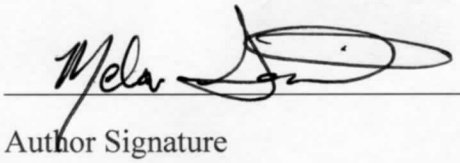
33. Qi, L. S. *et al.* Repurposing CRISPR as an RNA-guided platform for sequence-specific control of gene expression. *Cell* **152,** 1173–1183 (2013).

34. Yoon, J.-H., Srikantan, S. & Gorospe, M. MS2-TRAP (MS2-tagged RNA affinity purification): tagging RNA to identify associated miRNAs. *Methods San Diego Calif* **58,** 81–87 (2012).

Publishing Agreement

It is the policy of the University to encourage the distribution of all theses, dissertations, and manuscripts. Copies of all UCSF theses, dissertations, and manuscripts will be routed to the library via the Graduate Division. The library will make all theses, dissertations, and manuscripts accessible to the public and will preserve these to the best of their abilities, in perpetuity.

I hereby grant permission to the Graduate Division of the University of California, San Francisco to release copies of my thesis, dissertation, or manuscript to the Campus Library to provide access and preservation, in whole or in part, in perpetuity.



Author Signature

5·19·14

Date